Titulació:
Enginyeria Aeronàutica Superior

Alumne (nom i cognoms):
Orzuri Rique Garaizar

Títol PFC:
Design of a Solar Sail as the Propulsion System for a Nanosatellite

Director del PFC:
Dr. Elena Fantino

Convocatòria de lliurament del PFC:
Quadrimestre de primavera 2013 - Defensa Juny 2013

Contingut d'aquest volum: **-**MEMÒRIA**-**

Design of a Solar Sail as the Propulsion System for a Nanosatellite

-Project Report-

by

Orzuri Rique Garaizar

orzuri.rique@gmail.com

Tutor: Dr. Elena Fantino

June 2013

A dissertation submitted to the Department of Aerospace Engineering,

ETSEIAT- *Universitat Politècnica de Catalunya*,

in partial fulfillment of the requirements for the degree of

Aeronautical Engineer

Escola Tècnica Superior d'Enginyeries Industrial i Aeronàutica de Terrassa

UNIVERSITAT POLITÈCNICA DE CATALUNYA

ABSTRACT

This project presents the design of a solar sail as a feasible solution to thrust nanosatellites. A solar sail is a high-energy space propulsion system that uses solar radiation pressure to push large ultra-thin mirror to high speed, enabling the combination of low-cost operations with long operating lifetimes. In this project, the Solar Sail Module (SSM) is designed to be packed into a Plug and Play (PnP) module of 2U size ($20\text{cm} \times 10\text{cm} \times 10\text{cm}$). The solar sail is aimed for cubesats performing missions orbiting the Moon. Basically, the sail is sized for a trajectory that departs from GEO, follows a spiral to escape from the Earth and finally drives the nanosatellite to the target lunar orbit.

The SSM detailed design has been done using Commercial Off-The-Shelf (COTS) components. The overall design of the SSM is presented by a CAD design done in CATIAv5. With respect to the trajectory calculation, a 4 body problem is implemented through a self-developed Matlab® code with RKF7 integrator. The trajectory calculation enables the validation of the SSM design to propel spacecraft up to 8kg in less than 3.6 years to the vicinity of the Moon.

The main contribution of this work is to provide the nanosatellites community with a feasible PnP SSM that can drive this kind of satellites from the Earth to the Moon.

Keywords: solar sail, nanosatellite, Moon orbit, GEO, Plug and Play and COTS.

ACKNOWLEDGEMENTS

This project represents the last stage in my path for obtaining the Degree of Aeronautical Engineer. Due to being a milestone in my life, with these few words I want to show my gratitude to all those who have supported me during this last years and especially in the development of this project. Firstly, I would like to acknowledge my tutor Dr. Elena Fantino. During her classes of Space Vehicles, Design of Space Vehicles I and II, she transmitted me her passion for space. This passion led me to decide doing a space-related Final Year Project, hence getting inside this wonderful field.

Secondly, I would like to show my gratefulness to Helena Pons Lorente, who aided me printing and delivering the project documents.

Finally, I would like to thank all my family, but specially my parents Koldo and Edurne and my sister Larraitz. Furthermore, I specially want to thank my boyfriend Arnau, my support during this complicated time, for his constant patience and understanding.

I hope that you enjoy the reading of this document.

Sincerely,

Orzuri Rique Garaizar

Quo natura negat, reddere cura potest.

TABLE OF CONTENTS

LIST OF FIGURES

LIST OF TABLES

LIST OF ACRONYMS

AFRL	Air Force Research Labs
ASTM	American Section of the International Association for Testing Materials
AU	Astronomical Unit
BDM	Booms deployment mechanism
BRC	Bi-stable reeled
CAD	Computer-aided Design
CAE	Computer-aided Engineering
CFRP	Carbon-fiber Reinforced Plastic
CI	Creasing Indicator
CM	Center of Mass
COTS	Commercial Off-The-Shelf
CTM	Collapsible Tube Mast
DFM	Design for Manufacturability
DRL	German Aerospace Center, Deutsches Zentrum für Luft- und Raumfahrt
ECI	Earth-centered inertial
ESA	European Space Agency
FEM	Finite Element Method
GEO	Geostationary Earth Orbit
GSO	Geosynchronous Earth Orbit
GRC	Glenn Research Center
IKAROS	Interplanetary Kite-craft Accelerated by the Radiation of the Sun
IR	Ideal Reflection
ISSS	International Symposium on Solar Sailing
JAXA	Japan Aerospace Exploration Agency

JD	Julian Date
JPL	Jet Propulsion Laboratory
MEO	Medium-Earth Orbit
NASA	National Aeronautics and Space Administration
NPR	Non-Perfectly Reflecting
PnP	Plug and Play
P-POD	Poly-PicoSatellite Orbital Deployer
RAQL	Radio-Quiet Lunar
RKF	Runge-Kutta-Fehlberg
s/c	Spacecraft
SI	Le Système international d'unités
SOI	Sphere of Influence
SPF	Space Power Facility
SRP	Solar Radiation Pressure
SSM	Solar Sail Module
STEM	Storable Tubular Extendable Member
TRAC	Triangular Retractable and Collapsible
TRL	Technology Readiness Level
ηPR	η-Perfect Reflection

LIST OF SYMBOLS

Symbol	Definition	Units
a	Absorption coefficient	---
a_c	Characteristic acceleration	m/s^2
A	Sail area	m^2
A_{eff}	Effective solar sail area	m^2
c	Speed of light	m
$d_\odot$	Time parameter	m
$D_\leftmoon$	Moon's mean elongation with respect to Sun	degrees
L	Length of the quadrant-shaped solar sail side	m
L_{booms}	Length of each boom	m
L_s	Solar luminosity	W
$L_\odot$	Mean longitude of the Sun corrected for the aberration of light	degrees
$L_\leftmoon$	Longitude of the Moon	degrees
m	Mass of the s/c	kg
m_{booms}	Total mass of booms	kg
m_{s_c}	Mass of each sail quadrant	kg
$M_\odot$	Sun mean anomaly	degrees
$M_\leftmoon$	Moon mean anomaly	degrees
P	Solar Radiation Pressure	Pa
$r_\odot$	Earth-Sun distance	AU
$r_\leftmoon$	Geocentric distance	m
R_1	Inner radius of the BDM	m
R_2	Outer radius of the BDM	m
$R_\oplus$	Equatorial radius of the Earth	m
$R_\leftmoon$	Equatorial radius of the Earth	m
s	Specular reflection factor	---

S_o	Solar Constant	W/m^2
t_f	Thickness of flattened booms	m
t_s	Thickness of the membrane	m
$T_\odot$	Time parameter	
$\vec{a}$	Acceleration vector of the satellite	m/s^2
$\vec{a}_{pert}$	Satellite acceleration due to all the perturbations	m/s^2
$\vec{a}_{SRP}$	Satellite acceleration due to SRP	m/s^2
$\vec{F}_{SRP}\big\vert_{Ideal}$	SRP force for ideal solar sail model	N
$\vec{F}_{SRP}\big\vert_{NPR}$	SRP force for NPR solar sail model	N
$\vec{L}$	Orbital angular momentum vector	m^2/s
$\hat{n}$	Solar sail unit normal vector	---
$\vec{r}$	Position vector of the satellite	m
$\vec{r}_{moon}$	Moon positioning vector	m
$\vec{r}_{ms}$	Moon-to-satellite vector	m
$\vec{r}_{ss}$	Sun-to-satellite vector	m
$\vec{r}_{sun}$	Sun position vector	m
$\vec{v}$	Velocity vector of the satellite	m/s^2
α	Pitch angle of the satellite	degrees
α_{ra}	Right ascension	degrees
β	Ecliptic latitude	degrees
δ	Declination	degrees
ε	Emission coefficient	---
ε_b	Back emission coefficient	---
ε_f	Front emission coefficient	---
$\epsilon_\odot$	Obliquity of the ecliptic plane	degrees
η_{eff}	Efficiency factor	
λ	Ecliptic longitude	---
λ_L	Lightness number	---

$\lambda_{\odot}$	Longitude of the ecliptic plane	$\mathrm{degrees}$
$\mu_{\odot}$	Gravitational parameter of the Sun	$\mathrm{m}^3/\mathrm{s}^2$
$\mu_{\oplus}$	Gravitational parameter of the Earth	$\mathrm{m}^3/\mathrm{s}^2$
$\mu_{\leftmoon}$	Gravitational parameter of the Moon	$\mathrm{m}^3/\mathrm{s}^2$
ρ	Reflection coefficient	---
ρ_{b}	Back reflection coefficient	---
ρ_{d}	Diffuse reflection coefficient	---
ρ_{s}	Specular reflection coefficient	---
τ	Transmission coefficient	---
$\pi_{\leftmoon}$	Equatorial horizontal parallax	$\mathrm{minutes}$
$\Omega_{\leftmoon}$	Mean longitude of the ascending node	$\mathrm{degrees}$
$\mathcal{B}_{\mathrm{b}}$	Back non-Lambertian coefficient	---
$\mathcal{B}_{\mathrm{f}}$	Front non-Lambertian coefficient	---

1. INTRODUCTION

1.1. AIM OF THE PROJECT

The aim of the project consists of designing a solar sail propulsion module to thrust a nanosatellite.

1.2. SCOPE

The scope of the different areas in which the project is divided is:

- **Mission analysis**
  - Research of the state of the art of solar sail missions.
  - Justified selection of a mission.
  - Systems engineering: definition of the propulsion subsystem objectives, drivers, requirements, constraints and trade-offs.
- **Mission trajectory analysis**
  - Research of the solar sail trajectories state of the art.
  - Development of the formulation to simulate the trajectory followed by a satellite propelled by the solar sail.
  - Implementation of the formulation into a numerical code.
  - Development of a basic solar sail steering law.
  - Validation of the feasibility of the solar sail design to fulfill the propulsive requirements of the selected mission.
  - Out of scope:
    - Optimization of the trajectory followed by the s/c.
    - Modeling of complex maneuvers such as planet targeting or planet capture in the formulation and numerical code.
    - Consideration of the attitude control of the solar sail.
- **Design of the Solar Sail Module**
  - Research of the state of the art of solar sailing technology.
  - Downselection of the configuration of the solar sail module.
  - Definition of the materials for the solar sail module.
  - Sizing of the solar sail:
    - Sizing of the solar sail booms.
    - Sizing of the solar sail quadrants.
    - Matching of the booms and sail quadrants sizes.
  - Detailed 3D CAD design of the solar sail module.
  - Estimation of the mass budget of the solar sail module.
  - Estimation of the inertia matrices of the solar sail module.
  - Out of scope:

        - Precise structural analysis of the solar sail module.
        - Thermal analysis of the solar sail module.
        - Charging analysis of the solar sail module.
        - Application of the sail as a radiofrequency antenna.
        - Design of the rest of the s/c subsystems.
- **Economic aspects**
    - Estimation of the design engineering work cost and budget.
    - Estimation of the Solar Sail Module development cost.
- **Environmental aspects**
    - Estimation of the environmentally harmful effects of solar sailing.
    - Estimation of the environmental benefits reached through this design.
- **Documentation and marketing**
    - Composition of the Project Report.
    - Composition of the Solar Sail Module Technical Datasheet.
    - Generation of Solar Sail Module drafts.
    - Generation of mission trajectory videos.

1.3. REQUIREMENTS

The basic requirements that the project shall fulfill are:

- The designed solar sail module shall be able to fulfill the propulsive requirements of the selected mission.
- The designed solar sail module shall fulfill the nanosatellites general dimensional, structural, electrical, operational and testing requirements.
- The designed solar sail module shall follow the Plug and Play philosophy.
- The designed solar sail propulsive module shall be in compliance with international space law.
- The trajectory calculation numerical code shall be written in Matlab®.
- The CAD design shall be done in CATIAv5.

1.4. JUSTIFICATION

In recently years, nanosatellites have experienced a boost growth thanks to the Cubesat concept developed by Jordi Puig-Suari (Cal Poly) and Bob Twiggs (Stanford University) in 1999. Besides, the current advancements in miniaturizing space-borne systems have allowed nanosatellites to perform similar missions to that of bigger satellites. Indeed, the CubeSats are filling a niche in space that larger systems, with their higher cost and longer design-to-space cycles are not designed to fill. Furthermore, due to the industrial standardization of these designs, nongovernmental organizations, such as universities or nonprofit scientific associations (e.g. The Planetary Society) are now capable of taking part

into space-exploration. In addition, taking into account that as stated in [50], the weight of a space shuttle at launch is approximately 95 percent fuel, the nanosatellites have arrived to stay and be the test-bench for checking new technologies in space environment.

However, due to their limited size and weight, the propulsion system is still an impediment for performing longer and more complex missions, such as non-inertial orbits or interplanetary missions. Thereby, finding a cutting-edge lightweight propulsion system is the only way to broaden the horizon of nanosatellites. Due to offering the combination of high performance capability, solar sails are the most suitable candidates to thrust nanosatellite with long lifetimes. In fact, one of the great advantages of solar sailing is that it requires no fuel, because the use the sunlight to thrust. NASA researchers have found that at 1 Astronomical Unit (AU), sunlight can produce about $1.4\mathrm{kW}$ of power ([50]). Taking $1.4\mathrm{kW}$ and dividing it by the speed of light, it would be found that the force exerted by the Sun is about $3.5 \cdot 10^{-6}\mathrm{N/m^2}$. To compare with, note that the thrust provided by a conventional chemical rocket, such as the space shuttle main engine, is $1.67\mathrm{MN}$. Nonetheless, the continuous force of the sunlight on a solar sail may thrust a satellite to speeds five times faster than in case of the traditional rockets. Bearing in mind the propulsion system of nanosatellites is not aimed to lift off, the value of the maximum nominal thrust required is small. Conversely, the amount of total impulse required is big, especially when long continuous operating-times are required. Besides, the compactness offered by solar sails as well as their lightweight make them suitable to deal with the strict volume constraints of nanosatellites.

In this way, through this project a hot demand of the current space-community is intended to supplement: the design of a solar sail to be used as propulsion system for nanosatellites. Although much progress is still required to fulfill the wishes of Galileo or to make true the dreams of Julio Verne, all possible efforts are required.

Provide ships or sails adapted to the heavenly breezes, and there will be some who will brave even that void.

Galileo, 1610 ([51])

2. SOLAR SAIL CONCEPT

A solar sail is a high-energy space propulsion system that uses the radiation pressure of the light from a star to push large ultra-thin mirror to high speed. In case of the Solar System, the light source to thrust the solar sail is the Sun and consequently, the radiation pressure is known as Solar Radiation Pressure (SRP). Note that light is made up of packets of energy "photons" that act like atomic particles but with more energy. In this way, when a beam of light is pointed at a bright mirror surface the photons reflect it back transmitting their momentum twice: once by the initial impact and again by reflecting back from the surface. Consequently, if there is a steady stream of reflective photons, the solar sail is pushed forward, even little by little. In other words, the thrust of a solar sail although small, is continuous and acts for the life of the mission enabling the combination of low-cost operations with long operating lifetimes.

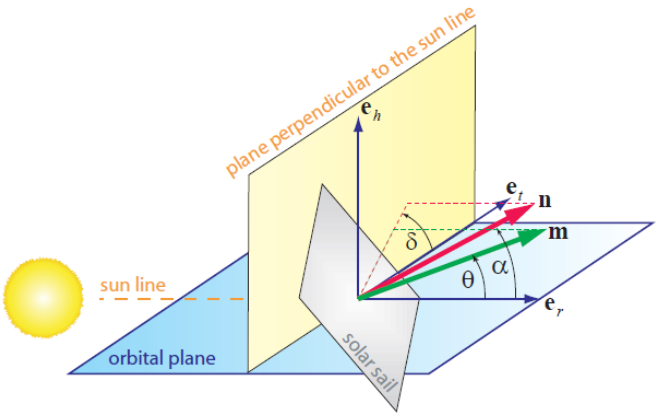

Figure 1. Definition of the sail normal vector $\hat{\mathrm{n}}$ and thrust unit vector $\hat{\mathrm{m}}$ (source [1]).

In order to describe the force exerted on the solar sail by the SRP, the reference frame stated in [1]-[2] and attached through Figure 1 is used. The reference frame $\mathcal{O}^3 = \{\mathrm{e_r}, \mathrm{e_t}, \mathrm{e_h}\}$ is an orthogonal right-handed polar coordinate frame where $\mathbf{e_r}$ points always along the sun-spacecraft line, $\mathbf{e_h}$ is the orbit plane normal pointing along the s/c orbital angular momentum vector and $\mathbf{e_t}$ completes the coordinate frame. The first unit vector defined in this reference frame is the unit vector perpendicular to the sail always directed away from the Sun called $\hat{\mathrm{n}}$. This vector $\hat{\mathrm{n}}$ can be utilized to describe the sail's attitude and its direction with respect to the frame of Figure 1 is given through the pitch angle α and clock angle δ. Furthermore, the second unitary vector is the thrust unit vector identified with $\hat{\mathrm{m}}$. This vector points along the direction of the SRP. Similar to the case of vector the $\hat{\mathrm{n}}$, the direction of the vector $\hat{\mathrm{m}}$ in the reference frame of Figure 1 can be given by the cone angle θ and the clock angle δ. The value of the SRP at the position of the satellite known as P is:

$$P = \frac{L_s}{4\pi c \cdot \|\vec{r}_{ss}\|^2} \ [Pa] \tag{2.1}$$

where $\vec{r}_{ss}$ is the Sun-to-satellite vector expressed in meters, c is the speed of light in vacuum equal to $c = 299792459 m/s$ and L_s is the solar luminosity. For the calculations presented in this project, it has been assumed that $L_s = 3.856 \cdot 10^{26} W$ (see [3]). Note that the value of the solar luminosity is not constant. It varies by about $\pm 0.5\%$ due to the 11-years solar cycle. The solar luminosity value here acquired is an average and implies a Solar Constant of S_o of $S_o = 1371.1 W/m^2$.

According to the simplifications made concerning the optical characteristics of a solar sail, the magnitude and direction of the SRP force can be modeled in different ways. In this project, the two models of defined in [2] are presented: the ideal solar sail and the Non-perfectly Reflecting (NPR) solar sail.

2.1. IDEAL SOLAR SAIL

The ideal solar sail is the simplest model. As shown in Figure 2, it assumes that the solar sail is an ideally reflecting surface. This assumption can be denoted model Ideal Reflection (IR): the vector $\hat{n}$ and the thrust vector $\hat{m}$ are parallel, hence the SRP force is always perpendicular to the sail's surface. As a result, from Figure 2 one can conclude that:

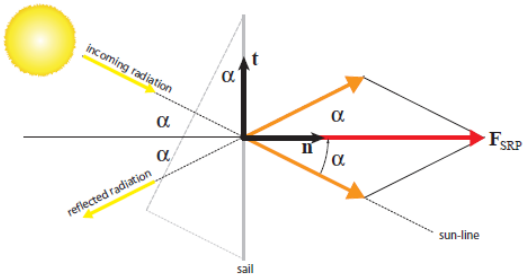

Figure 2. Scheme of the SRP force on an ideal solar sail (source [2]).

$$\vec{F}_{SRP}\big|_{Ideal} = 2PA\cos\alpha\cos\alpha\,\hat{n} \ [N] \tag{2.2}$$

where P is the value of the SRP at the position of the satellite given by the expression (2.1) in Pa, A is the total area of the satellite in m^2 and α is the angle between the sunlight and the solar sail normal vector:

$$\alpha = \cos^{-1}\left(\frac{\vec{r} - \vec{r}_{sun}}{\|\vec{r} - \vec{r}_{sun}\|} \cdot \hat{n}\right) \ [rad] \tag{2.3}$$

where, $\vec{r}$ is the satellite position vector and $\vec{r}_{sun}$ is the Sun position vector.

Also, note that in this case the effective solar sail area that contributes to the SRP force, A_{eff} is implicitly considered in expression (2.2). Indeed, A_{eff} is equal to $A_{eff} = A\cos\alpha$, hence the expression (2.2) can be rewritten as:

$$\vec{F}_{SRP}\big|_{Ideal} = 2PA_{eff}\cos\alpha\,\hat{n} \quad [N]. \tag{2.4}$$

When characterizing and comparing specific implementations of solar sails, there are two important parameters to be considered: the characteristic acceleration a_c and the lightness number λ_L. The former is the most commonly used solar sail performance parameter. It is defined as the SRP acceleration acting on a solar sail that is oriented perpendicularly to the sun line ($\mathbf{e_r} = \hat{n}$) at 1 AU ($r_0 = 1AU = 1.49597870 \cdot 10^{11}m$). In case of ideal solar sail, the characteristic acceleration is calculates through:

$$a_c = \frac{2P_0A}{m}\ [m/s^2] \tag{2.5}$$

where P_0 is the value of the SRP at 1AU. Note that the value of P_0 is given by:

$$P_0 = \frac{L_s}{4\pi c \cdot \|r_0\|^2} = \frac{L_s}{4\pi c \cdot \|1.49597870 \cdot 10^{11}\|^2}\ [Pa]. \tag{2.6}$$

Note that although in this project all of the magnitudes are expressed in SI, a_c is convenient to use mm/s^2, due to being really small magnitude.

The lightness number λ_L represents the dimensionless ratio of the SRP force to the Sun gravitational force at 1AU. In the case of ideal sail, it is given by:

$$\lambda_L = \frac{a_c r_0^2}{\mu_\odot} \quad [dimensionless] \tag{2.7}$$

where a_c is the characteristic acceleration obtained from (2.5) and $\mu_\odot$ gravitational parameter of the Sun equal to $\mu_\odot = 1.327124 \cdot 10^{20} m^3/s^2$.

2.2. NON-PERFECTLY REFLECTING SOLAR SAIL

The Non-perfectly Reflecting (NPR) is a more sophisticated SRP force model than the ideal one, due to the fact it takes into account the optical coefficients of the solar sail film. This SRP force model is described [1]-[2] is illustrated in Figure 3.

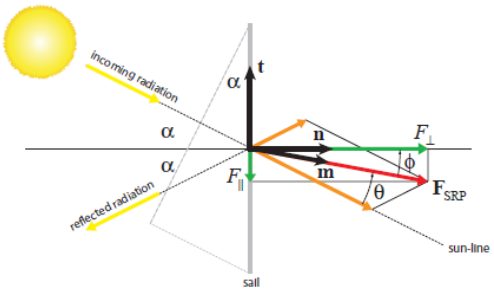

Figure 3. Scheme of the SRP force on a Non-perfectly Reflecting solar sail (sources [1]-[2]).

In this model the optical characteristics of the sail film are parameterized by the absorption coefficient a, the reflection coefficient ρ, the transmission coefficient τ, and the emission coefficient ε. These coefficients are constrained through:

$$a + \rho + \tau = 1. \tag{2.8}$$

Note that $\tau = 0$ in the reflecting side of the solar sail. As well, due to the fact that not all the photons are reflected specularly, the reflection coefficient can be further divided into a specular reflection coefficient ρ_s, a diffuse reflection coefficient ρ_d and a back reflection coefficient ρ_b, combined in such way that $\rho = \rho_s + \rho_d + \rho_b$. Furthermore, considering that the back reflection coefficient is negligible ($\rho_b = 0$), a specular reflection factor s can be also used: $s = \rho_s/\rho \rightarrow \rho_s = s\rho$ and then, $\rho_d = (1 - s)\rho$. The expression (2.8) can be rewritten as:

$$a = 1 - \rho = 1 - (\rho_s + \rho_d). \tag{2.9}$$

The emission coefficient ε is used to describe the power emitted from a surface of area A at an absolute temperature T. Bearing in mind that the front and the back of the solar sail have different coatings, the power emitted from the two sides different. The emission coefficient of the front is identified with ε_f and that of the back as ε_b. Moreover, the non-Lambertian coefficients of the front $\mathcal{B}_f$ and back $\mathcal{B}_b$ side of the sail are defined with the aim of describing the angular distribution of the emitted and the diffusely reflected photons. Consequently, the NPR model parameterizes the optical characteristics of the sail film through:

$$\mathcal{P} = \{\rho, s, \varepsilon_f, \varepsilon_b, \mathcal{B}_f, \mathcal{B}_b\}. \tag{2.10}$$

Following the formulation developed in [2] and looking at Figure 3, a sail-fixed 2D coordinate frame called $\mathcal{S} = \{\hat{n}, \hat{t}\}$ in introduced, where $\hat{n}$ is the unit vector normal to the sail's surface and $\hat{t}$ is the unit vector tangent to the sail surface. In this way, the SRP force exerted on the solar sail is represented by a normal component $F_\perp$ along $\hat{n}$ and transverse component $F_\parallel$ along $\hat{t}$ as follows:

$$F_{\perp} = F_{SRP} \cdot \hat{n} = 2PA\cos\alpha\,\psi_{\perp} \;\; [N] \tag{2.11}$$

$$F_{\parallel} = -F_{SRP} \cdot \hat{t} = -2PA\cos\alpha\,\psi_{\parallel} \;\; [N] \tag{2.12}$$

where the values $\psi_{\perp}$ and $\psi_{\parallel}$ are given by:

$$\psi_{\perp} = \frac{1}{2}(1+s\rho)\cos\alpha + \frac{1}{2}\left[\mathcal{B}_f(1-s)\rho + (1-\rho)\frac{\varepsilon_f\mathcal{B}_f - \varepsilon_b\mathcal{B}_b}{\varepsilon_f+\varepsilon_b}\right] \tag{2.13}$$

$$\psi_{\parallel} = \frac{1}{2}(1-s\rho)\sin\alpha. \tag{2.14}$$

In order to simplify equations (2.13) and (2.14), in [2] the following three characteristic optical sail coefficients are defined:

$$a_1 = \frac{1}{2}(1+s\rho) \tag{2.15}$$

$$a_2 = \frac{1}{2}\left[\mathcal{B}_f(1-s)\rho + (1-\rho)\frac{\varepsilon_f\mathcal{B}_f - \varepsilon_b\mathcal{B}_b}{\varepsilon_f+\varepsilon_b}\right] \tag{2.16}$$

$$a_3 = \frac{1}{2}(1-s\rho) \tag{2.17}$$

Consequently, substituting the expressions (2.15), (2.16) and (2.17) into (2.13) and (2.14), yields:

$$\psi_{\perp} = a_1\cos\alpha + a_2 \tag{2.18}$$

$$\psi_{\parallel} = a_3\sin\alpha. \tag{2.19}$$

Therefore, the total SRP force exerted on the solar sail can be written as:

$$\vec{F}_{SRP}\big|_{NPR} = \sqrt{{F_{\perp}}^2 + {F_{\parallel}}^2}\,\hat{m} = 2PA\cos\alpha\sqrt{{\psi_{\perp}}^2 + {\psi_{\parallel}}^2}\,\hat{m} = 2PA\cos\alpha\,\psi\,\hat{m}\;[N] \tag{2.20}$$

where $\psi = \sqrt{{\psi_{\perp}}^2 + {\psi_{\parallel}}^2}$ depends only on the pitch angle α and on the optical coefficients of the sail defined in equation (2.10). In case of the NPR solar sail, the characteristic acceleration a_c is defined as:

$$a_c = \frac{2P_0A}{m}(a_1 + a_2) \;\; [m/s^2] \tag{2.21}$$

where a_1 and a_2 are the characteristic optical sail coefficients defined by the expressions (2.15) and (2.16). Finally, note that the value of the lightness λ_L in the case of NPR solar sail is obtained by substituting the value of characteristic acceleration of (2.21) into expression (2.7).

3. STATE OF THE ART

Although the solar sailing notion has been in the consciousness of the scientific community since the early part of the 20th century, the first engineering efforts date back to the 1970's. Indeed, in the 1970's National Aeronautics and Space Administration (NASA) began to dabble in the concept of solar sailing. As indicated in [52], Dr. Louis Friedman at NASA's Jet Propulsion Laboratory (JPL) led a project to try the first solar sail flight. The main idea was to propel a probe through solar sail to rendezvous with the Halley's Comet that would have its closest approach to the Earth in 1986. Unfortunately, the project was discarded although the feasibility of solar sailing was shown by that preliminary design.

The next relevant reference for solar sailing is found in 1993, when the Russian Space Agency launched Znamya 2, a 20m spinning solar mirror aimed to beam solar power back to the ground. Znamya 2 is considered as solar sailing approach by Les Johnson of NASA Marshall Space Flight Center , as discussed in [52], because it was made of a large, lightweight reflector and unfurled as a solar sail might be unfurled. After the default of the failure of deployment of the follow-up mission called Znamya 2.5, this Russian proto-sail program was scrapped. Meanwhile, other space agencies continued with the development of the solar sailing technology and demonstration missions. A brief summary of NASA's solar sailing technology status in 1999 is found in [4]. As well, solar sails were used as accessory to offset the torque resulting from solar pressure on India's INSAT 2A (circa 1992) and INSAT 3A (circa 2003) satellites.

The first real attempts to deploy and ground-test the solar sails began to take place in the 2000's. Precisely, as a part of In-Space Propulsion Technology Program, during a five-week period testing from April to May 2004 NASA's solar sail propulsion team and industry partner, Able Engineering successfully deployed their solar system at Langley Research Center (see [50]). Afterwards, in July 2004, NASA's solar sail propulsion team and industry partner, L'Garde Inc., also saw successful deployment of their solar sail system at Glenn Research Center (GRC). This In-Space Technology Program was divided in several phases. Indeed, the highlight of phase 2 was the successful testing of a 10 m four-quadrant sub-scale solar sail system test article in vacuum and thermal environment conditions at the 30m Space Power Facility (SPF) vacuum chamber, located at NASA GRC (for further information see [5]). The next step of this program (phase 3) was the testing of two 20m four-quadrat solar sail system. The two solar sails were designed and developed by Alliant Techsystems Space Systems and L'Garde Inc., respectively. During the testing, which took place in June-July 2005 in the SPF at GRC, a vacuum deployment test and structural

statics and vibration tests of two of the beam assemblies and the entire four-quadrant sail membrane were carried out in order to measure the static and dynamic response (for further information see [6]). After these ground demonstrations were completed, NASA terminated funding the solar sails and other advanced space propulsion technologies. The investments made in the In-Space Technology Program managed by NASA's Science Mission Directorate in Washington D.C. and implemented by the In-Space Technology Project reached $30milion (see [7]). In this way, with the aim of capitalizing the investments made in solar sail technology to that point, NASA Marshall Space Flight Center founded the NanoSail-D, which is explained in the section 3.1.

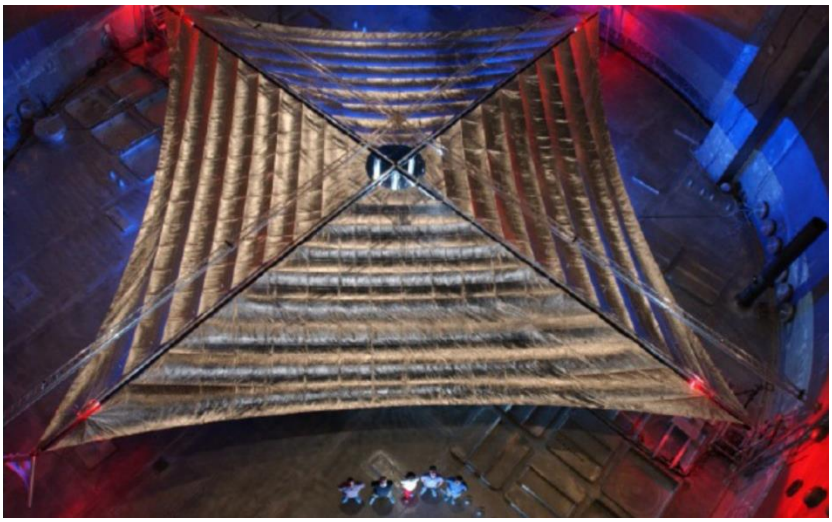

Figure 4. 20m solar sail system tested at NASA GRC Plum Brook Station Space Power Facility (source [53]).

Simultaneously, while NASA was developing the aforementioned program, the Japanese Aerospace Exploration Agency (JAXA) deployed solar sail materials in a sub-orbital environment from a sounding rocket. Although it is not considered as a demonstration of a free-flying solar sail, this experiment is largely valuable due to the difficulty associated to the deployment of gossamer sheets from a fast-moving vehicle. All these acquired knowledge by JAXA was then used in the development of IKAROS-1 (Interplanetary Kite-craft Accelerated by the Radiation of the Sun). IKAROS-1 is the first successful solar sail mission launched in May 2010 and currently on its way to Venus. Note that Znamya 2 is considered as a solar mirror, while IKAROS is the first proper solar sail. It has a mass of 300kg and it consists of 14m x 14m spinning solar sail. In order to deploy the sail, a centripetal force generated by its spinning (angular rate) is used. As well, this spinning motion also produces gyroscopic rigidity for attitude stabilization. Through the launch of this s/c, launch, space deployment and characteristic acceleration's real data were obtained. As mentioned before, IKAROS-1 is an ongoing JAXA research program.

It should be pointed out that IKAROS-1 is not the first ever attempt of launching a solar sail. This attribution belongs to Cosmos-1, a s/c developed by The Planetary Society and Cosmos Studios. In order to test a solar sail in space, the sail was designed with the aim of increasing the radius of its orbit around the Earth. The solar sail configuration was based on a spinning disk shape composed of eight blades of 15m long that could rotate about a single pitch axis for attitude control. It was launched on June 21, 2005 from the Russian submarine Borisoglebsk. Unluckily, quoting The Planetary Society, the rocket failure did not permit the s/c to reach its desired orbit. After this failure, The Planetary Society planned to launch the Cosmos-2, the successor of Cosmos-1. Nonetheless, advancements in solar sailing technology as well as the capability of lower mass slots due to the piggyback launch configuration, led The Planetary Society to change its initial plans. In this way, in November 2009 the design and development of LightSail-1 was announced [54] and consequently, the Cosmos-2 project was not carried out. For further reading about LightSail-1, please see section 3.1.

With respect to Europe, there are several solar sail project unfinished, aborted or failed due to the shortage in funding (e.g. GeoSail, European Solar Sail Demonstrator or Odissee). At present, the European Space Agency (ESA) together with the German Aerospace Center (DRL) has a solar sailing road map called Gossamer and consisting of the successive development of three s/c (see [8]). Gossamer-1 will try to demonstrate the deployment of a 5m x 5m sail with lenticular carbon fiber booms developed by DLR. Later, in 2015 Gossamer-2 will attempt to deploy a 20m x 20m solar sail at 500km. Finally, the Gossamer-3 is planned to deploy a 50m x 50m sail in Medium-Earth Orbit (MEO) in 2018 with the purpose of escaping from the Earth.

To date, only two solar sails have been successfully launched and space tested: IKAROS-1 and NanoSail-D2. Nonetheless, the research effort on solar sailing has increased significantly over the recent years. A good proof of that are the International Symposiums of Solar Sailing (ISSS), which aim to share solar sailing know-how and technology: ISSS 2007 [55], ISSS 2010 [56] and ISSS 2013 [57]. As well, most of the solar sailing projects under way are carried out through nanosatellites, due to the lower budget required.

3.1. SOLAR SAILING AND NANOSATELLITES

In order to enhance the feasibility of the solar sailing missions, the Technology Readiness Level (TRL) must be increased. One possible solution is the use of simpler missions (e.g. nanosatellite based missions) that will space-test the

critical and risky subsystems of sail deployment and attitude control, thus enabling researchers to increase the knowledge of solar sailing.

In the following, some of the most important solar sailing nanosatellite missions are presented. Note that the BMSTU solar sail being developed by Bauman Moscow State Technical University is not here included due to lack of information.

- **NanoSail-D & NanoSail-D2.** As stated in [7], in order to capitalize investments done in the In-Space Propulsion Technology Program, NASA Marshall Space Flight Center founded the NanoSail-D at the beginning of 2008, aiming at the design of a subscale solar sail system designed for possible small s/c applications (see Figure 5 Left). The primary objectives were the successfully stow and deploy of the sail as well as the demonstration of de-orbiting functionality. NanoSail-D was a 3U size CubeSat class spacecraft, from which the upper 1/3 (1U) was occupied by the bus. Consequently, 2/3 (2U) of the volume corresponded to the furled sails and booms. Note that the size "1U" means "1 Unit" and it is the basic CubeSat standard 10cm x 10cm x 10cm. Hence, the size "2U" corresponds to 20cm x 10cm x 10cm and "3U" to 30cm x 10cm x 10cm. The s/c closeout panels protected the sail and booms during the launch phase and possessed spring-loaded hinges that were released on orbit, as shown in Figure 5 (Right). The sail is a four-quadrant solar sail of $10m^2$. The sail membranes were made of aluminum-coated CP1^{TM}, which was originally utilized in the aforementioned NASA's large solar sail ground demonstration project. For the launch phase, the sail membrane was z-folded and rolled onto a sail spool. The four Triangular Retractable and Collapsible (TRAC) booms used were also rolled onto the spool. These booms, which were developed by the Air Force Research Labs (AFRL), were made of Elgiloy® steel. The NanoSail-D project lasted six months from desk to launch. According to what stated in [58], the building and testing of the s/c cost about $250,000. The reader is referred to [9]–[11].

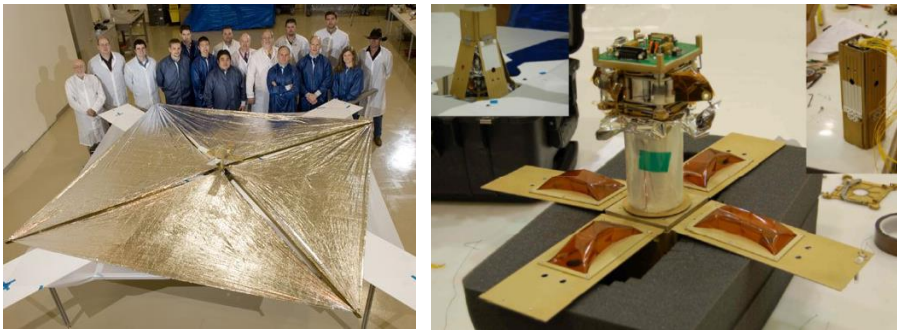

Figure 5. Huntsville-based NanoSail-D team standing with the fully unfurled (Left) and with the stowed configuration of the NanoSail-D (Right) (source [59] and [10]).

The NanoSail-D was launched on August 3, 2008 on board a Falcon 1 rocket. Unfortunately, due to a malfunction of the rocket during the stage separation, NanoSail-D had little chance to achieve its desired orbit. So, the team decided to fly the NanoSail-D ground spare, called NanoSail-D2, improved during the two years after following the NanoSail-D failure. The satellite was launched on a Minotaur IV rocket in November 2010. After 240 days in orbit, the NanoSail-D2 re-entered the atmosphere on September 17, 2011 becoming the second solar sail that flew in space.

- **LightSail-1.** LightSail is a program developed by The Planetary Society, a global non-profit organization ([60]). Indeed, as stated in [12], LightSail-1 is the first of three s/c of the program and its main objectives are to measure the thrust and to demonstrate controlled solar sail flight in order to develop solar sail-related key technologies: sail deployment, sail material management during flight, gossamer structure dynamics and navigation and tracking. The LightSail-1 will be launched through Cal Poly's Poly-PicoSatellite Orbital Deployer (P-POD) and shall orbit above 800km of altitude. Note that the design is based on a 3U CubeSat, whose weight is less than 5kg. From this CubeSat, four TRAC booms are deployed in order to achieve a $32m^2$ of square 3-axis stabilized sail. These TRAC booms, which are made of Elgiloy® steel, have been developed by the AFRL and used before in the NanoSail-D and –D2. As well, the sail is made of aluminized Mylar™ of 4.5microns. The packed volume of the solar sail considering the sail itself, the four 4m x 4m TRAC booms and the deployment mechanism is 2U. As described in [61], Stellar Exploration Inc. of San Louis Obispo is the systems integrator for LightSail-1, whose budget is estimated in $2.2 million.
- **CubeSail.** As indicated in [13] and [62], CubeSail is a 3U s/c being developed by Surrey Space Center with the industrial partnership of Astrium and Surrey Satellite Technology Ltd. A key feature of the mission is the deployment of a $25m^2$ four-quadrant solar sail in order to demonstrate the propulsive characteristics of the sail as well as the de-orbiting capabilities during a year of period. The sail is supported through four 3.6m long four booms, made from two Copper-Beryllium tape springs forming a lenticular cross-section and encased in a Kapton® sheath. This enables to obtain a simple, robust and ultra-light boom structure of less than 2kg (note that the s/c mass is 3kg). The sail membrane is made of aluminized Kapton® and it is fit around a 15-16mm long spindle. The satellite bus volume is approximately 1U and the remaining 2U are used to house the two axis translation stage and sail-deployment subsystem.
- **CU Aerospace's CubeSail.** As stated in [14]-[15], the University of Illinois together with the company CU Aerospace is designing a mission, whose

objective is to demonstrate the deployment and measure the thrust given by a 20m^2 membrane. The sail will be a rectangular 250m x 77mm x 6.2µm of aluminized double coated Mylar™. Two 1.5U CubeSats that will separate from each other in orbit will be used to carry the sail. Therefore, equal lengths of the membrane will be rolled onto two motorized reels (exactly, 125m of membrane in each CubeSat). This mission is the precursor towards a sail concept called UltraSail, which is based on multiple structures similar to CubeSail that would extend kilometers long film blades to finally form a heliogyro. According to [63], the initial cost of CubeSail is estimated in $600,000.

In Table 1 the available main characteristic of the aforementioned nanosatellites and corresponding solar sails are summarized. Note that $\mathrm{a_c}$ is expressed in units of g, the gravitational acceleration at the Earth's surface ($\mathrm{g} = 9.81\mathrm{m/s^2}$).

	NanoSail-D & NanoSail D-2	**LightSail-1**	**CubeSail (Europe)**	**CubeSail (US)**
Developer	Marshall Space Flight Center (NASA)	The Planetary Society	Surrey Space Centre, Astrium, Surrey Satellite Technology Ltd.	CU Aerospace and Illinois University
Type of Sail	Four-quadrant	Four-quadrant	Four-quadrant	Rectangular
$\mathbf{A}\ [\mathbf{m^2}]$	10	32	25	20
Weight of s/c $[\mathbf{kg}]$	3.86 (8.5 pound)	4.54	3	1.5 (each CubeSat)
$\mathbf{a_c}$	$2 \cdot 10^{-6}\mathrm{g}$ ([16])	$6.3 \cdot 10^{-6}\mathrm{g}$ ([16])	--	--
Booms	4 Elgiloy® TRAC booms	4 Elgiloy® TRAC booms	4 lenticular booms	No booms
Membrane material	3µm thick Al-coated CP1™	4.5µm thick Al coated Mylar™	Aluminized Kapton®	6.2µm thick Al coated Mylar™
Packed volume	2U	2U	2U	0.5U (each CubeSat)
Space tested [Y/N]	NanoSail-D: No NanoSail-D2: Yes	No	No	No
Cost	$250,000	$2.2million (estimated)	--	$600,000

Table 1. Main characteristics of some nanosatellites and their solar sails.

4. MISSION ANALYSIS

To date, NanoSail-D2 has demonstrated the feasibility of solar sails as propulsion system for nanosatellites. Moreover, other missions of the same nature are very close to be launched such as LightSail-1 and CubeSail (Europe). Hence, the focus of the research community is now pointing to missions beyond Low Earth Orbit including interplanetary missions. Indeed, Interplanetary CubeSats were selected by the NASA Innovative Advanced Concepts (NIAC) program in 2011 for further investigation.

After analyzing the state of the art of different nanosatellite interplanetary missions aimed to be propelled by solar sails (e.g. polar-sitters or CubeSats performing highly Non-Keplerian Orbits), the Radio Quiet Lunar Cubesat (RAQL) has been selected. Among all the interplanetary missions, RAQL represents the least technological leap from the current space-flown nanosatellite solar sail technology. So, this work continues the trend from CubeSat community, providing a feasible solar sail module design to the proposal made during the First Interplanetary CubeSat Workshop held at Massachusetts Institute of Technology in May 2012 ([17]), where RAQL mission was firstly presented and discussed.

The RAQL is an astrophysics mission whose main objective is to assess radio quiet volume shielded zone behind the Moon for future redshifted 21cm cosmology missions. Note that the usable volume behind the Moon for high sensitivity 21cm cosmology observations determines the utility of the lunar surface versus the orbiting missions. For this mission, [17] and [18] proposed the use of a 6U ($10\text{cm} \times 20\text{cm} \times 30\text{cm}$) nanosatellite, with the same size to the one shown in Figure 6. The distribution of this 6U s/c should be: 1U for s/c housekeeping, 2U for solar sail propulsion system, 1U for telecommunications and 2U for payload.

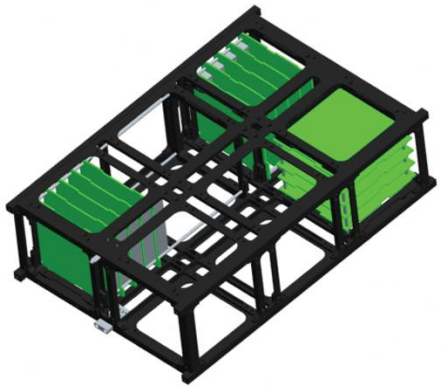

Figure 6. Illustration of the structure of a characteristic 6U satellite (source [64]).

Additionally, in order to reach the desired lunar orbit, the RAQL mission departs from GEO and uses the solar sail to follow a spiral to Earth escape. Then, the s/c should perform a flyby loose capture into Highly Elliptical Orbit at Moon in order to map its surface. The entire mission is constrained to cost less than $30M and last up to 5 years.

The RAQL is designed to be propelled only by a solar sail. Thereby, the Solar Sail Module (SSM) is one of the most critical parts of the entire mission. Following, the systems engineering for the solar sail module for RAQL mission is presented. Then, in Chapter 5 the RAQL mission trajectory analysis is performed. In this analysis, in order to assess the feasibility of the SSM design, only the spiral phase from GEO to Earth scape is considered. Later, in Chapter 6 the design of the SSM proposed to fulfill the requirements of the RAQL mission is presented.

4.1. SSM SYSTEMS ENGINEERING

4.1.1. SSM OBJECTIVES

Primary objectives

- To thrust and guide a 6U nanosatellite from GEO to the lunar target orbit.

Secondary objectives

- To advance and enhance solar sailing technology for nanosatellites.
- To contribute to the development of Commercial-Off-The-Shelf Plug and Play propulsion systems for CubeSats.

The RAQL mission is still in a conceptual phase and hence, the final lunar orbit is not specified yet. Nonetheless, by proving that the SSM is able to drive the satellite from GEO to Earth escape is enough to demonstrate its capability to reach any lunar orbit.

4.1.2. SSM DRIVERS

Parameter	Mission performance issues	Design impact
Volume	Flight time	The SSM volume limits directly the size of the sail and hence the thrust provided to the s/c. Increasing the volume leads to more thrust, but adds weight and reduces the space for payload and other subsystems.

Boom length	Flight time	Increasing the booms length allows for a bigger sail but increases weight, volume and loading level (bending moment).
Sail area	Flight time	A bigger sail provides more thrust and hence reduces the flight time. Nevertheless, it is heavier, occupies more volume and increases the loads hold by the booms.

Table 2. Solar Sail Module drivers.

In this case, the departure orbit is not a mission driver because it is already fixed by the mission statement. However, it has a big influence on the flight time and energy budget. For instance, departing from a LEO orbit implies presence of drag force, hence requiring stronger booms, which are heavier and bulkier. On the other side, by departing from higher altitudes, the booms can be less stiff and the orbital energy (Δv needed) and flight time are lower.

4.1.3. SSM REQUIREMENTS

Top-level requirements

- The Solar Sail Module shall be capable of propelling a 6U nanosatellite from GEO to the lunar target orbit.
- The SSM cost shall not exceed 1M$.
- The SSM shall give preference to space-tested technology and Commercial-Off-The-Shelf components.

Critical requirements

- The SSM shall be fitted into a 2U volume ($20\text{cm} \times 10\text{cm} \times 10\text{cm}$).
- The SSM shall not exceed 2kg mass.

Functional requirements

- The SSM shall be designed according to CubeSat standard ([19]) and deployer requirements ([20]).
- The SSM shall be able to be attached to the rest of the 6U nanosatellite.
- The SSM dimensions shall adapt to 6U CubeSat lateral panels.
- The SSM structure shall be self-sustainable and independent.
- The SSM shall be able to deploy completely the solar sail quadrants and booms.

- The SSM primary structure material shall have a similar expansion coefficient to that of Aluminum 7075-T73.
- The SSM shall use hard anodized rails to prevent cold-welding.
- The SSM shall be able to withstand the outer Van Allen radiation belt.

Performance requirements

- The SSM shall be able to propel the nanosatellite to the desired lunar orbit in less than 4 years.
- The Solar Sail Module shall be operative for at least 5 years.
- The solar sail module shall contain a sail area of at least $40\mathrm{m}^2$.
- The SSM shall have vertical columns of at least $8.5\mathrm{mm}\ \mathrm{x}\ 8.5\mathrm{mm}$ cross-section.
- The SSM shall have smooth rails and rounded edges to a minimum radius of $1\mathrm{mm}$.

Most of the functional and performance requirements are determined by the CubeSats standards ([19]) and deployer requirements ([20]). Furthermore, in order to reduce cost and increase the reliability COTS components and flight-proven technology is desired. This fact has a big impact on the design philosophy because it constraints the availability of the engineering solutions. Finally, due to departing from GEO, the SSM will stay a relatively short time exposed to the outer Van Allen belt. Thereby, this exposure to the radiation is not a strong limitation.

4.1.4. SSM CONSTRAINTS

- Occupying a maximum volume of 2U ($20\mathrm{cm}\ \mathrm{x}\ 10\mathrm{cm}\ \mathrm{x}\ 10\mathrm{cm}$).
- Not exceeding a total mass of 2kg.
- Have smooth rails and rounded edges to a minimum radius of $1\mathrm{mm}$.
- Use of hard anodized rails to prevent cold-welding.
- Have at least 75% of the flat rail contact with the deployer.
- Have constrained deployables by the SSM.
- No use of pyrotechnics.
- Deploy the booms and sail quadrants at least 30 minutes after launching.

The most important constraints, the SSM mass and volume, are already determined by the RAQL mission. In this way, these two constraints limit the achievable maximum solar sail area and hence, the maximum thrust. Furthermore, the SSM is constrained to the CubeSat standards adapted for the case of 6U nanosatellite. However, following the CubeSats standards is a great advantage for the availability of COTS components, community knowledge and flight experience heritage.

4.1.5. SSM TRADE-OFFS

- **Solar sail packed volume vs. stowed booms volume.** The SSM is restricted to be fitted into a 2U volume. However the distribution of this volume can be done in several ways: a) giving priority to the maximum sail packed volume or b) giving more volume for stowed booms. In most of the cases, the factor that limits the maximum achievable sail area is the stowed booms volume. Then, in order to maximize the sail area it is necessary to give the booms the most space as possible. However, the shape of the available volume for the stowed booms plays a significant role in the maximum booms length. It should be pointed out that the deployment and stowage mechanism of the booms has a set of minimum dimensions, hence limiting the possible design solutions. Then, the portion of volume dedicated to sail and booms must be carefully balanced.
- **Maximum booms length vs. SSM mass.** Depending on the booms material, if the sail thickness is around $5\mu m$ (like current solar sails for nanosatellites), it is very likely to happen that the booms weigh significantly more than the sail. Then, not only the volume represents a constraint but the mass can play an important role in the final sizing process. This way, the longer the booms are the bigger the sail area becomes. Nevertheless, the $2kg$ mass constraint can effectively limit the booms length even though the available volume would allow for longer booms.

5. MISSION TRAJECTORY ANALYSIS

This chapter presents the trajectory analysis of the satellite propelled by the solar sail. This study is focused on a trajectory from initial GEO parking orbit to Earth escape. As it has been aforementioned in the scope, modeling of complex maneuvers such as planet targeting or planet capture is not considered in this project. Moreover, although the main aim of this project is to design the Solar Sail Module (SSM), the mission trajectory analysis is a fundamental step in order to verify the feasibility of the final design. Indeed, through the formulation, modelling and algorithms presented in this section and implemented in Matlab®, it is assessed if the solar sail area selected is sufficient to arrive to the final desired selenocentric orbit in less than 5 years. Nonetheless, it should be pointed out that the trajectory analysis here presented is not optimized. Further information related with this section is available in the annexes of the projects. Precisely, the coefficients of the RKF 7(8) are enclosed are enclosed in the ANNEX A, whereas the Matlab® code developed is included in the ANNEX B.

In the following, a brief organization of the chapter is presented. First, an introduction of the reference frames as well as the Sun, Moon and satellite positioning system utilized in development of the Matlab® code are presented. Then, the forces affecting the satellite are indicated. The gravitational attractive force, the perturbation forces and the Solar Radiation Pressure (SRP) force are considered. Afterwards, the Matlab® numerical codes as well as the trajectory calculation algorithm developed are briefly described. Finally, in the last section, the simulation results for a s/c mass of $\mathrm{m} = 6\mathrm{kg}$ with sail area of $\mathrm{A} = 50\mathrm{m}^2$ and for $\mathrm{m} = 8\mathrm{kg}$ with sail area of $\mathrm{A} = 50\mathrm{m}^2$ are included.

5.1. REFERENCE FRAMES AND POSITIONING

In order to describe the mission trajectory analysis, the Earth-centered inertial (ECI) coordinate frame referred to J2000.0 is acquired as the main reference frame. As stated in [21], this frame has its origins at the center of mass of the Earth and its fundamental plane is the equatorial. The $\vec{\mathrm{x}}$ axis is considered positive towards the mean vernal equinox point at J2000. Note that the vernal equinox lies at the intersection of the ecliptic and the Earth's equatorial planes. The $\vec{y}$ axis belongs to the mean equatorial plane at J2000, is perpendicular to the $\vec{\mathrm{x}}$ axis and in the sense of the Earth's rotation (eastwards). Finally, the $\vec{\mathrm{z}}$ axis is obtained by the cross product $\vec{\mathrm{x}} \times \vec{\mathrm{y}}$ following the right-hand rule. The resulting orthonormal basis spanning $\mathbb{R}^3$ is shown in Figure 7.

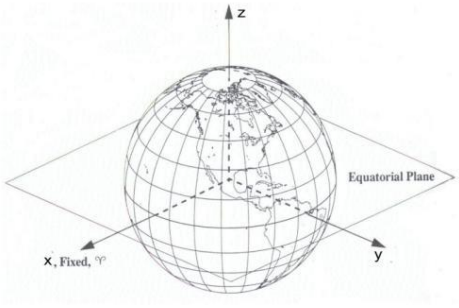

Figure 7. Earth-centered inertial (ECI) reference frame (source [65]).

Note that the ECI reference frame is referred to J2000.0, which means January 1, 2000 at 12:00 Terrestrial Time (TT) and the prefix "J" is used to indicate that it is a Julian epoch. Consequently, due to the use of the Julian epoch as reference, time has been expressed in Julian Date (JD) when calculating the position of Sun and Moon.

5.1.1.SATELLITE POSITION

The velocity and position of the satellite are obtained from the integration of the acceleration of the satellite. Therefore, if the acceleration of the satellite expressed in the ECI coordinate frame is defined as $\vec{a}(x,y,z) = [a_x, a_y, a_z]$ in m/s^2, the velocity and the position are given by:

$$\vec{v}(x,y,z) = [v_x, v_y, v_z] = \left[\int a_x dt + C_{v\_x}, \int a_y dt + C_{v\_y}, \int a_z dt + C_{v\_z}\right] \quad [m/s] \tag{5.1}$$

$$\vec{r}(x,y,z) = [r_x, r_y, r_z] = \left[\int v_x dt + C_{r\_x}, \int v_y dt + C_{r\_y}, \int v_z dt + C_{r\_z}\right] \quad [m] \tag{5.2}$$

Furthermore, apart from the ECI coordinate frame and in order to ease calculation, NTW satellite coordinate system has also been defined following [22], with the origin of NTW is defined in the satellite's center of mass, the $\vec{T}$ axis lies in the orbital plane and parallel to the velocity vector, the $\vec{W}$ axis is normal to the orbital plane and parallel to the orbital angular momentum vector $\vec{L}$ and the axis $\vec{N}$ completes the right-handed triad. In other words:

$$\hat{T} = \frac{\vec{v}(x,y,z)}{\|\vec{v}(x,y,z)\|} \tag{5.3}$$

$$\hat{W} = \hat{L} = \frac{\vec{r} \times \vec{v}}{\|\vec{r} \times \vec{v}\|} \tag{5.4}$$

$$\hat{N} = \hat{T} \times \hat{W}. \tag{5.5}$$

A vector defined in NTW coordinate system can be expressed in ECI reference through the transformation:

$$\begin{bmatrix} x \\ y \\ z \end{bmatrix}_{ECI} = \begin{bmatrix} N_x & T_x & W_x \\ N_y & T_y & W_y \\ N_z & T_z & W_z \end{bmatrix} \begin{bmatrix} x \\ y \\ z \end{bmatrix}_{NTW}. \tag{5.6}$$

5.1.2. POSITION OF THE SUN

The position of the Sun in ECI reference frame is calculated introducing the value JD in the Matlab® code developed. For that, first following the formulation given by [21], the parameter of time $T_\odot$ is calculated as:

$$T_\odot = \frac{JD - 2451545}{36525} \tag{5.7}$$

Then, the mean longitude of the Sun corrected for the aberration of light $L_\odot$, the mean anomaly $M_\odot$ are given by and the longitude $\lambda_\odot$ and the obliquity of the ecliptic plane $\epsilon_\odot$ are given by:

$$L_\odot = 280^o.460 + 36000^o.770T_\odot \ [\text{degrees}] \tag{5.8}$$

$$M_\odot = 357^o.528 + 35999^o.050T_\odot \ [\text{degrees}] \tag{5.9}$$

$$\lambda_\odot = L_\odot + 1^o.915 \sin M_\odot + 0^o.020 \sin 2M_\odot \ [\text{degrees}] \tag{5.10}$$

$$\epsilon_\odot = 23^o.4393 - 0^o.01300T_\odot \ [\text{degrees}] \tag{5.11}$$

Note that the longitude and the obliquity of the reference plane are utilized in ecliptic coordinate system. So, in order to relate ecliptic coordinate frame with equatorial coordinate frame trigonometry and rotations can be used as described in [23] obtaining:

$$\begin{gathered} \cos\alpha_{ra}\cos\delta = \cos\beta\cos\lambda \\ \sin\alpha_{ra}\cos\delta = \cos\epsilon\cos\beta\sin\lambda - \sin\epsilon\sin\beta \\ \sin\delta = \sin\epsilon\cos\beta\sin\lambda + \cos\epsilon\sin\beta \end{gathered} \tag{5.12}$$

where α_{ra} is the right ascension, δ is the declination and β is the ecliptic latitude. Particularizing for the case of Sun and taking into account that due to being in the ecliptic plane, $\beta_\odot$ is approximately $\beta_\odot = 0$, expression (5.12) yields:

$$\alpha_\odot = \tan^{-1}\left(\cos\epsilon_\odot \tan\lambda_\odot\right) \quad [\text{rad}] \tag{5.13}$$

$$\delta_\odot = \sin^{-1}\left(\sin\epsilon_\odot \sin\lambda_\odot\right) \ [\text{rad}]. \tag{5.14}$$

Then, the Earth-Sun distance expressed AU and following [21] is given by:

$$r_{\odot} = 1 - 0.017 \cos M_{\odot} \ \ [\mathrm{AU}]. \tag{5.15}$$

Finally, the position of the Sun in ECI reference frame is given by:

$$\vec{r}_{\mathrm{sun}} = (1 - 0.017 \cos M_{\odot}) 1.49597870 \cdot 10^{11} \begin{bmatrix} \cos \delta_{\odot} \cos \alpha_{\odot} \\ \cos \delta_{\odot} \sin \alpha_{\odot} \\ \sin \delta_{\odot} \end{bmatrix} [\mathrm{m}]. \tag{5.16}$$

5.1.3. POSITION OF THE MOON

The position of the Moon in ECI reference frame is also calculated introducing the value JD in the Matlab® code developed. For that, first following the formulation given by [21], the parameter of time $d_{\leftmoon}$ is calculated as:

$$d_{\leftmoon} = \mathrm{JD} - 2454465.5 \tag{5.17}$$

The mean longitude of Moon $L_{\leftmoon}$, the mean anomaly $M_{\leftmoon}$, the mean longitude of ascending node $\Omega_{\leftmoon}$ and the mean elongation with respect to Sun $D_{\leftmoon}$ are given by:

$$L_{\leftmoon} = 179^{\mathrm{o}}.992337 + 13^{\mathrm{o}}.17639646 d_{\leftmoon} \ [\ \mathrm{degrees}] \tag{5.18}$$

$$M_{\leftmoon} = 131^{\mathrm{o}}.284857 + 13^{\mathrm{o}}.06492298 d_{\leftmoon} \ [\ \mathrm{degrees}] \tag{5.19}$$

$$\Omega_{\leftmoon} = 330^{\mathrm{o}}.393027 - 0^{\mathrm{o}}.05295375 d_{\leftmoon} \ [\ \mathrm{degrees}] \tag{5.20}$$

$$D_{\leftmoon} = 260^{\mathrm{o}}.942409 + 12^{\mathrm{o}}.19074910 d_{\leftmoon} \ [\ \mathrm{degrees}]. \tag{5.21}$$

True ecliptic longitude, $\lambda_{\leftmoon}$ and the true ecliptic latitude, $\beta_{\leftmoon}$ are calculated as:

$$\begin{aligned} \lambda_{\leftmoon} = \left(L_{\leftmoon} - 360 \cdot \mathrm{integer}\left(\frac{L_{\leftmoon}}{360}\right)\right) 60' + 377' \sin M_{\leftmoon} + 76' \sin\left(2D_{\leftmoon} - M_{\leftmoon}\right) \\ + 40' \sin\left(2D_{\leftmoon}\right) + 13' \sin\left(2M_{\leftmoon}\right) \quad [\mathrm{minutes}] \end{aligned} \tag{5.22}$$

$$\beta_{\leftmoon} = 309' \sin\left(\lambda_{\leftmoon} \frac{1}{60} - \Omega_{\leftmoon}\right) \ [\mathrm{minutes}]. \tag{5.23}$$

Note that in case of $\lambda_{\leftmoon}$, in equation (5.21) is given in minutes. Thereby, in order to use it in the equation (5.23) it is expressed in degrees dividing it by 60. Furthermore, in this case the obliquity of the ecliptic plane for the position of the Moon $\epsilon_{\leftmoon}$ is given by expression (5.11), where $T_{\leftmoon}$ is found from equation (5.7). In order to find the right ascension $\alpha_{\leftmoon}$ and declination $\delta_{\leftmoon}$ for the Moon, $\lambda_{\leftmoon}, \beta_{\leftmoon}$ and $\epsilon_{\leftmoon}$ are substituted into expression (5.12).

Moreover, as described in [21], the equatorial horizontal parallax $\pi_{\leftmoon}$ is calculated from:

$$\pi_{\leftmoon} = 57'.0 + 3' \cos \mathrm{M}_{\leftmoon} \ [\mathrm{minutes}] \tag{5.24}$$

. Once $\pi_{\leftmoon}$ is calculated, the geocentric distance $\mathrm{r}_{\leftmoon}$ is given by:

$$\mathrm{r}_{\leftmoon} = \frac{\mathrm{R}_{\oplus}}{sin\left(\frac{\pi_{\leftmoon}}{60}\right)} \ [\mathrm{m}] \tag{5.25}$$

where $\mathrm{R}_{\oplus}$ is the equatorial radius of Earth and equal to $\mathrm{R}_{\oplus} = 6378.14 \cdot 10^4 \mathrm{m}$. Finally, the position of the Moon is expressed as:

$$\vec{\mathrm{r}}_{\mathrm{moon}} = \mathrm{r}_{\leftmoon} \begin{bmatrix} \cos \delta_{\leftmoon} \cos \alpha_{\leftmoon} \\ \cos \delta_{\leftmoon} \sin \alpha_{\leftmoon} \\ \sin \delta_{\leftmoon} \end{bmatrix} \ [\mathrm{m}]. \tag{5.26}$$

5.2. FORCES ACTING ON THE SATELLITE

From the orbital mechanics viewpoint, the performance of a general solar sail can be measured by thrust, drag and stability/control. The purpose of this project is not to optimize the trajectory of the satellite propelled by the solar sail. Therefore, the stability/control of the solar sail is not deeply developed, although a basic steering law has been implemented. Besides, due to departing from a GEO altitude, the influence of Earth's atmospheric drag on the solar sail trajectory is negligible. As a result, the performance of the satellite is going to be mainly influenced by the thrust given by the solar sail. Note that this thrust is a consequence of the Solar Radiation Pressure (SRP) force, which is broadly explained in section 5.2.2. So, the following hypotheses are assumed for this trajectory study:

- The solar sail is a flat plate.
- The sun is a point mass and a point light source.
- The motion of the satellite is only due to the gravitational forces of Earth, Moon and Sun and Solar Radiation Pressure (SRP).
- The attitude of the solar sail can be changed instantaneously.

Note that the attitude control and an optimum control algorithm are out of the scope of the project. Hence, the last assumption has been considered towards simplifying the solar sail steering law as it is done in [1].

Following the hypothesis stated in the third assumption, in this project, orbital mechanics, Newton's Law of Gravitation and SRP have been combined developing a dynamical model of four-body problem with thrust. The four bodies

considered are the satellite, the Earth, the Sun and the Moon. Hence, the acceleration of the satellite expressed in the ECI reference coordinate frame is:

$$\vec{a} = -\frac{\mu_{\oplus}}{\|\vec{r}\|^3}\vec{r} + \vec{a}_{\text{pert}} + \vec{a}_{\text{SRP}} \quad [\text{m/s}^2] \tag{5.27}$$

where $\mu_{\oplus}$ is the gravitational parameter of Earth and equal to $\mu_{\oplus} = 3.98600448 \cdot 10^{14}\ \text{m}^3/\text{s}^2$, $\vec{r}$ is the position vector of the satellite in ECI coordinate frame given by (5.2), $\vec{a}_{\text{pert}}$ is the contribution of all the perturbations to the satellite acceleration expressed in $[\text{m/s}^2]$ and $\vec{a}_{\text{SRP}}$ is the satellite acceleration due to the SRP. Section 5.2.1 contains a description of how $\vec{a}_{\text{pert}}$ is calculated. Analogously, in section 5.2.2 the assumptions and procedure followed to obtain $\vec{a}_{\text{SRP}}$ are presented.

5.2.1. PERTURBATION FORCES

Since SRP is the source to propel the solar sail of the satellite, it is not considered as a perturbation force. Indeed, in the trajectory analysis three main perturbation forces are considered: Sun-gravity $\vec{a}_{\odot\text{pert}}$, Moon-gravity $\vec{a}_{\mathbb{C}\text{pert}}$ and second potential harmonic J_2 of the gravitational potential of the Earth $\vec{a}_{\text{J2}\oplus\text{pert}}$. So, the term $\vec{a}_{\text{pert}}$ of equation (5.27) can be discomposed into:

$$\vec{a}_{\text{pert}} = \vec{a}_{\odot\text{pert}} + \vec{a}_{\mathbb{C}\text{pert}} + \vec{a}_{\text{J2}\oplus\text{pert}} \quad [\text{m/s}^2]. \tag{5.28}$$

Hereunder, the three kinds of perturbations are described. Note that the perturbation due to the second zonal harmonic of J_2 of the gravitational potential of the Moon is not considered. As stated in [24], the perturbation acceleration due to this term is approximately equal to 10^{-4} at an altitude of 1000km from the lunar surface and $9 \cdot 10^{-6}$ at $10{,}000\text{km}$ altitude. Thereby, bearing in mind that over the major portion of the trajectory the satellite's distance from the lunar surface is larger than $10{,}000\text{km}$, it is reasonable to neglect this perturbation effect in this preliminary trajectory analysis. However, for the final low lunar orbit, the perturbations due to this harmonic term should be taken into account together with the effects generated by the mass concentrations (e.g. mascons).

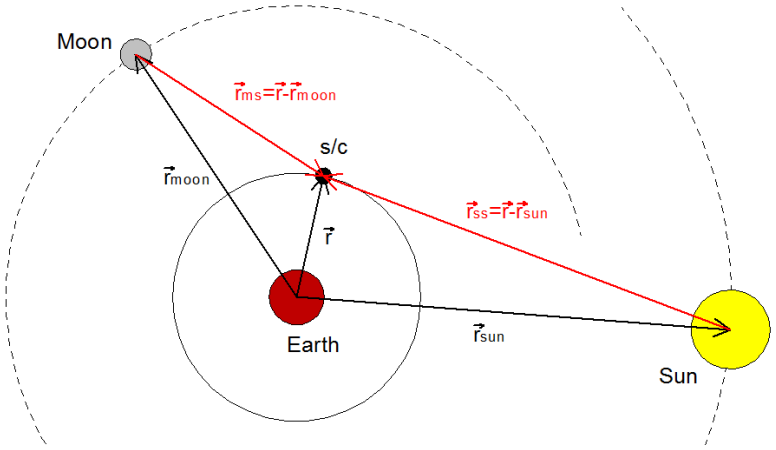

Figure 8. Scheme of the Moon, Sun and s/c position vectors used in the ECI coordinate frame (drawing not scaled).

- **Perturbation $\vec{a}_{\odot pert}$ induced by Sun's gravity.** This perturbation has two contributions when expressed in the ECI coordinate frame. Precisely, it is equal to:

$$\vec{a}_{\odot pert} = -\frac{\mu_{\odot}}{\|\vec{r}_{ss}\|^3}\vec{r}_{ss} - \frac{\mu_{\odot}}{\|\vec{r}_{sun}\|^3}\vec{r}_{sun} \quad [m/s^2] \tag{5.29}$$

where $\mu_{\odot}$ is the gravitational parameter of Sun equal to $\mu_{\odot} = 1.327124 \cdot 10^{20} m^3/s^2$, $\vec{r}_{sun}$ is the position of the Sun in the ECI coordinate frame given by equation (5.16) and $\vec{r}_{ss}$ is the vector from the Sun to satellite. As indicated in Figure 8, $\vec{r}_{ss}$ can be written as:

$$\vec{r}_{ss} = \vec{r} - \vec{r}_{sun} \quad [m] \tag{5.30}$$

where $\vec{r}$ is the position of the satellite given by (5.2) and $\vec{r}_{sun}$ is obtained with (5.16).

- **Perturbation $\vec{a}_{\leftmoon pert}$ induced by the Moon's gravity.** This perturbation has two contributions when expressed in the ECI coordinate frame:

$$\vec{a}_{\leftmoon pert} = -\frac{\mu_{\leftmoon}}{\|\vec{r}_{ms}\|^3}\vec{r}_{ms} - \frac{\mu_{\leftmoon}}{\|\vec{r}_{moom}\|^3}\vec{r}_{moon} \quad [m/s^2] \tag{5.31}$$

where $\mu_{\leftmoon}$ is the gravitational parameter of Moon equal to $\mu_{\leftmoon} = 4.902799 \cdot 10^{12} m^3/s^2$, $\vec{r}_{moon}$ is the position of Moon in the ECI coordinate frame as given by equation (5.26) and $\vec{r}_{ms}$ is the Moon-to-satellite vector As indicated in Figure 8,

$$\vec{r}_{ms} = \vec{r} - \vec{r}_{moon} \quad [m], \tag{5.32}$$

where $\vec{r}$ is the position of the satellite given by (5.2) and $\vec{r}_{moon}$ is found by equation (5.26).

- **Perturbation $\vec{a}_{J2\oplus pert}$ due to the J_2 spherical harmonics term of the Earth's gravitational potential.** Following the formulation of [25], the perturbation due to J_2 of the Earth expressed in the spherical ECI coordinate system is:

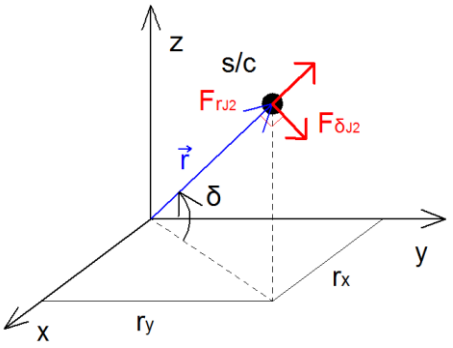

Figure 9. Perturbations due to J_2 of the Earth expressed in the spherical ECI coordinate frame.

$$\left\|\overrightarrow{F_{r_{J2}}}\right\| = \frac{\mu_\oplus}{\|\vec{r}\|^4} J_2 R_\oplus{}^2 \left(3\sin^2\delta - 1\right) \ [N] \tag{5.33}$$

$$\left\|\overrightarrow{F_{\delta_{J2}}}\right\| = \frac{\mu_\oplus}{\|\vec{r}\|^4} J_2 R_\oplus{}^2 \sin(2\delta) \ [N] \tag{5.34}$$

where J_2 is the second zonal harmonic J_2 of the gravitational potential of the Earth equal to $J_2 = 0.001082626$ and δ is the declination defined in equation (5.12). In case of the s/c, in order to calculate δ Figure 10 (Left) and (Right) yields:

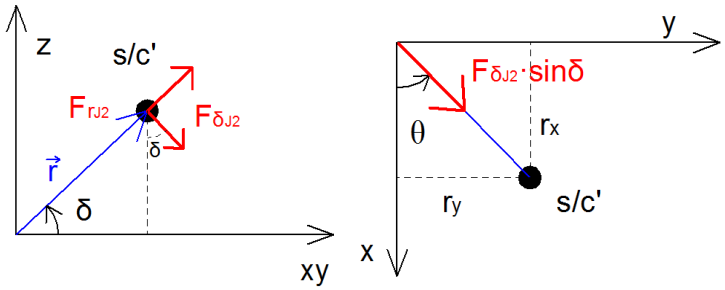

Figure 10. Some vertical (Left) and horizontal (Right) projections.

$$\delta = \tan^{-1}\left(\frac{\mathrm{abs}(r_z)}{\sqrt{r_x^2 + r_y^2}}\right) \ [rad] \tag{5.35}$$

where r_x, r_y and r_z are the components of the vector $\vec{r}$ defined in (5.2). Furthermore, as illustrated in Figure 9 that the contribution due to $\overrightarrow{F_{r_{J2}}}$ can be easily expressed in Cartesian ECI coordinate frame as:

$$\overrightarrow{F_{r_{J_2}}}(x,y,z) = \left\|\overrightarrow{F_{r_{J_2}}}\right\| \frac{\vec{r}}{\|\vec{r}\|} \quad [N] \tag{5.36}$$

where $\left\|\overrightarrow{F_{r\_J2}}\right\|$ is the modulus given by expression (5.33). In case of the contribution due to $\overrightarrow{F_{\delta_{J_2}}}$, the resulting expression in Cartesian ECI coordinate system is:

$$\overrightarrow{F_{\delta_{J_2}}}(x,y,z) = \left\|\overrightarrow{F_{\delta_{J_2}}}\right\| \left[\sin\delta \frac{r_x}{\sqrt{r_x^2 + r_y^2}} , \sin\delta \frac{r_y}{\sqrt{r_x^2 + r_y^2}} , -\text{sign}(r_z)\cos\delta \right] \quad [N] \tag{5.37}$$

where $\left\|\overrightarrow{F_{\delta_{J_2}}}\right\|$ is given by expression (5.34). Thereby, the value of the perturbation $\vec{a}_{J2\oplus pert}$ is:

$$\vec{a}_{J2\oplus pert} = \frac{\overrightarrow{F_{r_{J_2}}}}{m} + \frac{\overrightarrow{F_{\delta_{J_2}}}}{m} \quad [m/s^2] \tag{5.38}$$

where m is the mass of the satellites in kg.

Summarizing, the expression (5.28) considering (5.29), (5.31) and (5.38) can be rewritten as:

$$\begin{aligned} \vec{a}_{pert} = \vec{a}_{\odot pert} + \vec{a}_{\leftmoon pert} + \vec{a}_{J2\oplus pert} = -\frac{\mu_\odot}{\|\vec{r}_{ss}\|^3}\vec{r}_{ss} - \frac{\mu_\odot}{\|\vec{r}_{sun}\|^3}\vec{r}_{sun} - \\ -\frac{\mu_{\leftmoon}}{\|\vec{r}_{ms}\|^3}\vec{r}_{ms} - \frac{\mu_{\leftmoon}}{\|\vec{r}_{moom}\|^3}\vec{r}_{moon} + \frac{\overrightarrow{F_{r_{J_2}}}}{m} + \frac{\overrightarrow{F_{\delta_{J_2}}}}{m} \quad [m/s^2]. \end{aligned} \tag{5.39}$$

5.2.2. SOLAR RADIATION PRESSURE

Solar Radiation Pressure (SRP) proportioned the acceleration, called $\vec{a}_{SRP}$ in equation (5.27) that thrust the satellite. In order to calculate this acceleration, two possible solar sail models have been considered: ideal solar sail model and Non-Perfectly Reflecting (NPR) solar sail model. On the one hand, the former is the simplest model, but the results given differ from what happens in reality; on the other hand, the latter estimates better the solar sail performance, but it is more sophisticated and the resulting code is more time-consuming. Thereby, after implementing both codes and checking the time required to compile, it is concluded that it is better not to use the NPR in the entire simulation of the trajectory. The simulation time required by NPR model does not compensate the accuracy obtained in the results while the main aim of this chapter is to assure that the solar sail area selected is capable of achieving the desired selenocentric in less than 5 years. Nonetheless, in order to assure a balance on the trade-off

results accuracy vs. simulation time, it has been decided to add an efficiency factor to the ideal solar sail model from equation (2.2) as follows:

$$\vec{F}_{SRP} = \eta_{eff}\vec{F}_{SRP}\big|_{Ideal} = 2\eta_{eff}PA\cos\alpha\cos\alpha\,\hat{n}\ \ [N] \tag{5.40}$$

where η_{eff} is the efficiency factor. This equation represents a pseudo-ideal solar sail model often called η-Perfect Reflection (ηPR). As well, as stated in [26], this model reduces only the magnitude of the SRP force but leaves its direction unaltered (non-ideal reflection but perfect reflection). Consequently, while analyzing the attitude of a solar sail, the NPR sail model must be used. However, in the trajectory analysis here presented and following the discussed in [26], the ηPR model has been constrained to give the same characteristic acceleration modulus than the model NPR (equation (2.21) must be equal to equation (2.5) multiplied by η_{eff}). In this way:

$$\eta_{eff} = \ a_1 + a_2 \tag{5.41}$$

where a_1 is defined in equation (2.15) and a_2 in (2.16). For a highly reflective Aluminum-coated from and back side, references [2] and [26] stated that the expression (2.10) is equal to:

$$\mathcal{P} = \{\rho = 0.88, s = 0.94, \varepsilon_f = \varepsilon_b = 0.05, \mathcal{B}_f = \mathcal{B}_b = 0.79\} \tag{5.42}$$

Thereby, substituting (2.15), (2.16) and (5.42) into (5.41) the efficiency factor for Aluminum coated front and back side sail is:

$$\eta_{eff} = \ a_1 + a_2 = \frac{1}{2}(1+s\rho) + \frac{1}{2}\left[\mathcal{B}_f(1-s)\rho + (1-\rho)\frac{\varepsilon_f\mathcal{B}_f - \varepsilon_b\mathcal{B}_b}{\varepsilon_f + \varepsilon_b}\right] = 0.934456 \tag{5.43}$$

Due to being the sunlight the origin of SRP, the solar sail shall be in the illuminated part of the orbit to be propelled (out of eclipse). As seen from the position of s/c, two kinds of solar eclipses can happen: a) Earth passes between Sun and the s/c and b) Moon passes between Sun and the s/c fully or partially blocking the sunlight. So, $\vec{a}_{SRP}$ must consider the eclipse condition as follows:

$$\vec{a}_{SRP} = \frac{(1-\text{Eclipse})}{m}\vec{F}_{SRP} = 2\frac{(1-\text{Eclipse})}{m}\eta_{eff}PA\cos\alpha\cos\alpha\,\hat{n}\ \ [m/s^2] \tag{5.44}$$

where Eclipse is a parameter to mesure when the satellite is into a solar eclipse and η_{eff} is the efficiency factor equal to (5.43).The parameter Eclipse, explained in section 5.2.2.1, shall be equal to $\text{Eclipse} = 0$ when the satellite is in the illuminated part of the orbit and equal to $\text{Eclipse} = 1$ when the sunlight is blocked by the Earth or the Moon.

Furthermore, in order to slightly control the solar sail and thus, adapt the value of the SRP thrust to perform the desired orbit, three steering laws have been

considered: throttle, brake and coasting. These steering laws, which control the orientation of the sail normal vector $\hat{n}$, are explained in section 5.2.2.2. Lastly, the section 5.2.2.3 describes how to calculate the Δv of the s/c during the trajectory.

5.2.2.1. Eclipse calculation

In the 4 body problem implemented to analyze the trajectory of the satellite, as seen from s/c's position, Earth and Moon can provoke solar eclipses. Considering that the shadow zone is cylindrical and following the formulation presented in [27]:

- **Solar eclipse due to Earth.** It is generated when Earth passes between Sun and the s/c. The eclipse condition is used to determine if the satellite is into eclipse or not. For that, firstly it is necessary to define the angles $\beta_{\oplus \mathrm{eclip}}$ and $\alpha_{\oplus}$ as:

$$\beta_{\oplus \mathrm{eclip}} = \sin^{-1}\left(\frac{R_{\oplus}}{\|\vec{r}\|}\right) \quad [\mathrm{rad}] \tag{5.45}$$

$$\alpha_{\oplus \mathrm{eclip}} = \cos^{-1}(\hat{\rho}_{\mathrm{sun}} \cdot \hat{r}) \quad [\mathrm{rad}] \tag{5.46}$$

  where $\hat{r}$ is the unit vector of the satellite position calculates as $\hat{r} = \frac{\vec{r}}{\|\vec{r}\|}$ and $\hat{\rho}_{\mathrm{sun}}$ is the unit anti-Sun unitary vector given by:

$$\hat{\rho}_{\mathrm{sun}} = -\frac{\vec{r}_{\mathrm{sun}}}{\|\vec{r}_{\mathrm{sun}}\|} \,. \tag{5.47}$$

  Note that $\vec{r}_{\mathrm{sun}}$ is given by equation (5.16). Finally, the eclipse condition is:

$$\begin{aligned} \text{Eclipse condition:} \quad & \alpha_{\oplus \mathrm{eclip}} \leq \beta_{\oplus \mathrm{eclip}} \rightarrow \mathrm{Eclipse} = 1 \\ \text{Out of eclipse if:} \quad & \alpha_{\oplus \mathrm{eclip}} > \beta_{\oplus \mathrm{eclip}} \rightarrow \mathrm{Eclipse} = 0 \end{aligned} \tag{5.48}$$

- **Solar eclipse due to Moon.** It happens when the Moon passes between the Sun and the s/c. These eclipses are less frequent and mainly occurred when the s/c is in the vicinity of the Moon. Firstly, the angles $\beta_{\mathbb{C}}$ and $\alpha_{\mathbb{C}\mathrm{eclip}}$ are defined as:

$$\beta_{\mathbb{C}\mathrm{eclip}} = \sin^{-1}\left(\frac{R_{\mathbb{C}}}{\|\vec{r}_{\mathrm{ms}}\|}\right) \quad [\mathrm{rad}] \tag{5.49}$$

$$\alpha_{\mathbb{C}\mathrm{eclip}} = \cos^{-1}(\hat{\rho}_{\mathrm{sm}} \cdot \hat{r}_{\mathrm{ms}}) \quad [\mathrm{rad}] \tag{5.50}$$

  where $\hat{r}_{\mathrm{ms}}$ is the Moon-to-satellite unit vector calculated as $\hat{r}_{ms} = \frac{\vec{r}_{ms}}{\|\vec{r}_{ms}\|}$ and $\hat{\rho}_{\mathrm{sm}}$ is the Sun-to Moon unit vector given by:

$$\hat{\rho}_{sm} = -\frac{\vec{r}_{moon} - \vec{r}_{sun}}{\|\vec{r}_{moon} - \vec{r}_{sun}\|} \tag{5.51}$$

Finally, the eclipse condition due to Moon is:

$$\begin{aligned} &\text{Eclipse condition:} \quad \alpha_{\mathbb{C}eclip} \leq \beta_{\mathbb{C}eclip} \rightarrow \text{Eclipse} = 1 \\ &\text{Out of eclipse if:} \quad \alpha_{\mathbb{C}eclip} > \beta_{\mathbb{C}eclip} \rightarrow \text{Eclipse} = 0 \end{aligned} \tag{5.52}$$

5.2.2.2. Steering Law

The solar sail steering law is the algorithm of control of the sail thrust direction. Thus, by controlling the thrust direction, the spacecraft trajectory can be guided with the aim of arriving to the desired destiny. As it has been aforementioned in the scope of the project, no optimum control algorithm has been developed in this work, but a basic steering law has been implemented. In this project, three attitude states have been considered: positive thrust (accelerating), brake (decelerating) and coasting (zero thrust).

The steering law controls the trust direction by determining at any time the pitch and yaw angles of the sail normal vector about the NTW reference frame. As it has been explained before, the solar sail thrust goes in the sail's normal direction due to the solar sail has been modelled using the ηPR model. In this way, the pitch (μ) is the angle between the thrust vector and the orbital plane, while the yaw (ψ) is the angle in the orbital plane between the thrust and the spacecraft velocity (that goes in the $\vec{T}$ direction). The pitch and yaw angles and their relationship with the NTW reference are shown in Figure 11.

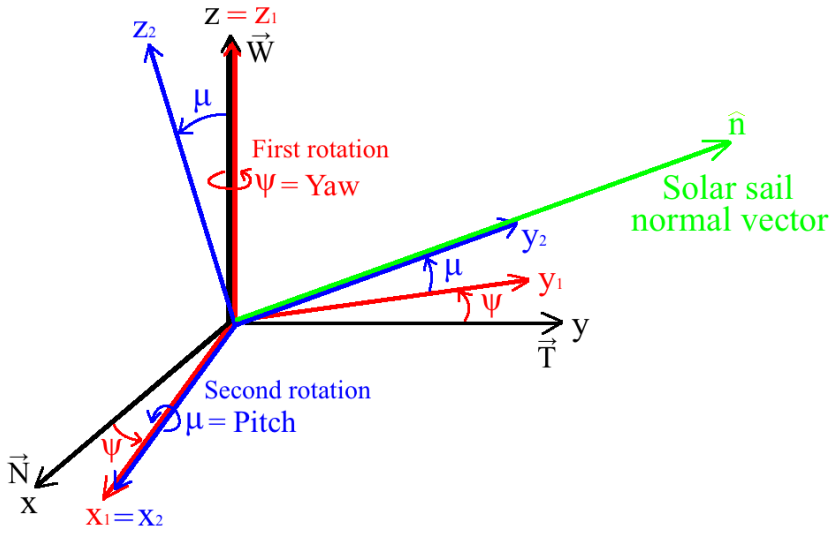

Figure 11. Rotation from solar sail normal vector coordinate to NTW reference frame.

In order to represent the solar sail normal vector with respect the NTW reference frame, it is necessary to perform two rotations: first rotation about z axis ($\vec{W}$) and

second rotation about x_1 axis. In this way, the reference frame 1 ($[x_1 \quad y_1 \quad z_1]$) is obtained from the NTW frame by rotating an angle ψ about z ($\overrightarrow{W}$) axis:

$$\begin{bmatrix} x_1 \\ y_1 \\ z_1 \end{bmatrix} = \Re_z(\psi) \begin{bmatrix} x \\ y \\ z \end{bmatrix}_{NTW} = \begin{bmatrix} \cos\psi & \sin\psi & 0 \\ -\sin\psi & \cos\psi & 0 \\ 0 & 0 & 1 \end{bmatrix} \begin{bmatrix} x \\ y \\ z \end{bmatrix}_{NTW} \tag{5.53}$$

Then, the reference frame 2 ($[x_2 \quad y_2 \quad z_2]$) is obtained from the reference frame 1 by rotating an angle μ about $\mathbf{x_1}$ axis:

$$\begin{bmatrix} x_2 \\ y_2 \\ z_2 \end{bmatrix} = \Re_{x_1}(\mu) \begin{bmatrix} x_1 \\ y_1 \\ z_1 \end{bmatrix} = \begin{bmatrix} 1 & 0 & 0 \\ 0 & \cos\mu & \sin\mu \\ 0 & -\sin\mu & \cos\mu \end{bmatrix} \begin{bmatrix} x_1 \\ y_1 \\ z_1 \end{bmatrix} \tag{5.54}$$

Hence, the reference frame 2 can be obtained from the NTW reference frame by performing the two rotations of (5.53) and (5.54)in chain:

$$\begin{aligned} \begin{bmatrix} x_2 \\ y_2 \\ z_2 \end{bmatrix} &= \Re_{x_1}(\mu) \cdot \Re_z(\psi) \begin{bmatrix} x \\ y \\ z \end{bmatrix}_{NTW} \\ &= \begin{bmatrix} 1 & 0 & 0 \\ 0 & \cos\mu & \sin\mu \\ 0 & -\sin\mu & \cos\mu \end{bmatrix} \begin{bmatrix} \cos\psi & \sin\psi & 0 \\ -\sin\psi & \cos\psi & 0 \\ 0 & 0 & 1 \end{bmatrix} \begin{bmatrix} x \\ y \\ z \end{bmatrix}_{NTW} \end{aligned} \tag{5.55}$$

In this way, the opposite process can be achieved by inverting the rotation matrices. Due to the rotation matrices are orthogonal, their inverse matrix is directly the transposed matrix:

$$\Re_{x_1}(\mu)^{-1} = \Re_{x_1}(\mu)^T; \qquad \Re_z(\psi)^{-1} = \Re_z(\psi)^T; \tag{5.56}$$

Then, the transformation from the reference frame 2, where the sail normal vector is expressed, to the NTW frame is:

$$\begin{bmatrix} x \\ y \\ z \end{bmatrix}_{NTW} = \Re_z(\psi)^T \cdot \Re_{x_1}(\mu)^T \begin{bmatrix} x_2 \\ y_2 \\ z_2 \end{bmatrix} \tag{5.57}$$

Developing the previous expression the final transformation is obtained:

$$\begin{bmatrix} x \\ y \\ z \end{bmatrix}_{NTW} = \begin{bmatrix} \cos\psi & -\sin\psi & 0 \\ \sin\psi & \cos\psi & 0 \\ 0 & 0 & 1 \end{bmatrix} \cdot \begin{bmatrix} 1 & 0 & 0 \\ 0 & \cos\mu & -\sin\mu \\ 0 & \sin\mu & \cos\mu \end{bmatrix} \begin{bmatrix} x_2 \\ y_2 \\ z_2 \end{bmatrix} \tag{5.58}$$

So, recalling equation (5.6) the sail normal vector and hence the solar radiation pressure force can be expressed in ECI reference frame, just like all the other forces, by transforming the NTW coordinates to ECI coordinates:

$$\begin{bmatrix} x \\ y \\ z \end{bmatrix}_{ECI} = \begin{bmatrix} N_x & T_x & W_x \\ N_y & T_y & W_y \\ N_z & T_z & W_z \end{bmatrix} \cdot \begin{bmatrix} \cos\psi & -\sin\psi & 0 \\ \sin\psi & \cos\psi & 0 \\ 0 & 0 & 1 \end{bmatrix} \cdot \begin{bmatrix} 1 & 0 & 0 \\ 0 & \cos\mu & -\sin\mu \\ 0 & \sin\mu & \cos\mu \end{bmatrix} \begin{bmatrix} x_2 \\ y_2 \\ z_2 \end{bmatrix} \tag{5.59}$$

Given that the solar sail normal is directly located at the $\mathbf{y_2}$ axis:

$$\hat{n} = 1 \cdot \hat{j}_2 = \begin{bmatrix} 0 \\ 1 \\ 0 \end{bmatrix}_2 \tag{5.60}$$

Finally, the expression of the solar sail normal vector with respect the ECI reference frame can be obtained:

$$\hat{n} = \begin{bmatrix} n_x \\ n_y \\ n_z \end{bmatrix}_{ECI} = \begin{bmatrix} N_x & T_x & W_x \\ N_y & T_y & W_y \\ N_z & T_z & W_z \end{bmatrix} \begin{bmatrix} \cos\psi & -\sin\psi & 0 \\ \sin\psi & \cos\psi & 0 \\ 0 & 0 & 1 \end{bmatrix} \begin{bmatrix} 1 & 0 & 0 \\ 0 & \cos\mu & -\sin\mu \\ 0 & \sin\mu & \cos\mu \end{bmatrix} \begin{bmatrix} 0 \\ 1 \\ 0 \end{bmatrix} \tag{5.61}$$

Therefore, due to the force goes in the sail's normal direction, the solar radiation pressure force expressed in ECI reference frame is:

$$\vec{F}_{SRP}\big|_{ECI} = \left\|\vec{F}_{SRP}\right\| \cdot \hat{n}|_{ECI} = 2\eta_{eff} P A \cos\alpha \cos\alpha \cdot \hat{n}|_{ECI} \qquad [N] \tag{5.62}$$

Thereby, by controlling the pitch and yaw angle with the steering law, the solar sail thrust is determined by (5.61) and (5.62).

The steering law proposed in this project is based on controlling only the yaw angle and applying the sail's thrust always in the orbital plane i.e. the pitch angle is always zero. In this way, the steering law uses two user inputs: the φ_c constant angle and the "*att"* parameter. Firstly, φ_c is a constant angle that represents the offset angle between the sun light direction and the solar sail tangent vector, when the spacecraft is aligned with the Earth and the Sun, as shown in Figure 12 when $\theta = \frac{\pi}{2}$. Secondly, the *"att"* parameter represents the attitude state of the sail steering law:

$$\text{att} = \begin{cases} 1 \longrightarrow \text{positive thrust (accelerating)} \\ -1 \longrightarrow \text{brake (decelerating)} \\ 0 \longrightarrow \text{coasting (zero thrust)} \end{cases}$$

Figure 12 shows a scheme of the solar sail steering law. It should be pointed out that this scheme is a top view of the orbital plane, where the spacecraft performs one turn about the Earth. The scheme shows a circular orbit for simplicity but any type orbit is allowed. In this figure, $\vec{r}$ is the spacecraft position vector, $\vec{v}$ is the spacecraft velocity, $\vec{n}$ is the solar sail normal vector, $\vec{r}_{sun}$ is the Sun position vector (not in scale in the scheme of Figure 12) and $\hat{r}_{ss}$ is the satellite position unit vector with respect the Sun. As well, φ_c is the user-defined steering law control angle, υ is the angle between $\vec{r}$ and $\vec{r}_{sun}$, θ is the angle between $\hat{r}_{ss}$ and $\vec{v}$, and ψ, which represents the sail normal yaw angle, is the angle between $\vec{n}$ and $\vec{v}$. Note that $\nu \in [0, 2\pi]$, $\psi \in [-\pi, \pi]$ and both angles are considered positive in counter-clockwise sense. On the other side, $\theta \in [0, \pi]$ and so, it is always positive.

It should be pointed out that $\vec{n}$ belongs to the orbital plane because the pitch angle has been set to 0. Thereby all the vectors shown in Figure 12 belong to the orbital plane except $\vec{r}_{sun}$ and $\hat{r}_{ss}$, which are the projected in this plane. This fact is due to the spacecraft orbital plane is not the ecliptic plane.

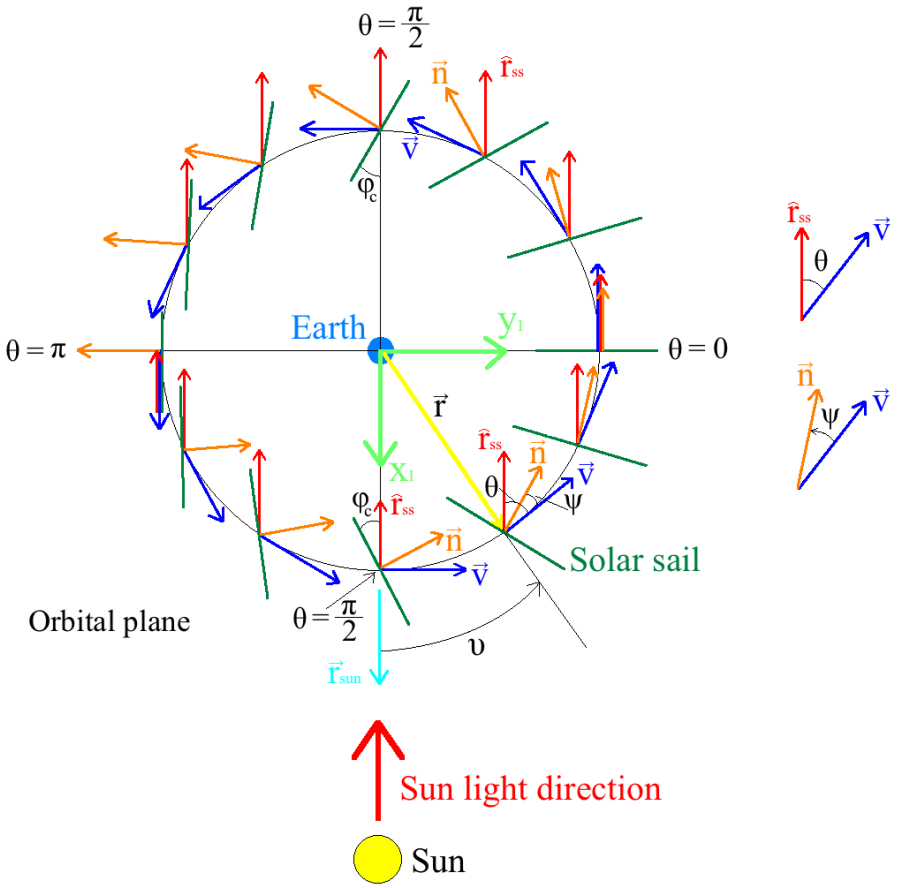

Figure 12. Scheme of the vectors and angles of the solar sail steering law (positive thrust attitude state).

In Figure 12, the reference frame I ($[\vec{x}_I \quad \vec{y}_I \quad \vec{z}_I]$) is used as a tool for delimiting the four quadrants of the orbital plane with respect the sunlight. This reference frame has the origin at the Earth's centre and its $\vec{z}_I$ axis is the unit orbital angular momentum vector of the spacecraft:

$$\vec{z}_I = \hat{L} = \frac{\vec{r} \times \vec{v}}{\|\vec{r} \times \vec{v}\|} \tag{5.63}$$

The $\vec{y}_I$ axis is perpendicular to the sunlight and belongs to the orbital plane:

$$\vec{y}_I = \hat{L} \times \frac{\vec{r}_{sun}}{\|\vec{r}_{sun}\|} \tag{5.64}$$

Finally, the $\vec{x}_I$ axis completes the right-handed triad:

$$\vec{x}_I = \vec{y}_I \times \vec{z}_I \tag{5.65}$$

This reference frame is calculated every time step so that the steering law always has the sunlight as reference. On the other side, the satellite position unit vector with respect the Sun, $\hat{r}_{ss}$, is given by:

$$\hat{r}_{ss} = \frac{\vec{r} - \vec{r}_{sun}}{\|\vec{r} - \vec{r}_{sun}\|} \tag{5.66}$$

Also, the angle ν, which is used as a reference for delimiting the four quadrants of the orbital plane, is calculated as follows:

$$\text{If} \quad \vec{r} \cdot \vec{y}_I \geq 0 \implies \nu = \cos^{-1}\left(\frac{\vec{r}_{sun} \cdot \vec{r}}{\|\vec{r}_{sun}\| \cdot \|\vec{r}\|}\right) \quad [\text{rad}] \tag{5.67}$$

$$\text{If} \quad \vec{r} \cdot \vec{y}_I < 0 \implies \nu = 2\pi - \cos^{-1}\left(\frac{\vec{r}_{sun} \cdot \vec{r}}{\|\vec{r}_{sun}\| \cdot \|\vec{r}\|}\right) \quad [\text{rad}] \tag{5.68}$$

Note that $\nu \in [0, 2\pi]$, $\psi \in [-\pi, \pi]$ and both angles are considered positive in counter-clockwise sense. The last angle in the figure $\theta \in [0, \pi]$ and so, it is always positive. This angle is calculated by:

$$\theta = \cos^{-1}\left(\hat{r}_{ss} \cdot \frac{\vec{v}}{\|\vec{v}\|}\right) \quad [\text{rad}] \tag{5.69}$$

Using these angles and definitions the steering law can be implemented with its three different attitude states: positive thrust, brake and coasting.

- **Positive thrust (accelerating).** In the positive thrust attitude state, the aim is to accelerate the spacecraft as much as possible allowing it to escape from the Earth gravity. Thereby, the objective is to orientate the sail, for every time step, in such a way that the thrust provides a positive impulse to the spacecraft. This attitude state is used to raise the spacecraft orbit from GEO to Earth escape. Note that because the pitch angle is 0, the yaw angle is the only variable that determines the sail orientation. The evolution of this attitude state, which is shown in Figure 12, is defined in the expressions below:

$$\begin{cases} 0 \leq \nu < \frac{\pi}{2} \longrightarrow \Psi = \varphi_c \cdot \sin\theta \\ \frac{\pi}{2} \leq \nu < \pi \longrightarrow \Psi = -\varphi_c \cdot \sin\theta \\ \pi \leq \nu < \frac{3\pi}{2} \longrightarrow \Psi = \left(\varphi_c - \frac{\pi}{2}\right) \cdot \sin\left(\theta - \frac{\pi}{2}\right) - \varphi_c \\ \frac{3\pi}{2} \leq \nu < 2\pi \longrightarrow \Psi = \left(\varphi_c - \frac{\pi}{2}\right) \cdot \sin\theta + \frac{\pi}{2} \end{cases}$$

In the first and second quadrants (right side of the circle) of Figure 12 the sail provides the most of the impulse to the spacecraft because it has the sunlight behind. On the contrary, on the third and fourth quadrants the sail provides a very little impulse because the spacecraft has the sunlight at its forward direction. Then, in the third and fourth quadrant, in order to avoid a negative thrust that slows the spacecraft down, the sail must remain practically tangent to the sunlight in a large portion of both quadrants. Moreover, it has been noticed that with this steering law, the maximum impulse Δv per turn is obtained for $\varphi_c = 45º$.

- **Brake (decelerating).** In order to adjust the trajectory it is necessary that the spacecraft has the ability to slow down when necessary. This attitude state may be needed when the spacecraft approaches fast to the Moon, and hence it is necessary to slow down in order to get captured by the Moon gravity. Basically, the expressions that drive the yaw in this attitude state have the same form to that of the positive thrust attitude state, but with the opposite objective. The evolution of the yaw angle in this attitude state is defined in the expressions below:

$$\begin{cases} 0 \leq \nu < \frac{\pi}{2} \longrightarrow \Psi = \left(\frac{\pi}{2} - \varphi_c\right) \cdot \sin\theta + \frac{\pi}{2} \\ \frac{\pi}{2} \leq \nu < \pi \longrightarrow \Psi = \left(\varphi_c - \frac{\pi}{2}\right) \cdot \sin\theta - \frac{\pi}{2} \\ \pi \leq \nu < \frac{3\pi}{2} \longrightarrow \Psi = -\varphi_c \cdot \sin\left(\theta - \frac{\pi}{2}\right) - \pi + \varphi_c \\ \frac{3\pi}{2} \leq \nu < 2\pi \longrightarrow \Psi = -\varphi_c \cdot \sin\theta + \pi \end{cases}$$

Because the brake attitude state is modelled in the same way to that of the positive thrust attitude state, the maximum braking impulse has been found when $\varphi_c = 45º$.

- **Coasting (zero thrust).** Finally, due to low thrust trajectories are so complex, there may be some parts in the trajectory when the spacecraft should provide no thrust so that only the gravity forces drive it. In this case, the aim is to orientate the sail in such a way that it is always tangent to the sunlight and hence, produces zero thrust. The evolution of the yaw angle in this attitude state is defined in the expressions below:

$$\begin{cases} 0 \leq \nu < \frac{\pi}{2} \longrightarrow \Psi = \theta - \frac{\pi}{2} \\ \frac{\pi}{2} \leq \nu < \pi \longrightarrow \Psi = -\theta - \frac{\pi}{2} \\ \pi \leq \nu < \frac{3\pi}{2} \longrightarrow \Psi = \frac{\pi}{2} - \theta \\ \frac{3\pi}{2} \leq \nu < 2\pi \longrightarrow \Psi = \theta - \frac{3\pi}{2} \end{cases}$$

With this attitude state the thrust is not always zero but sometimes is either positive or negative (with maximum values below $10^{-8}\mathrm{N}$ for a $50\mathrm{m}^2$ sail). However, it follows a symmetric trend so that if the thrust is positive in a portion of the orbit, it becomes negative in the opposite part of the orbit, resulting in a practically zero impulse $\Delta\mathrm{v}$.

5.2.2.3. Δv calculation

In the spacecraft propelled by rocket engines, in which the stored propellant is expulsed through the nozzle at high velocity, the $\Delta\mathrm{v}$ impulse (velocity change) provided to the spacecraft by the rocket engine is calculated using Tsiolkovsky rocket equation:

$$\Delta\mathrm{v} = \mathrm{v_e} \cdot \ln\left(\frac{\mathrm{M_0}}{\mathrm{M_f}}\right) \quad \left[\frac{\mathrm{m}}{s}\right] \tag{5.70}$$

Where $\mathrm{v_e}$ is the jet exhaust velocity, $\mathrm{M_0}$ is the initial spacecraft mass (before the orbital maneuver) and $\mathrm{M_f}$ is the final spacecraft (after performing the maneuver). Hence, Tsiolkovsky rocket equation states that the impulse provided to a spacecraft by a rocket engine is proportional to the logarithm of the mass ratio before and after the maneuver. Thereby, the bigger this ratio is (by expulsing more propellant mass in the maneuver) the higher the $\Delta\mathrm{v}$ impulse becomes. In this way, using Tsiolkovsky equation it is very easy to relate the impulse provided to the spacecraft and the propellant mass invested in each maneuver. However, a solar sail is a propellant-less propulsion system and hence Tsiolkovsky equation cannot be applied on it. Nevertheless, a solar sail generates a thrust force which, although small, can provide much bigger $\Delta\mathrm{v}$ impulse than conventional chemical rockets. It should be pointed out that only the projection of the thrust on the velocity direction contributes to the velocity modulus change. Indeed, a force normal to the velocity generates no variation in the velocity modulus, but only a deviation of its direction. So, the SRP projected acceleration is given by:

$$\vec{a}_{SRP} = \frac{\vec{F}_{SRP}}{m} \Longrightarrow \vec{a}_{SRP}|_{\vec{v}} = \frac{\vec{F}_{SRP}}{m} \cdot \frac{\vec{v}}{\|\vec{v}\|} \quad \left[\frac{m}{s^2}\right] \tag{5.71}$$

Therefore, in solar sails the Δv impulse is calculated by integrating the acceleration due to SRP projected on the velocity direction.

$$\Delta v = \int_0^t \frac{\vec{F}_{SRP}}{m} \cdot \frac{\vec{v}}{\|\vec{v}\|} dt \quad \left[\frac{m}{s}\right] \tag{5.72}$$

5.3. TRAJECTORY CALCULATION

In order to calculate the trajectory of the satellite numerically, the formulation developed from section 5.1 to section 5.2 has been implemented in Matlab®. In order to obtain the velocity (5.1) and the position (5.2) of the satellite for each instant, the satellite acceleration defined in equation (5.27) must be integrated. For that, the Runge-Kutta-Fehlberg 7(8) numerical integrator implemented in Matlab® has been used. The main principles of this numerical integrator are briefly presented in section 5.3.1. The principles of Runge-Kutta-Fehlberg method are further explained in [28]. Furthermore, the coefficients of RKF 7(8) are indicated in ANNEX A.

Furthermore, additional functions have been created to calculate the diverse effects that should be considered in order to calculate the acceleration defined in (5.27). These functions are briefly described in section 5.3.2. Afterwards, in section 5.3.3 the inputs, constant and outputs that should be defined in the code are presented. Note that all the Matlab® developed is presented in ANNEX B.

5.3.1. NUMERICAL INTEGRATOR

The Runge-Kutta-Fehlberg (RKF) 7(8) improves the 4th order Runge-Kutta method providing an estimate of the truncation error for higher orders. Indeed, the RKF 7(8) has a variable step size method of order 7th with an 8th order error estimation, used to change the step size during the integration. In order to integrate numerically the satellite acceleration defined in (5.27) through RKF 7(8), it is required to reduce the three second order differential equations to six first order differential equations. Note that the equation (5.39) can be written as:

$$\begin{aligned} \vec{a} &= -\frac{\mu_\oplus}{\|\vec{r}\|^3}\vec{r} + \vec{a}_{pert} + \vec{a}_{SRP} = \\ &= -\frac{\mu_\oplus}{\|\vec{r}\|^3}\vec{r} - \frac{\mu_\odot}{\|\vec{r} - \vec{r}_{sun}\|^3}\vec{r} - \frac{\mu_\leftmoon}{\|\vec{r} - \vec{r}_{moon}\|^3}\vec{r} + \mathcal{F}\ [m/s^2\ ] \end{aligned} \tag{5.73}$$

where $\mathcal{F}$ is equal to:

$$\mathcal{F} = \frac{\mu_{\odot}}{\|\vec{r} - \vec{r}_{sun}\|^3}\vec{r}_{sun} + \frac{\mu_{\leftmoon}}{\|\vec{r} - \vec{r}_{moon}\|^3}\vec{r}_{moon} - \frac{\mu_{\odot}}{\|\vec{r}_{sun}\|^3}\vec{r}_{sun} - \\ - \frac{\mu_{\leftmoon}}{\|\vec{r}_{moom}\|^3}\vec{r}_{moon} + \frac{\overrightarrow{F_{r_{J2}}}}{m} + \frac{\overrightarrow{F_{\delta_{J2}}}}{m} + \vec{a}_{SRP}\ [m/s^2\ ] \tag{5.74}$$

In order to reduce the equation (5.73) the auxiliary Γ is defined as:

$$\begin{matrix} \Gamma_1 = r_x & \Gamma_2 = r_y & \Gamma_3 = r_z \\ \Gamma_4 = \dot{r}_x = v_x & \Gamma_5 = \dot{r}_y = v_y & \Gamma_6 = \dot{r}_z = v_z \quad \Gamma_7 = \Delta v \end{matrix} \tag{5.75}$$

Then, the derivatives of Γ, called $\dot{\Gamma}$ are defined as:

$$\begin{matrix} \dot{\Gamma}_1 = \dot{r}_x = \Gamma_4 & \dot{\Gamma}_2 = \dot{r}_y = \Gamma_5 & \dot{\Gamma}_3 = \dot{r}_z = \Gamma_6 \\ \dot{\Gamma}_4 = \ddot{r}_x = a_x & \dot{\Gamma}_5 = \ddot{r}_y = a_y & \dot{\Gamma}_6 = \ddot{r}_z = a_z \quad \dot{\Gamma}_7 = \dot{\Delta v} \end{matrix} \tag{5.76}$$

Consequently, forming a system of first order differential equations such as:

$$\dot{\Gamma} = f(t, \Gamma) = \begin{bmatrix} \Gamma_4 \\ \Gamma_5 \\ \Gamma_6 \\ -\frac{\mu_{\oplus}}{\|\vec{r}\|^3}\Gamma_1 - \frac{\mu_{\odot}}{\|\vec{r} - \vec{r}_{sun}\|^3}\Gamma_1 - \frac{\mu_{\leftmoon}}{\|\vec{r} - \vec{r}_{moon}\|^3}\Gamma_1 + \mathcal{F} \\ -\frac{\mu_{\oplus}}{\|\vec{r}\|^3}\Gamma_2 - \frac{\mu_{\odot}}{\|\vec{r} - \vec{r}_{sun}\|^3}\Gamma_2 - \frac{\mu_{\leftmoon}}{\|\vec{r} - \vec{r}_{moon}\|^3}\Gamma_2 + \mathcal{F} \\ -\frac{\mu_{\oplus}}{\|\vec{r}\|^3}\Gamma_3 - \frac{\mu_{\odot}}{\|\vec{r} - \vec{r}_{sun}\|^3}\Gamma_3 - \frac{\mu_{\leftmoon}}{\|\vec{r} - \vec{r}_{moon}\|^3}\Gamma_3 + \mathcal{F} \\ \frac{\vec{F}_{SRP}}{m} \cdot \frac{\vec{v}}{\|\vec{v}\|} \end{bmatrix} \tag{5.77}$$

where $\vec{F}_{SRP}$ is equal to $\vec{F}_{SRP} = m\vec{a}_{SRP}$, being $\vec{a}_{SRP}$ defined in equation (5.44). This system of equations is solved by the explicit Runge-Kutta method written as:

$$\Gamma_{j+1} = \Gamma_j + Hf(t_j, \Gamma_j, H) \tag{5.78}$$

where $f(t_j, \Gamma_j, H)$ is an increment function evaluated at several mid-points in the time interval $[t_j, t_j + H]$. Furthermore, accuracy is increased through the use of the embedded method, which implies combining two adjacent Runge-Kutta methods. In other words, an automatic step size solution is included, which generates larger step size for larger changes and a smaller for smaller changes.

Following the formulation with the notation of [28], for Γ_{j+1} is obtained that:

$$\tilde{t}_m = t_j + a_n H \quad m = 1,2,\dots,s \tag{5.79}$$

$$\tilde{\Gamma}_m = \Gamma_j + H\sum_{n=1}^{m-1} b_{mn}\tilde{f}_n \quad m = 1,2,\dots,s \tag{5.80}$$

$$7^{th}\ \text{order} \quad \Gamma_{j+1} = \Gamma_j + H\sum_{m=1}^{s} c_m\tilde{f}_n(\tilde{t}_m, \tilde{\Gamma}_m) \quad s = \text{No. of stages} \tag{5.81}$$

$$8^{\text{th}}\ \text{order} \quad \Gamma_{j+1}^{*} = \Gamma_j + H\sum_{m=1}^{s} c_m^{*}\tilde{f}_n\left(\tilde{t}_m, \tilde{\Gamma}_m\right) \quad s = \text{No. of stages} \tag{5.82}$$

where $\{a\}$ are the nodes, $[b]$ are the coupling coefficients $\{c_m\}$ and $\{c_m^{*}\}$ are the weights. The values of these coefficients are included in the ANNEX A of this project. Moreover, in order to compute the step size is necessary to define the difference between the solutions of equations (5.81) and (5.82). In this way, the maximum scalar value for all the N first equations is determined and the local error estimated as:

$$e = \Gamma_{j+1} - \Gamma_{j+1}^{*} \rightarrow e = \max(|e_1|, \dots, |e_N|). \tag{5.83}$$

Considering this error e, the value of H is updated after each step. So, H is decreased if it is higher than a tolerance value Tol or increasing it if it is smaller. This is expressed as:

$$H^{*} = H_{old}\left(\frac{Tol}{e}\right)^{\frac{1}{p+1}}$$
$$\beta = 0.25^{\frac{1}{p+1}} \rightarrow \begin{cases} \beta_{max} = 1 & \text{for step rejection} \\ \beta_{max} = 1.5 & \text{for step rejection} \end{cases} \rightarrow H_{new} = min(\beta H^{*}, \beta_{max} H_{old}) \tag{5.84}$$

where p is the order of the method ($p = 7$). During the iteration process, the result is only accepted if the error is smaller than Tol. It should be pointed out that the integrator numerical code has been developed with [28] as reference.

5.3.2. FUNCTIONS

In this section the functions generated to implement the formulation are briefly described. For that, in Table 3 their name and main purposes are explained. Note that although the main code is not included in Table 3, it is presented in the section B.1. of ANNEX B.

Matlab® code functions and their description	
Name	**Description**
calc_Eclipse.m	It calculates the Eclipse condition defined in section 5.2.2.1.
calc_SRP.m	It estimates the value of the SRP force as explained in section 5.2.2.
el_trans.m	Defining the initial orbital elements, it returns the position and velocity of the s/c.
f_derivatives.m	It is used to calculate the derivatives defined in equation (5.77).

J2_perturbation.m	It is used to calculate the perturbations due to J_2 of Earth, as given in section 5.2.1.
juliandate.m	It is used to calculate the JD.
new_step.m	It is used to update the step size following the stated in expression (5.84).
pos_moon.m	It is used to calculate the position of Moon while knowing JD as explained in section 5.1.3.
pos_sun.m	It is used to calculate the position of Sun while knowing JD as explained in section 5.1.2.
RKF7_integrator.m	It is integrates the numerical integrator. It is related with f_derivatives.m and new_step.m.
sail_control.m	It integrates the steering law as explained in section 5.2.2.2.
sm_relative.m	It calculates the relative position of the s/c with respect to the Moon.
trajectory_video.m	It is used for the generation of a video. Other function called trajectory_video2.m is also included in the code.

Table 3. Summary of the functions developed in Matlab® and their descriptions.

The Matlab® code of these functions is enclosed in section B.2. of ANNEX B.

5.3.3. IMPUTS, CONSTANTS AND OUTPUTS

The Matlab® code has been developed to assess the feasibility of the designed solar sail for the mission presented in 4. However, the code itself is not constrained to study a satellite departing from GEO and arriving to the vicinity of the Moon's surface. Indeed, the user is allowed to define the initial orbit of the satellite and the departing time, inter- alia, as shown in Table 4.

Inputs of the Matlab® code			
Area	**Name**	**Description**	**Units**
s/c	m	Mass of the satellite	kg
	A	Area of the solar sail	m^2
Steering law	Phi_control	Alpha angle for the sail control law in º.	º
	att	Type of attitude state for the steering law.	---
Departure time	year0	Departure year.	---
	day0	Departure day (0-365).	---
	h_UTC_0	Departure hour (0-24).	---
	m_UTC_0	Departure minute (0-60).	---
	s_UTC_0	Departure second (0-60).	---

Initial orbital elements	a0	Semi-major axis of the initial orbit	m
	e0	Initial orbit eccentricity	
	i0	Initial orbit inclination	º
	RAAN0	Initial orbit Right Ascension of the Ascending Node	º
	w0	Argument of the perigee of the initial orbit	º
	Theta0	True anomaly	º
Simulation	stop_time	Numerical parameter of the RKF 7(8) function	s
	tolerance	Tolerance value used to define the step size	---
	t_0	Initial time for the simulation	s
	h	Initial time step	s
	Tsim	Trajectory simulation time	s
	Tsave	Time between vector saving	s
	N	Initial size of the vector arrays for memory preallocation	---

Table 4. Inputs for the Matlab® code and their description.

Note that in the code the perturbations due to atmospheric drag are not considered. Thereby, although as code-user it is possible to define LEO as initial orbit for the s/c, the results obtained will not be truthful. The constants defined in the code are: $R_{\oplus}$,$R_{\leftmoon}$, AU, J_2, $\mu_{\oplus}$, $\mu_{\leftmoon}$ and $\mu_{\odot}$. Finally, the outputs are shown in Table 5.

Outputs given by the Matlab® code	
Name	**Description**
r_x, r_y, r_z	Evolution of s/c trajectory in the ECI reference frame
F_{SRP} vs. t	Evolution of SRP force during the simulation
Δv vs. t	Evolution of Δv during the simulation
Ψ vs. t	Evolution of the yaw angle during the simulation
F_v vs. t	Evolution of the SRP force projected in the velocity direction during the simulation
E_{Earth} vs. t	Evolution of the s/c specific energy with respect to the Earth during the simulation

Table 5. Outputs given by the Matlab® code and their description.

5.4. RESULTS

This section presents the results of the trajectory analysis with the aim of determining whether or not a solar sail of $50\mathrm{m}^2$ can fulfill the mission propulsive requirements. This solar sail area value has been determined in the subsection 6.2.3 of the sizing section, as the maximum possible sail area for the current design. On the other side, the propulsive requirements determine that the solar sail module shall be able to drive the 6U nanosatellite from GEO to the target lunar orbit in less than 4 years. Nevertheless, as it has been aforementioned, the RAQL mission is still in a conceptual phase and so, the target lunar orbit is not specified yet. Thus, this trajectory analysis does not include planet targeting or planet capture maneuvers. However, proving that the SSM is able to propel the nanosatellite from GEO to Earth escape is enough to demonstrate its capability to reach any lunar orbit. Indeed, if the SSM is able to provide enough impulse within a limited time for reaching Earth escape, then it is capable of performing the planet capture maneuver, which requires much less impulse. Hence, the focus of this trajectory analysis lies on determining if the SSM can achieve reaching Earth escape in less than 4 years. To do so, two mass cases have been considered: 6U nanosatellite nominal mass of 6kg and 6U nanosatellite maximum mass of 8kg.

5.4.1. RESULTS FOR $\mathbf{m = 6kg}$ & $\mathbf{A = 50m^2}$

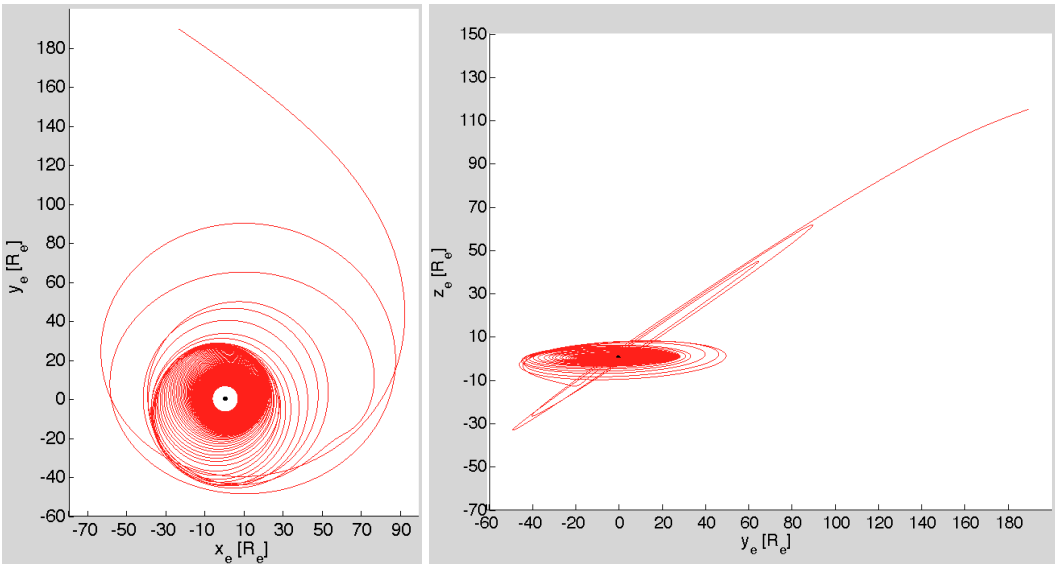

Figure 13. Top-view (Left) and side-view (Right) of the s/c trajectory from GEO to Earth scape for $\mathbf{m = 6kg}$ and $\mathbf{A = 50m^2}$. From $\mathbf{t = 0\ years}$ to $\mathbf{t = 2.7\ years}$.

Figure 13 shows the 6kg-nanosatellite with $50\mathrm{m}^2$ sail trajectory from GEO orbit ($\mathrm{t} = 0\ \mathrm{years}$) to a position very close to Earth escape ($\mathrm{t} = 2.7\ \mathrm{years}$). Precisely,

the nanosatellite is considered to escape the Earth after 1016 days (2.784 years) after departure. The escape condition has been identified as the point of the trajectory in which the spacecraft orbital energy is equal to 0. As shown in Figure 13 the spacecraft follows a spiral from GEO until it makes a flyby with the moon around $t = 2.4\ \text{years}$ which provokes a strong perturbation in the trajectory. In this flyby the spacecraft inclination changes dramatically from a value close to 0 to more than 30º. After running many simulations it was found that due to the process of raising the orbit from GEO is very slow, sooner or later the spacecraft will get close to the moon and experience a strong flyby, unless the conditions are suitable for capture. If the spacecraft arrives to this point in optimal conditions (adequate position and velocity) then it would be possible that the Moon gravity captures it. However, arriving to this condition at the right place and time is extremely difficult. Achieving this condition is only possible by performing an optimum control over the sail and implementing planet targeting and capture maneuvers, which are out of the scope. Nevertheless, it was found that in most of the cases the spacecraft reaches the escape condition close to the Moon (which orbits around a distance of 60 Earth radius (R_e)). So, in conclusion, with 6kg of mass and 50m^2 of sail area, the spacecraft would reach the target lunar orbit in much less than 4 years, hence fulfilling the mission propulsive requirements.

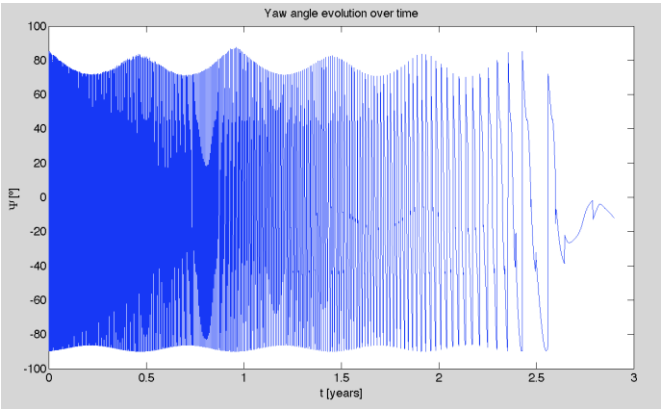

Figure 14. Yaw angle evolution over time for $m = 6kg$. From $t = 0\ \text{years}$ to $t = 2.9\ \text{years}$.

Figure 14shows the yaw angle evolution following the steering law developed for the positive thrust state. It is clear that as the time goes by and the spacecraft gets further from the Earth and so its orbital period is longer, the yaw evolves slower. The longer it takes for the spacecraft to perform one turn about the Earth, then the slower the yaw varies.

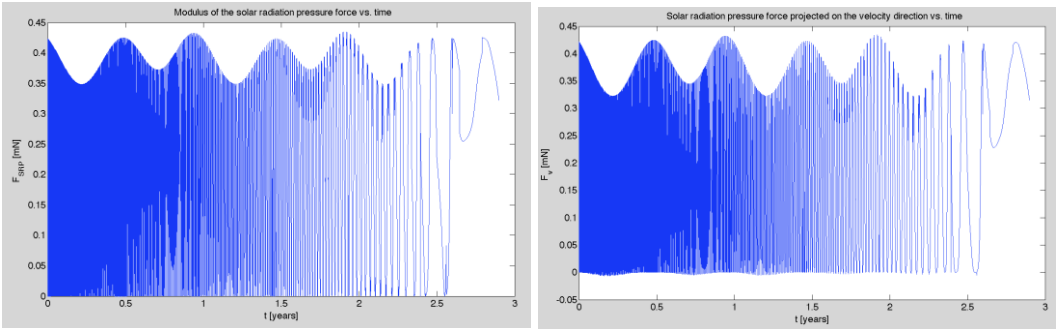

Figure 15. Evolution of SRP force modulus (Left) and SRP force projected on the velocity direction (Right) for $\mathbf{m = 6kg}$. From $\mathbf{t = 0\ years}$ to $\mathbf{t = 2.9\ years}$.

In Figure 15, the evolution of the solar radiation pressure force and its projection over the velocity direction is presented. The maximum thrust the solar sail provides is around 0.43mN considering an efficiency of $\eta_{\text{eff}} = 0.934456$. However, as it has been aforementioned, only the projection of the thrust on the velocity direction contributes to the impulse provided to the spacecraft. Then, it is useful to notice the differences between the left and right plots of Figure 15.

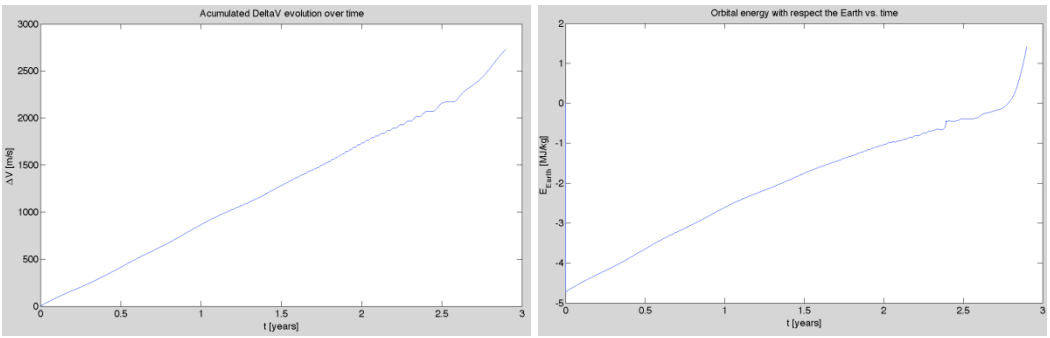

Figure 16. Evolution of accumulated Δv (Left) and s/c orbital energy with respect to the Earth (Right) for $\mathbf{m = 6kg}$. From $\mathbf{t = 0\ years}$ to $\mathbf{t = 2.9\ years}$.

The impact of the solar sail thrust in the spacecraft motion is also shown in Figure 16. Firstly, on the left, it can be noticed how the Δv impulse increases very linearly over the time. This feature is characteristic of the spiral trajectory phase, where the spacecraft turns about the Earth each time at bigger distance. As well, as the spacecraft approaches the escape point the Δv impulse varies because the trajectory has changed significantly from the spiral phase. So, as the trajectory is different as it gets close to this condition, the way the solar sail receives the sunlight varies hence changing the Δv slope. Indeed, the slope varies because the spacecraft stops turning about the Earth and follows a single direction. In the spiral phase, a portion of the turn provides the most of the impulse (Sun behind the spacecraft) and the other portion provides very little Δv. Then, if the sail keeps the same direction and does not turn around, then the thrust is continuous thereby changing the Δv slope. On the other side, in the right

plot of Figure 16, it can be noticed the time when the spacecraft reaches the Earth escape condition i.e. energy equal to zero. Same as it happened for the Δv, when the spacecraft approaches the escape condition the energy slope varies.

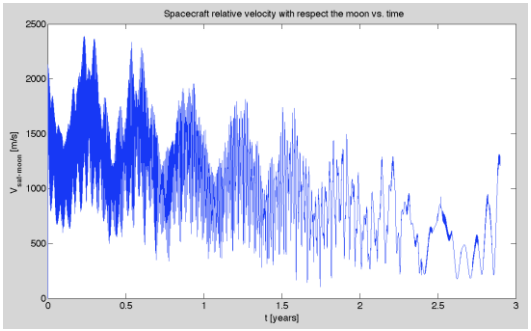

Figure 17. Evolution of s/c relative velocity with respect the Moon for $\mathbf{m = 6kg}$. From $\mathbf{t = 0}$ years to $\mathbf{t = 2.9}$ years.

Figure 17 shows the evolution of the spacecraft relative velocity about the Moon. As the time goes by, the spacecraft gets closer to the Moon hence reducing the relative distance and velocity. However, as the spacecraft keeps accelerating it finally begins to get further from the Moon as it escapes the Earth.

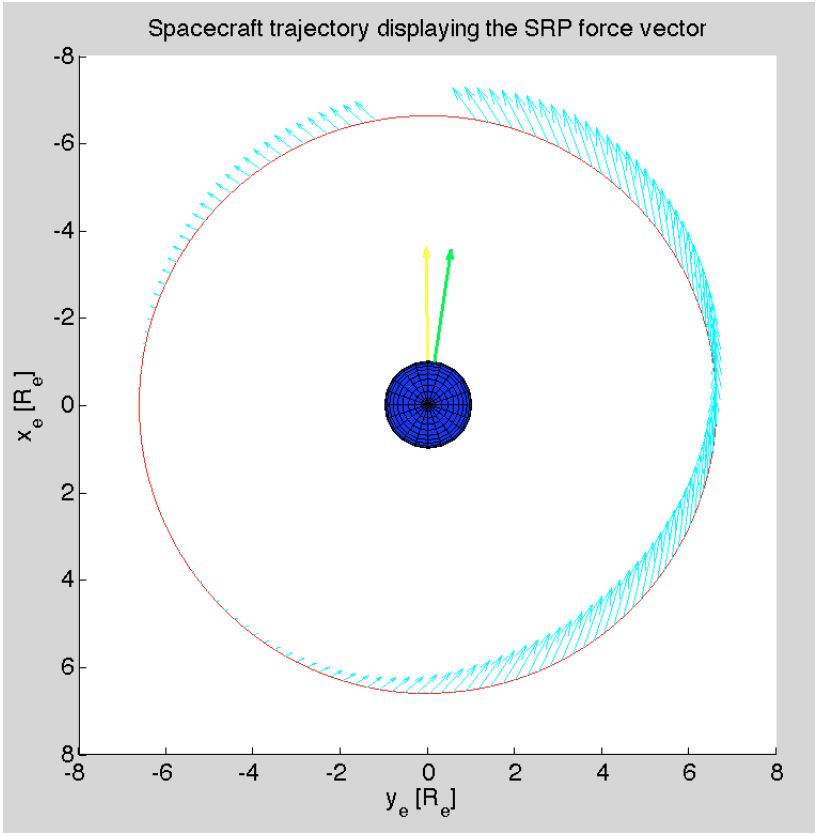

Figure 18. S/C trajectory showing the SRP force vector (in cyan), the sunlight (yellow arrow) and vector pointing to the Moon (green arrow) for $\mathbf{m = 6kg}$. 1 day in GEO orbit when the Sun is at the vernal equinox.

In order to show the steering law working process, Figure 18 presents the spacecraft trajectory in departure condition at GEO during 1 day. At GEO 1 day equals to 1 complete turn about the Earth, and hence the whole process of the steering law can be seen. Note that, the trajectory shadowed area provokes and eclipse condition which results in zero sail thrust. As well, it can be seen how the SRP force vector varies its modulus and direction along the complete turn about the Earth. By comparing this figure with Figure 12, the working process of the steering law can be easily understood. It should be pointed out that the advantage of the steering law developed in this project provides thrust even when the spacecraft has the Sun in front of.

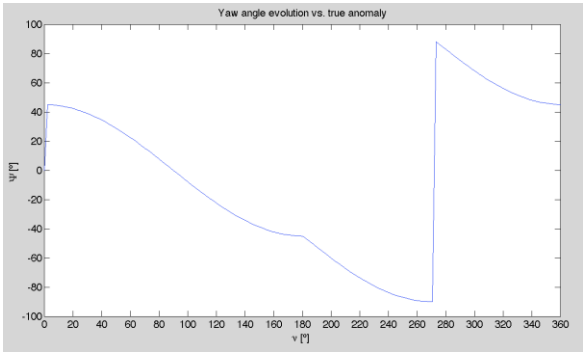

Figure 19. Yaw angle evolution vs. true anomaly in one turn for $\mathbf{m = 6kg}$. 1 day in GEO orbit when the Sun is at the vernal equinox.

In Figure 19, the yaw evolution is shown along the complete turn about the Earth. Note that when the spacecraft reaches 270º it performs a fast 180º turn to get the sail ready for providing thrust again.

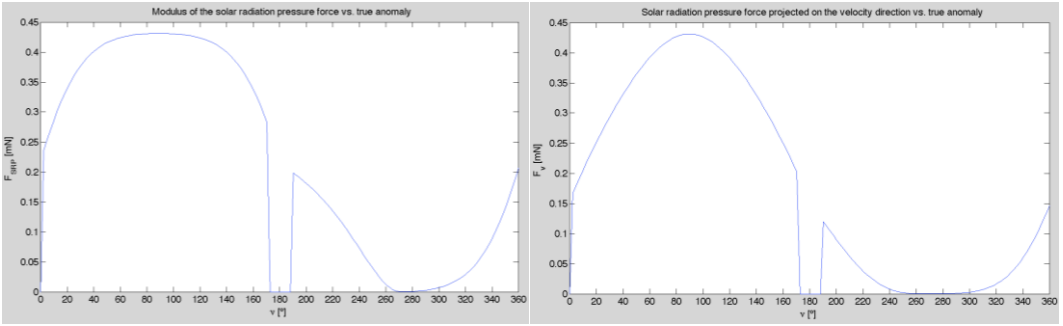

Figure 20. Evolution of SRP force modulus (Left) and SRP force projected on the velocity direction (Right) vs. true anomaly in one turn for $\mathbf{m = 6kg}$. 1 day in GEO orbit when the Sun is at the vernal equinox.

In Figure 20, the comparison between the SRP force modulus and its projection on the velocity direction can be easily done. Note that between $\nu = 40º$ and $\nu = 150º$, the thrust modulus is very close to the maximum however not all the force contributes to the net Δv provided to the s/c. Only the projection of the thrust on the velocity direction contributes to Δv.

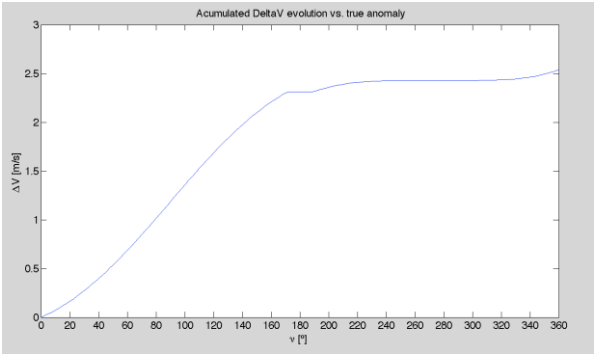

Figure 21. Evolution of accumulated Δv vs. true anomaly in one turn for $\mathbf{m = 6kg}$. 1 day in GEO orbit when the Sun is at the vernal equinox.

Finally, Figure 21 shows very clearly how the most of the impulse provided by the solar sail is obtained when the Sun is behind the spacecraft (from $\nu = 0º$ and $\nu = 180º$). Nevertheless, even when the spacecraft has the Sun in front of, some Δv is obtained.

5.4.2. RESULTS FOR $\mathbf{m = 8kg}$ & $\mathbf{A = 50m^2}$

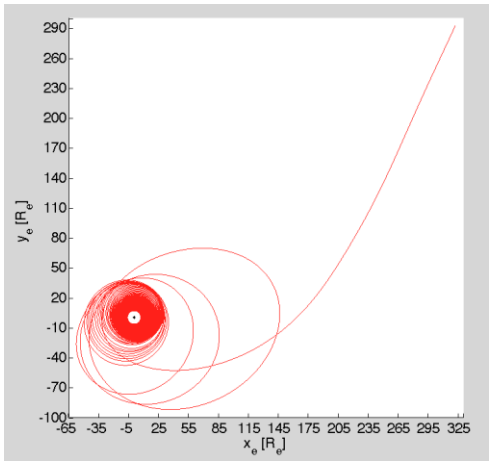

Figure 22. Top-view of the s/c trajectory from GEO to Earth scape for $\mathbf{m = 8kg}$. From $\mathbf{t = 0\ years}$ to $\mathbf{t = 3.65\ years}$.

Figure 22 and Figure 23 show the 8kg-nanosatellite with 50m^2 sail trajectory from GEO orbit ($t = 0$ years) to a position shortly after to Earth escape ($t = 3.65$ years). Precisely, the nanosatellite is considered to escape the Earth after 1317 days (3.607 years) after departure. Same as in the 6kg case, the escape condition is determined as the point of the trajectory in which the spacecraft orbital energy is equal to 0. Moreover, in the same way as it happened for the 6kg case, the spacecraft follows a spiral from GEO until it makes a flyby with the moon provoking a strong perturbation in the trajectory. In fact, it is easy to identify this point by the sudden change in the orbit inclination. Again, after running many simulations it was found that in the spiral climibing sooner or later the spacecraft

gets close to the moon and experiences a strong flyby. As it has been aforementioned, it is very difficult to arrive to the optimum conditions for lunar capture. Of course, after this flyby the trajectory changes dramatically as it is shown in the inclination change of Figure 23.

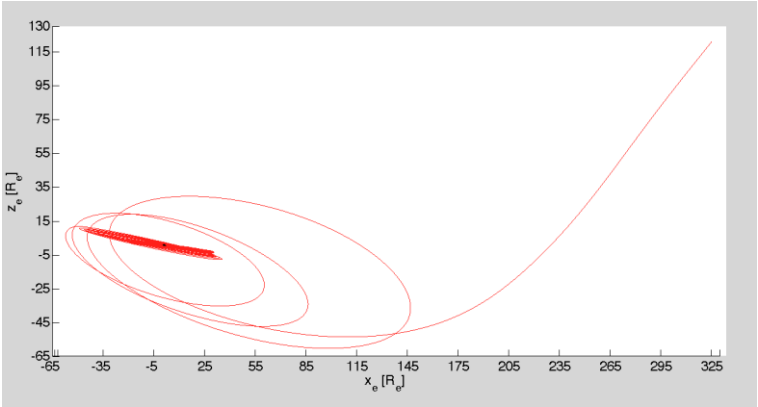

Figure 23. Side-view of the s/c trajectory from GEO to Earth scape for $\mathbf{m = 8kg}$. From $\mathbf{t = 0}$ years to $\mathbf{t = 3.65}$ years.

Nonetheless, it was found that the spacecraft reaches the escape condition close to the Moon (which orbits around a distance of 60 Earth radius (R_e)). In this case, the flight time increases significantly because the nanosatellite weighs 8kg but has the same thrust to that of the 6kg one. Then, the spacecraft acceleration due to the solar sail force is smaller because the thrust is the same but the mass is heavier. Altogether leads to a longer flight time that is close to the requirement limit. Thus, in conclusion, with 8kg of mass and 50m^2 of sail area, the spacecraft would reach the target lunar orbit in less than 4 years, hence fulfilling the mission propulsive requirements with a small safety margin.

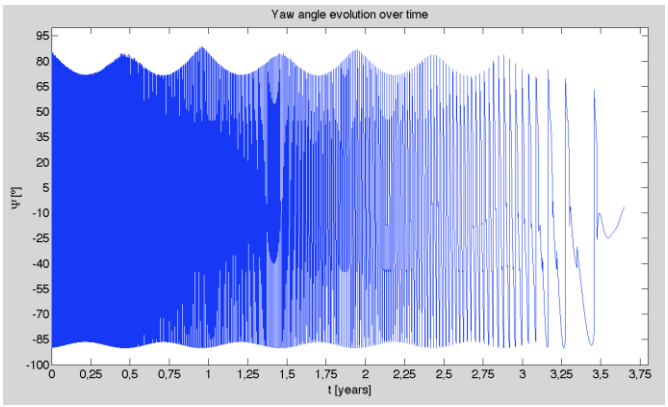

Figure 24. Yaw angle evolution over time for $\mathbf{m = 8kg}$. From $\mathbf{t = 0}$ years to $\mathbf{t = 3.65}$ years.

Figure 24 shows the yaw angle evolution following the steering law developed for the positive thrust state. As the time goes by and the spacecraft gets further from the Earth and its orbital period grows, the yaw angle evolves slower.

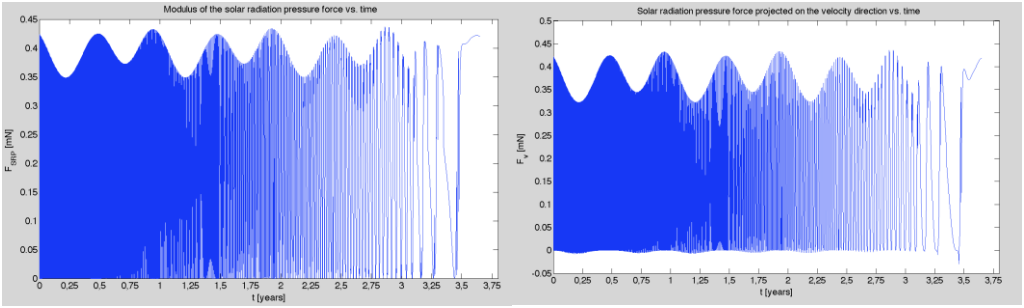

Figure 25. Evolution of SRP force modulus (Left) and SRP force projected on the velocity direction (Right) for $\mathbf{m = 8kg}$. From $\mathbf{t = 0\ years}$ to $\mathbf{t = 3.65\ years}$.

In Figure 25, the evolution of the solar radiation pressure force and its projection over the velocity direction is presented. In this case, due to the solar sail module is the same, the maximum thrust the solar sail provides is the same to that of the 6kg case, around 0.43mN considering an efficiency of $\eta_{\text{eff}} = 0.934456$. Note that only the projection of the thrust on the velocity direction contributes to the impulse provided to the spacecraft.

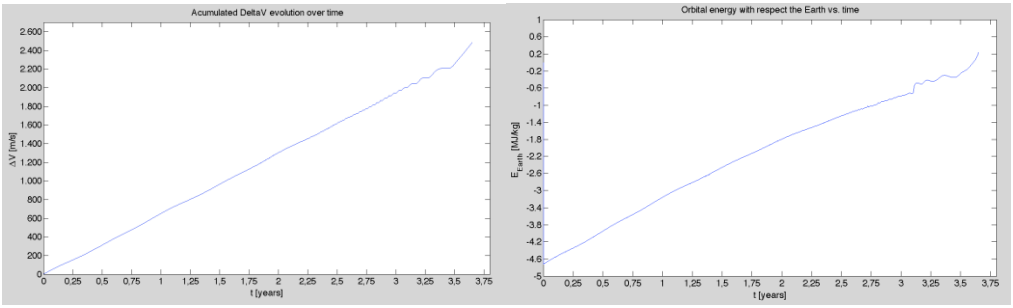

Figure 26. Evolution of accumulated Δv (Left) and s/c orbital energy with respect to the Earth (Right) for $\mathbf{m = 8kg}$. From $\mathbf{t = 0\ years}$ to $\mathbf{t = 3.65\ years}$.

The impact of the solar sail thrust in the spacecraft motion is also shown in Figure 26. Firstly, on the left, it can be noticed how the Δv impulse increases very linearly over the time. Approximately the Δv impulse until the Earth escape condition is the same to that of the 6kg case, but taking longer time to reach it. Moreover, as it has been aforementioned as the spacecraft approaches the escape point the Δv impulse varies because the trajectory has changed significantly from the spiral phase. This change is caused by the different way in which the solar sail receives the sunlight as the trajectory changes from the spiral phase. On the other side, in the right plot of Figure 26, it can be noticed the time when the spacecraft reaches the Earth escape condition i.e. energy equal to zero. Same as it happened for the Δv, when the spacecraft approaches the escape condition the energy slope varies.

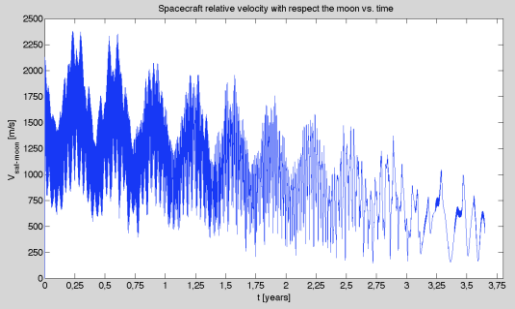

Figure 27. Evolution of s/c relative velocity with respect the Moon for $\mathbf{m = 8kg}$. From $\mathbf{t = 0}$ years to $\mathbf{t = 3.65}$ years.

Figure 27 shows the evolution of the spacecraft relative velocity about the Moon. Same as in the 6kg case, as the time goes by, the spacecraft gets closer to the Moon hence reducing the relative distance and velocity. However, as the spacecraft keeps accelerating it finally begins to get further from the Moon as it escapes the Earth.

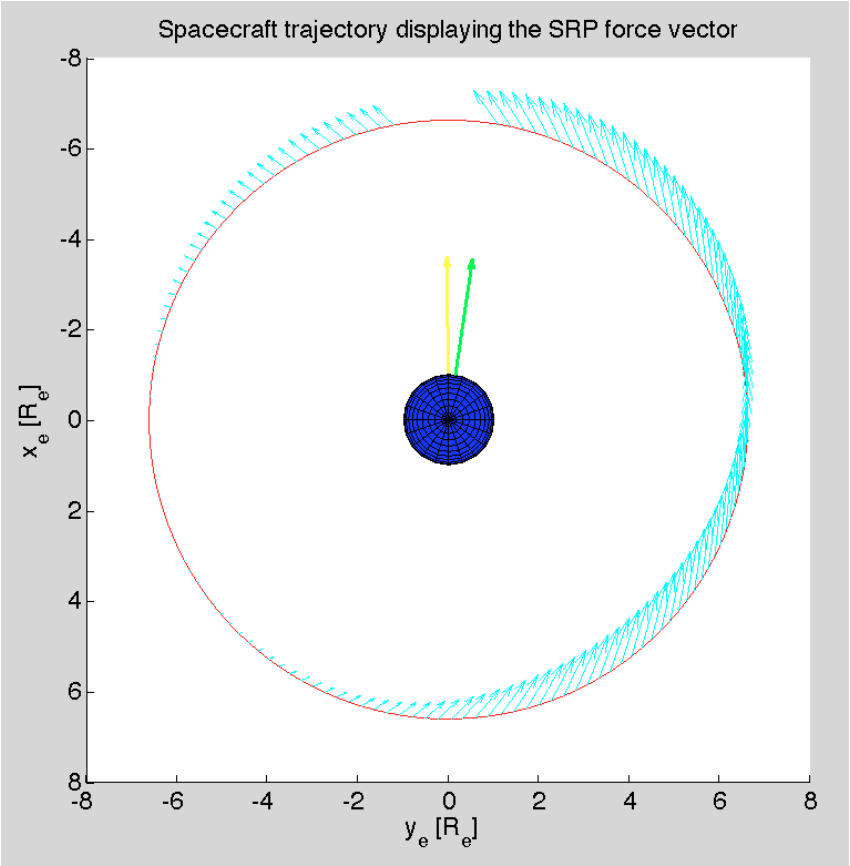

Figure 28. S/C trajectory showing the SRP force vector (in cyan), the sunlight (yellow arrow) and vector pointing to the Moon (green arrow) for $\mathbf{m = 8kg}$. 1 day in GEO orbit when the Sun is at the vernal equinox.

The steering law for the 8kg nanosatellite is the same to that of the 6kg case. So, the thrust capacity and evolution is the same but the satellite higher mass leads to an overall lower acceleration due to SRP force.

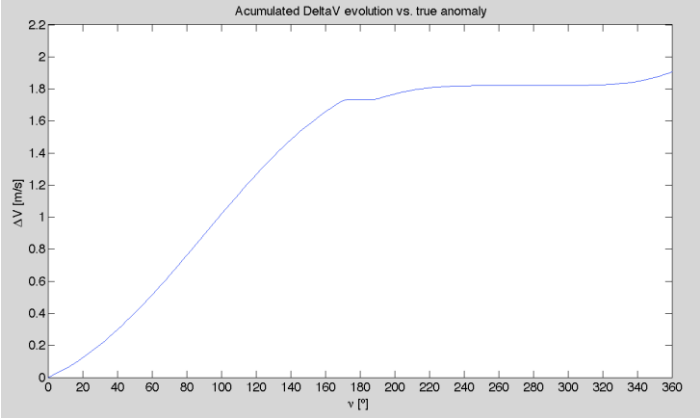

Figure 29. Evolution of accumulated Δv vs. true anomaly in one turn for $\mathbf{m = 8kg}$. 1 day in GEO orbit when the Sun is at the vernal equinox.

Finally, as it happened in the 6kg case, Figure 29 shows very clearly how the most of the impulse provided by the solar sail is obtained when the Sun is behind the spacecraft (from $\nu = 0º$ and $\nu = 180º$). Also, even when the spacecraft has the Sun in front of, some Δv is obtained. Comparing this figure with Figure 21, the Δv reached after a complete turn in GEO is about $1.9 m/s$ while in the 6kg nanosatellite it slightly above $2.5 m/s$. This represents a 25% less impulse per turn compared to the 6kg nanosatellite. This 25% value is equal to the mass difference between the 8kg nanosatellite and the 6kg one. However, the flight time has increased a 29.6% compared to the 6kg nanosatellite. This values confirm the critical influence of the mass in the nanosatellite performance.

6. SOLAR SAIL MODULE DESIGN

This chapter presents the design of the Solar Sail Module (SSM), which is the core of the project. This has been the most complex task due to the strict constraints and the need to find innovative solutions to fulfill all the requirements. Besides, it should be pointed out that this is a cutting-edge technology which is currently under development. To date, only two solar sails have successfully flown, therefore each new design represents a milestone for this technology.

The chapter begins with the conceptual design of the solar sail. For that, the designs of the solar sail, booms and SSM's structure are downselected based on the figures of merit defined from the mission's propulsion system analysis. Next, the sizing of the sail area and booms length is carried out. This has been achieved by a code Matlab® developed for the purpose. Eventually, the detailed design of the SSM is presented. The final result is a 3D Computer-aided Design (CAD) supplemented by 2D drawings, both made with CATIAv5. Note that these drawings are attached as separate appendices.

6.1. CONFIGURATION DOWNSELECT

The first phase of every engineering design project is the conceptual design; that is to say, a selection process of the main configuration parameters. Consequently, the decisions made in this first step will determine all the following design steps as well as the final space propulsion system's features and performance. In this way, the design of SSM for a nanosatellite involves a multidisciplinary view. This is fundamental because the solar sail configuration and the type of boom selected will imply fitting the module in 2U, designing the deployment process and reaching the final selenocentric orbit. Therefore, during this stage the following major configuration elements must be considered in the downselection process:

- **Solar sail.** It encompasses the sail general configuration as well as the sail membrane. Note that the general configuration is deeply related with the membrane global form, with the form of membrane quadrants and with the type of boom utilized. The major solar sail related points to discuss are the general configuration, the form of the quadrants (if any), membrane folding way, sail-boom attachment system and membrane materials. These downselection is described in section 6.1.1.
- **Booms.** The aforementioned sail general configuration drives the selection process of the booms. As well, the working space environment and the packing capabilities also determine the quantity and type of booms. Thereby,

in the boom downselection the type, the utilized deployment system, the configuration structure and the materials must be consciously determined. This procedure is exposed in section 6.1.2.

- **SSM structure layout.** This aspect constrained by the nanosatellite configuration, by the deployer (see [20]) and by the solar sail deployment process. Therefore, the downselection of the structure layout must be done once the sail and the booms are determined. Precisely, this is described in section 6.1.3.

The decision-making process in this conceptual design phase is driven by the mission propulsive requirements established in section 4.1.3. However, these propulsive requirements can be fulfilled in several ways, bearing in mind the broad number of available engineering solutions. Thereby, the chosen design is based on design criteria stated in few objectives to be pursued. These design criteria represent the design philosophy and the route map for achieving a successful final design. In the case of the SSM, the design criteria followed are summarized here below:

- **Fulfillment of mission propulsive requirements.** The solar sail shall be capable of propelling a 6U nanosatellite to reach a final selenocentric orbit departing from GEO and following a spiral orbit to escape from Earth. The SSM shall be packed into a 2U volume and have a lifetime of 5 years.
- **Maximizing the solar sail area while minimizing the SSM mass**. The magnitude of the SRP that acts on a solar sail while performing an orbit at 1AU distance from the Sun is small (around $4.6 \cdot 10^{-6}\mathrm{Pa}$). Therefore, the greater the area the greater the exerted force. Additionally, in order to increase the obtained acceleration, which is proportional to $\mathrm{A/m}$, it is necessary to minimize the satellite mass. That is to say, a high thrust to mass ratio is desired. Due to the fact that this project only concerns the SSM, the mass minimization is just applicable to the SSM.
- **Preference for space tested technology.** In order to minimize the design risks while reducing testing, it is preferred to select a space-qualified technology rather than a new approach. Note that although some of the components applied in the solar sail have TRL 9, the general TRL of the entire solar sail as propulsive subsystem is TRL 6. Therefore, in order to enhance the TRL of the final design, a minimum margin value of TRL 5 for the different components is established.
- **Preference for Commercial Off-The-Shelf (COTS) components.** One of the fundamentals of CubeSats is the utilization of Commercial Off-The-Shelf (COTS) components, with special focus on the electronics. The implementation of this kind of components allows the reduction of risk and cost and increase the reliability, mainly because they are already space

tested and qualified. Therefore, taking into account that the SSM is designed to be the propulsive system of a 6U nanosatellite, it is desired to follow the philosophy of CubeSat. Thus, priority is given to COTS components.

- **Design for Manufacturability (DFM).** In case no COTS components are available to solve a given problem, it is required to provide an innovative solution. In this case, priority is given to DFM, which implies designing the different components with the objective of making them easy to manufacture.
- **Minimization of Cost.** In order to guarantee the feasibility of the design, it is desired to minimize the final cost. For that, it is important to choose simplicity in design rather than for complexity, even if this may mean sacrificing some performance. As well, some of the criteria aforementioned (e.g. preference for space tested technology, use of COTS components or DFM) are in agreement with the reduction of the SSM development budget.
- **Plug and Play (PnP) module.** PnP is a manufacturing concept that deals with taking standard COTS components, assembling and integrating them within a satellite in a short period of time. The SSM here presented is meant to be a PnP module; precisely, the module corresponding to the propulsion subsystem. Therefore, it shall fulfill the CubeSat general dimensional, structural, electrical, operational and testing requirements stated in [19] and adapted for the requirements of a 6U CubeSat.

Taking into account the aforementioned criteria, in the next three sections, the downselection of the sail, the booms and the SSM structure layout are presented. Then, a summary of the final conceptual design is presented in the section 6.1.4.

6.1.1. SAIL DESIGN SELECTION

The first step of the conceptual design is determining the solar sail general configuration. Practically, every detail in the following design steps will be conditioned by the choice of this configuration. Considering that it is deeply related to the global form of the membrane, the form of the membrane quadrants and the type of booms adopted, an overall analysis must be done in Table 6.

Sail configuration downselect	
Square 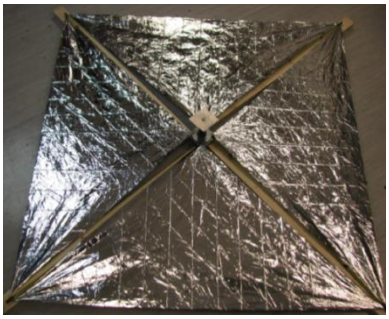	In this type of solar sail, generally only four booms are required. It is easy to fold and manufacture. So far, it is the highest thrust-to-mass design ground-assembled and tested. It has been space tested with IKAROS and NanoSail-D2. The main drawback is that it withstands the shear stress; so wrinkles are formed. Moreover, it must be stable in the 3D to allow the required precise pointing to control Sun-provided thrust (3 axis stabilized).
Heliogyro 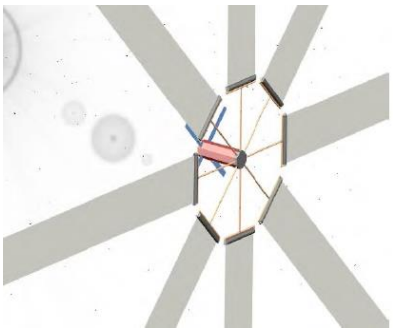	It is composed by several separate vanes that are deployed thanks to the spinning motion of the s/c (generally located at the center). It must rotate to be stable. Furthermore, attitude control can also be achieved changing the angle of the blades (cyclic and collective pitching). Its main advantage is based on the simple deploying mode of the sail. Nonetheless, it is not space tested and it is heavier than the square sail.
Disc (circular) 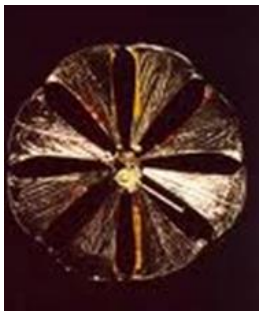	The centrifugal acceleration due to the spin puts the sail material under tension, thus keeping the sail flat. It can be also easily deployed due to the centrifugal acceleration. Furthermore, it does not withstand shear stress, hence it does not produce wrinkles. Nevertheless, it is more complicated to manufacture and it requires at least 8 booms. It must be controlled by moving the center of mass relative to the center of pressure. Similar to the Znamya 2 solar mirror.

Table 6. Sail configuration downselect (sources of the images: square [13], heliogyro [29] and disc [16]).

The square solar sail seems to be the best option, because of two main points: 1) it has been space tested and 2) it offers the best thrust-to-mass ratio. Although it has the disadvantage of wrinkles, they can be more or less avoided by choosing an adequate boom-membrane packing configuration as well as through a proper deployment system. Furthermore, it is the easiest sail configuration to be manufactured. Moreover, note that the square solar sail can be realized by three different forms of membranes discussed in Table 7.

Type of square-shaped sail downselect	
Triangular quadrant 	It is the type of quadrant mainly used in solar sails for nanosatellites. It is easy to manufacture, fold and deploy. The main drawback is that due to being tautened from three points, wrinkles may appear. As well, while increasing the size of the membrane, reinforcements in the three points are required. It is the type used in NanoSail-D and –D2, LighSail-1 and CubeSail (Europe).
Trapezoidal quadrant 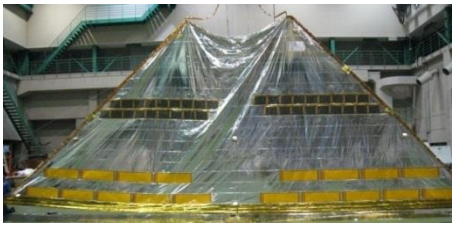	It is used in bigger solar sails. The smallest side of the trapezoid is connected to the s/c bus through a hardness and tether. Due to being tautened from four points, wrinkles are les relevant than in the triangular quadrant. It has been used in IKAROS.
Single membrane 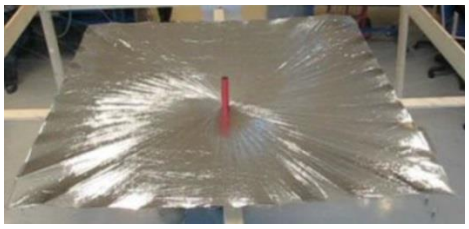	It is the most efficient type of sail considering the encompassed area. It is relatively easy to manufacture. However, the folding is complicated, especially when the size of the membrane increases (see Pattern 4 of Table 8). Additionally, the deployment integration with the 6U satellite structure layout is complex.

Table 7. Type of square sail downselect (sources of the images: triangular [30], trapezoidal [31] and single membrane [32]).

Between the three types of square-shaped, the triangular quadrant seems to be the best choice. However, the single membrane is not already discarded, although preference is given to the triangular one. The final selection between them is made after the discussion of Table 8. Moreover, bearing in mind the small space available for attachment between the sail container and the membrane, it is better to tauten the membrane from three points rather than from four points. Thereby, the trapezoidal quadrant is not further considered.

Folding influences the sail efficiency as well as how the sail deploys. It is important to avoid the potential of tearing. Moreover, the creases impact on the sail efficiency and so it must be minimized. Finally, the folded volume and the folded dimensions may be considered too. Five different ways of folding the membrane are considered in Table 8, obtained from [32] and [30].

Membrane folding downselect	
Pattern 1 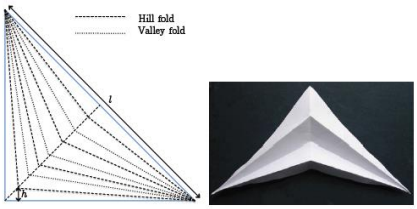	It uses a single fold in the middle as a guide for the subsequent folds. It is coiled around a spindle, easing the connection of the right-angle corner to the spindle. It is easily and compactly stowed. Nonetheless, large tension is required to keep the sail taught when the quadrants are deployed, because the tensions lines that keep the sail tauten are along the crease lines.
Pattern 2 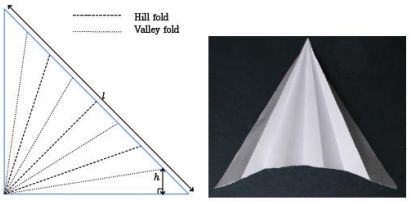	The crease lines begin at the right-angle corner of the triangle and spread out evenly. It is coiled around a spindle. It has two main advantages: a) the crease lines are not parallel to the tension lines and so that, a smaller force is required to tighten the sail and b) Folding and stowage are easier than in Pattern 1. Nevertheless, all the crease lines converge to a single point in the right angle of the membrane and this weakens the membrane. If it is just the attachment to the bus, a reinforcement should be required thus thickening the sail.
Pattern 3 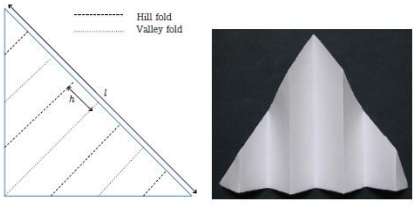	Crease lines are parallel to each other. It is coiled around a spindle. Its main pros are: a) there are no crease lines convergences to weaken the membrane, b) the tension lines and crease lines are closely perpendicular, c) folding is quite easy for any membrane size and, d) it is the best pattern to preserve the efficiency of the sail. Its main disadvantage is that the membrane is quite loose around the spindle. This is not really a hard problem if the SSM is covered by the bus side panels. It is used in CubeSail ([32]).
Pattern 4 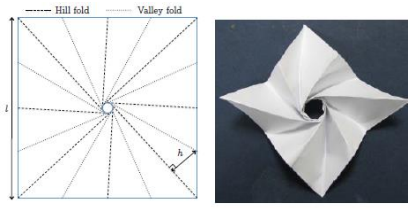	Coiled around a spindle, it is used to fold single membrane sails. It is the most compact way to fold a sail. Although there is a patented machine to fold the sail automatically [33], the folding complicates while the size increases. It is worse than Pattern 3 for preserving sail efficiency.

Z-folded & wedged 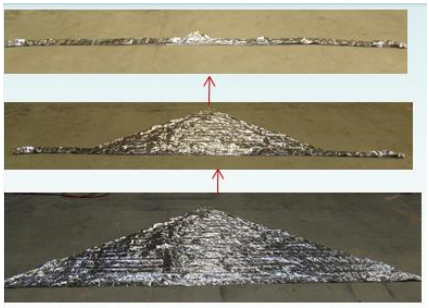	This kind of folding goes without coiling around a spindle. It is easy to fold and it is compact. It can be optimized to be fitted into different sizes of folded volume and dimensions independently of the membrane sizes. It provides a path for gases to escape and it has been verified with vacuum chamber test. Nonetheless, it should be restrained and covered by bus side panels. As well, it is not good to preserve the sail efficiency compared to the Pattern 3. It is used in LightSail-1 (see [30]).

Table 8. Membrane folding downselect (sources of the images: Patterns 1-4 [32] and z-folded [30]).

After considering Pattern 4, the single membrane option was discarded due to the complexity associated to the folding, especially when the size of the membrane increases, the single membrane was discarded. Furthermore, from Table 8 Pattern 3 looks the best candidate, thanks to its capability to preserve the membrane efficiency. Nonetheless, bearing in mind the height limitation to place the spindle into the SSM (less than 7.5cm available in the best case) and that the packing efficiency decreases while shortening the spindle, it is better not to use a spindle to fold the membrane. Note that the packing efficiency is defined as the packet sail volume per sail area. Moreover, the structure layout of the 2U SSM within the 6U nanosatellite is not suitable to utilize only one axis to guide the two typical spindles used to coil the four quadrants of the membrane and the boom, respectively, such as in case of NanoSail-D [10] and CubeSail [13]. Thereby, after discarding all of the coiled methods, the Z-folded and wedged is selected as membrane folding method.

Apart from the folding method, the sail attachments which are those parts that connect the sail to the s/c structures (e.g. boom or sail containers) must also be chosen. Three types of attachments are discussed in Table 9.

Sail attachment downselect	
Rigid triangle 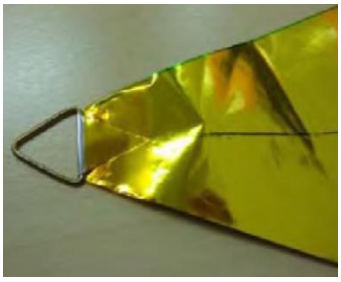	It attaches a rigid triangle to each of the corners and so, it requires thickening the membrane. Nonetheless, the thickening is not as relevant as in case of the eyelet corner. It assures conductivity and is easy to build. The main pro is that the membrane is not holed. However, the stretching performance is asymmetric.

Taped string along the border 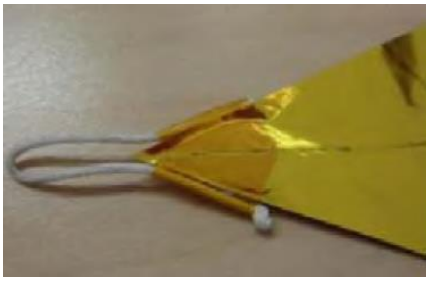	It consists in attaching a string along the border of the membrane. It is the easiest one to manufacture, the lightest and it assures the continuity of the membrane. As well, it provides flexibility to the joint. Its main disadvantage is that is not conductive. Besides, if the junction with the membrane is not well-done, may be break during tautening.
Eyelet on corner reinforcement 	In order to make the hole, it requires thickening the membrane and so that, its mass and volume is increased. Nonetheless, it provides symmetric and good tautening. As well, it is conductive and so that it helps not overcharging the membrane. Another drawback is that it interrupts the continuity of the membrane. It has been used in NanoSail-D &-D2 as well as in LightSail-1.

Table 9. Membrane folding downselect (sources of all the images [34]).

As suggested in [35], solar sail charging analyses demonstrated that minimal differential potentials and consequently, minimal threat of electrostatic discharge occur when the s/c is entirely made of conductive materials, as anticipated from standard guidelines for mitigation of spacecraft charging issues. Thereby, it is important to choose conductive sail attachments. Subsequently, the taped string along the border is rejected. The trade-off between symmetric stretching or smaller thickness (eyelet on corner vs. rigid triangle) is finally decided taking into account the aforementioned third design criterion. In this way, as the eyelet on corner has been already space tested, it is selected as the attachment system for the SSM's membrane. It is evident that the corners shall be reinforced; nonetheless, this is not insuperable problem and it should be considered during the sizing process. Furthermore, similarly to NanoSail-D, the joint between the eyelet corner of the membrane and that of the boom, the strings and a spring are going to be implemented too. As stated in [36], the beauty of this method is that it allows for the booms to be stored in the hub and the four quadrants to be stored in a nearby location with only the string having to pass through the interface. The spring is included to withstand thermal distortions. Indeed, it allows the adjustment of the stress caused by the different dilation coefficients between the booms and the membrane.

To end up the sail design downselect process, it is necessary to select the material for the membrane. The summary of several candidates of solar sail membrane materials is given in Table 10. These materials were selected due to their manufacturability, application and availability. Note that the critical properties for solar sail materials are low areal density, which means $\leq 1\mathrm{g/m^2}$ and long lifetimes, which means more than 10 years.

Sail membrane material downselect			
Name	**Base material**	**Reflective layer**	**Emissive Film**
Aluminized CP-1™	CP-1™	Aluminum	Aluminum
Aluminized Mylar™	Mylar™	Aluminum	Aluminum
Aluminized Mylar™ with Chromium	Mylar™	Aluminum	Chromium
Aluminized Kapton®	Kapton®	Aluminum	Aluminum

Table 10. Summary of solar sail membrane material candidates.

Solar sail materials with Mylar™ as base material are discarded due to their poor resistance to UV radiation. Moreover, although both CP-1™ and Kapton® have good UV resistance, as stated in [37] the main advantages that show CP-1™ with respect to Kapton® is its excellent thermal properties. Since CP-1 ™ is a colorless polyimide, with a solar α/ε of 0.1 compared to 0.7 of Kapton®, CP-1™ films are able to operate at much cooler temperature than the Kapton®. Furthermore, CP-1™ is a space-tested, space-durable material that can be stored for long period of times without property degradation. Finally, it should be pointed out that the thinnest material commercially available in the case of Kapton® is 8 microns thick with an areal density of $\sim 10\mathrm{g/m^2}$ (source [38]). In the case of CP-1™ the thinnest material commercially available is 2.5 microns thick with an areal density of $\sim 5\mathrm{g/m^2}$. Therefore, bearing in mind the outstanding properties of the CP-1 ™, it is chosen as the material for the SSM membrane. Nonetheless, before finalizing this downselection process, it is necessary to solve a doubt, i.e. including or not including an emissive film to the CP-1™: according to [39], this material does not require an emissive film whereas [35] and [40] suggested to use conductive surfaces on the backside of the sail in order to achieve an equipotential s/c structure and reduce the threat of discharges due to differential charging that could damage the film sail. So, a conductive emissive layer made of Aluminum is also added to the CP-1™ base material. As the CP-1™ manufacturer contemplates it, this little addition is completely feasible (see the CP-1™ datasheet included in ANNEX D).

6.1.2. SELECTION OF THE BOOMS

Solar sail booms are the structural element used to hold and tighten the solar sail membrane. As well, they drive the deployment process. Consequently, an inadequate downselection may cause the failure of the mission. Note that the booms downselection process is guided by the solar sail configuration, the operational space environment and the packing capabilities. As for the sail configuration, the square-shaped solar sail has been selected, which implies that at least four booms are required. The mission working environment encompasses geocentric distances from GEO to the Moon's vicinity. Therefore, there is influence of SRP, gravitational forces of Earth, Sun and Moon. Besides, at the beginning of the mission the spacecraft will absorb a considerable amount of radiation because GEO is inside the outer Van Allen radiation belt. On the other hand, due to the high initial altitude, trajectory departs from GEO, no drag force will act on the sail.

The first step in the selection process is to choose the type of boom from the three kinds available. Their characteristics are analyzed in Table 11.

Boom type downselect	
CoilABLE Masts 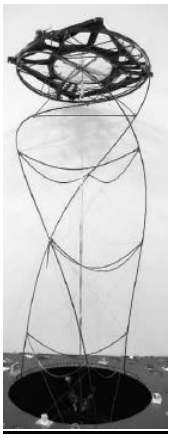	Widely used in space and available in many configurations (TRL 9 in general [41]). It can self-deployed self or extend driven by a motor. The specific mass is small ($\sim 0.24 \mathrm{kg/m}$). It has very good stiffness to weight ratio, high dimensional stability, it is conductive and exhibits robust deployment. It is usually used in big solar sail (e.g. the Layard spring system used in 20m x 20m solar sail tested by NASA). Additionally, the packed volume with respect to the volume available in a 2U SSM is big. It is used in IKAROS.
Inflatable booms with sub-T_g rigidization 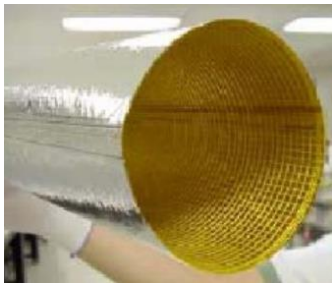	It is deployed by blowing it up. Then, it quickly becomes rigid, due to the boom's material. It is mechanically simple with few moving parts. Furthermore, the boom itself is light, conductive and it provides the possibility to scale to larger sizes without increasing the mass density. Nonetheless, while increasing the length, an additional spread system is required. Tested in the NASA's 20m x 20m solar sail.

Tapespring 	It consists of a long strip of material possessing a curved cross section. It is really compact, because the geometry of the springs allows to wind and stow a large length of spring around a circular spool through being elastically-strained. Additionally, the boom is not size limited. Furthermore, the TRL in general is high and it has been used since 1960's. Nonetheless, it requires an additional system to deploy and so that, the complexity is associated to the deployment method. It has been used in NanoSail-D & –D2, LightSail-1 and CubeSail (Europe).

Table 11. Boom type downselect (sources of the images: CoilABLE Masts [40], inflatable booms with sub-T_g rigidization [5] and Tapespring [13]).

From the analysis carried out in the Table 11, it can be basically concluded that whilst the first two types of booms are used with large solar sails; the last one is implemented in nanosatellite. So, at first sight, the tapespring boom seems to be the best choice. Nonetheless, the second boom type can be scaled creating medium-size booms. Besides, due to being mechanically simple and thus, more reliable and cheaper, the second type of booms is not disposable. In the case of the CoilABLE Mast, as the packed volume is large with respect to the 2U SSM, it is not further considered. In this way, the final decision whether applying inflatable booms with sub-T_g rigidization or tapespring will be made after analyzing the deployment system of each boom (Table 12).

Boom deployment system downselect	
Axially stowed 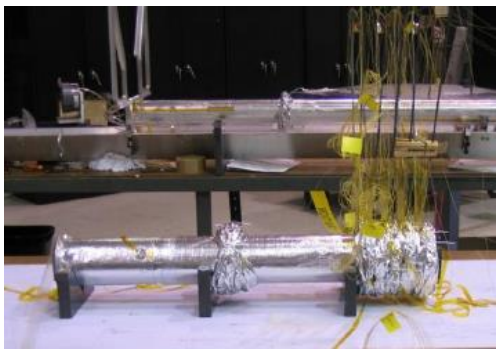	It is the deployment mechanism used with the inflatable booms mentioned in Table 11. The boom is stowed axially at one edge of cylinder that has a gas canister at the other edge. It is safe, simple, reliable and easy to fabricate. The big cons of this system are: a) it is not compact (for $7\mathrm{m}$ deployed boom approximately $5\mathrm{m}$ of deployment system are required [40]), b) one mechanism per each boom is required, c) the gas used to blow the booms should be carried in the s/c and d) booms embedment is complex.

Coiled around a spool 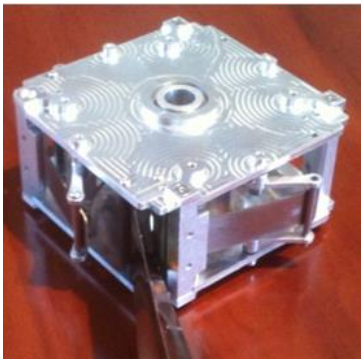	It is the deployment mechanism used with tapespring booms of Table 11. All the booms are coiled around a small spool and deployed through the rotation of this spool. It is a highly compact system (e.g. in LightSail-1 about 16m of boom are stowed in less than 0.5U). The main disadvantage is its complexity (design and manufacture) compared to the axially stowed one. Furthermore, it requires a motor to help in the deployment system. It is used in NanoSail-D & -D2, LightSail-1 and CubeSail (Europe).

Table 12. Boom deployment system downselect (sources of the images: telescopic [40] and coiled around a spool [30]).

Although the mechanism with the boom coiled around a spool is more complex, it is the best choice taking into account its compactness and the requirement to fit the entire SSM in 2U. As a result, the booms selected to be used in the SSM are tapespring booms. Hereunder, in Table 13 the shape of the tapespring boom is discussed. The tapespring shape selected shall be easy to manufacture, easy to coil and shall increase as much as possible the inertia in order to be as stiff as possible. From the state of the art, the most important six types of tapesprings have been selected to analyze: TRAC, STEM with overlap, lenticular boom, (tapespring, () tapespring and STEM without overlap.

Type of Tapespring boom downselect	
TRAC 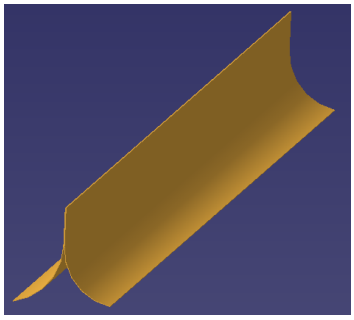	Developed by the AFRL, it incorporates the highest cross-sectional inertia and package height ratio. Due to the fact that buckling in the boom occurs along the most compliant axis, the lowest quantitative moment of inertia for each cross-sectional shape provides the valuable insight into the overall stiffness of the boom. It has TRL 8 ([41]). Nonetheless, it is difficult to construct, especially the flange zone. As well, it has poor torsional stiffness compared to the lenticular boom due to being an open cross-section. Finally, further development of Finite Element Method (FEMs) is required to predict properly its torsional behavior ([42]). It has been used in NanoSail-D &-D2 and LightSail-1.

STEM with overlap 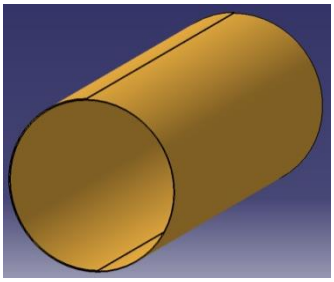	The Storable Tubular Extendable Member (STEM) is composed is composed of a single strip that, in the deployed state, forms a circular cross-section. In this case, through a part of this circular cross-section material is overlapped, which increases the stiffness and inertia compared to the STEM without overlap. It has TRL 9 ([41]). Its main pro is that its simplicity to fabricate and pack. However, a) it has really poor torsional stiffness, due to being an open cross-section and b) it results in a large package height. Nevertheless, the torsional can be enhanced by generating friction between the overlapped layers.
Lenticular boom (CTM) 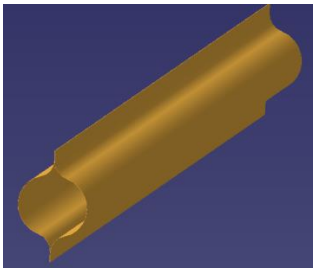	It is also known as Collapsible Tube Mast (CTM) boom. It is made from a pair of symmetric bell shape halves bonded at the edges. Although it can be flattened as the STEM boom, once deployed it forms a closed section, which is structurally efficient [42]. Indeed, it has the greatest torsional stiffness between tapesprings. It has TRL 9. For the same deployed circumference cross-section size, it has half package height compared to STEM; although it is still relatively tall with respect to the TRAC boom. Furthermore, for same package height, the moment of inertia of the lenticular boom is lower than that of the TRAC boom. It has been used in CubeSail ([13]).
(Tapespring 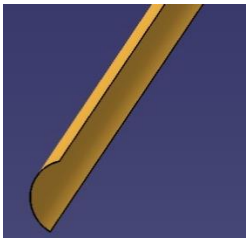	It consists in one semi-circumference tapespring. It is the simplest tapespring and so that, it is the easiest one to manufacture and package. Nonetheless, due to being an open cross-section, it has poor torsional stiffness. Its moment of inertia is really small too. Therefore, it tends to buckle easily.
() shaped boom 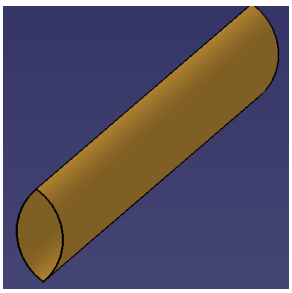	It is made from a pair of symmetric semi-circumference tapespring bonded at the edges. Although its torsional stiffness is greater than that one of the open cross-sections, it is complex to be bonded making it less reliable. Furthermore, its moment of inertia is smaller than that of the lenticular boom.

STEM without overlap	
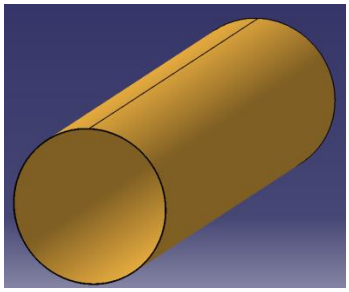	It is also composed is composed of a single strip that, in the deployed state, forms a circular cross-section. However, it does not have an overlapped section and thereby, the stiffness and moment of inertia is smaller compared to STEM with overlap. It has TRL 9 ([41]) too. Although it is simple to manufacture and package, it has really poor torsional stiffness as well as large package height.

Table 13. Type of Tapespring boom downselect.

Taking into account the structural efficiency of all of the types of tapesprings presented in Table 13, there are two potential candidates to be used in the SSM: the TRAC boom and the lenticular boom, also known as CTM. While the former has the highest moment of inertia and package height ratio, the latter has the greatest torsional stiffness and a good moment of inertia. At this moment, in order to select the most suitable tapespring shape, the third design criterion is applied: preference for COTS components. On the one hand, as already mentioned, the TRAC boom is a boom developed and manufactured by the AFRL especially for the NanoSail-D mission and later, provided to The Planetary Society to be implemented in LightSail-1. On the other hand, the lenticular boom has been invented in the 60's during the United States space program ([66]) and to date, many companies have the technology to manufacture it. Furthermore, it should be pointed out that the booms of the SSM shall not withstand the drag force. Consequently, the applied bending moment on SSM booms is less stringent compared to those of NanoSail-D and –D2 and LightSail-1 and so that, the moment of inertia of the cross-section could be smaller. As a result, bearing in mind the aforementioned reasons, the lenticular boom, also known as CTM boom, is selected.

Once the types of booms have been chosen, its configuration within the SSM structure and consequently, within the 6U structure should be decided. Bearing in mind the available space in a SSM of 2U of volume, three possible configurations are considered: centered, diagonal and web. These three configurations are analyzed in Table 14. Note that during this downselection process it is fundamental to maintain the symmetry with the purpose of easing the attitude control.

Boom configuration within structure downselect	
Centered 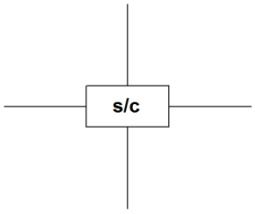	In this case, the booms are deployed from the center of the SSM. With this configuration, the booms are easily deployed, but not the four quadrants because they will collide with the SSM structure. Furthermore, if the coiled booms have the same length, once deployed the length of the booms out of the s/c will be different.
Diagonal 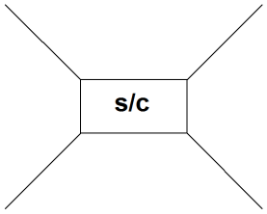	Here the booms are deployed from the diagonal of the SSM. Whereas the deployment of the booms is more complicated, the quadrants will be deployed without colliding. As well, it provides the possibility to make use of the stiffness of the SSM to tauten the booms. Moreover, if the coiled booms have the same length, once deployed the length of the booms out of the s/c will be the same.
Web 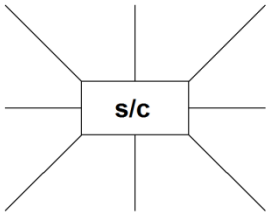	This configuration is intermediate between the centered and diagonal configuration. Its only advantage is that it provides greater stiffness. However, it is complicated to deploy and so , less reliable. In addition, for the same SSM, the booms would be shorter than in case of the centered or diagonal configuration.

Table 14. Boom configuration within structure downselect.

Considering the pros and cons of the three configuration of Table 14, the diagonal seems to be the best configuration. In this way, it is preferred to solve the complexity of booms deployment rather than sail quadrant deployment. Note that sail quadrants are more prone to tearing due to their small thickness.

Finally, to conclude the booms material must be chosen. In this case, it should be pointed out that the chosen material is constrained by the selected deployment mechanism as well as by the external forces and environment. Considering a safety factor of 1.0 the material shall not exceed a maximum strain of $\epsilon_{\max} \leq 0.4\%$ (source [43]), so that the stress levels are moderate. As mentioned in [36], it is not recommended to use materials thinner than 0.1mm (flattened) and it is desired to select material with high stiffness with the purpose of increasing allowable natural frequencies and critical loading. In this way, from the state of the art four types of boom materials have been considered and discussed in Table 15.

Boom material downselect	
Metallic: Elgiloy® steel 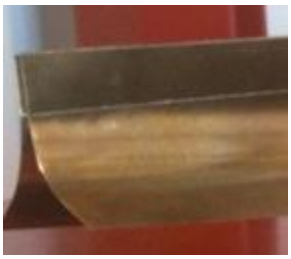	Elgiloy® is a high performance stainless steel, widely utilized in aerospace. It has excellent mechanical characteristics. It is corrosion resistant, exhibiting high strength, good fatigue life and ductility. Its main drawback is that it is heavy. It has been used in the TRAC booms of NanoSail-D and –D2 and LighSail-1.
Metallic: Cu-Be with Kapton® sleeve 	In this case Copper-Beryllium half-shells are covered by a Kapton® film. This film holds the two blades together, acts as a thermal barrier and stops atomic oxygen at LEO from reacting with blades and degrading them. It is simple to manufacture but it is not space tested. It is used in the testing process of CubeSail ([13]).
CFRP 	Carbon-fiber Reinforced Plastic (CFRP) is used to fabricate Bi-stable reeled (BRC) booms. In this type of booms single half-shell is made to be bi-stable. Its main advantage is that deployment energy is presented only at the transform between two states. As well, no constrain inside the deployment mechanism is required. It is used in the testing process of CubeSail ([13]).
Sub-T_g rigidizable fibers with bonded Kapton® bladder & Mylar™ 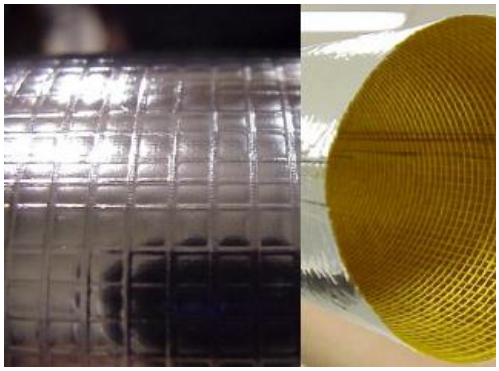	It consists of sub-T_g rigidizable material made from composite unidirectional fibers. Fibers are impregnated with resin that becomes rigid below -20^oC and it contains a spiral wrap that stabilizes the longitudinal fibers allowing over-pressurization for deployment anomalies. Furthermore, it has bonded Kapton® bladder and Mylar™ to make an encapsulation skin that carries shear. It is highly mass efficient ($\sim 36 \mathrm{g/m}$ linear density [40]) and it offers good mechanical properties. It is used in inflatable booms.

Table 15. Boom material downselect (sources of the images: Elgiloy® steel [30], Cu-Be with Kapton® sleeve [13], CFRP [13] and sub-T_g rigidizable fibers [40]).

In order to select the proper boom material, it should be remembered that according to [35], minimal differential potential and thereby minimal threat of electrostatic discharge occurs when the s/c is entirely constructed of conducting materials. This fact is anticipated from standard guidelines for mitigation of s/c charging issues. Consequently, metallic materials rather than dielectric materials for the booms are preferred. In this way, the last two materials from Table 15 are discarded. Furthermore, between the metallic materials it is manifest that the Cu-Be with Kapton® sleeve is against the design criterion of preference for space tested technology. Thereby, Elgiloy® steel is chosen, which not only fulfills the SSM design criteria but also provides exceptional mechanical properties. Its main characteristics are illustrated in section 6.1.4.

6.1.3. STRUCTURE LAYOUT SELECTION

To sum up, the structure layout of the SSM must be downselected. For that, it is important to bear in mind the configuration of a 6U satellite, such as the one attached in Figure 6. According to this s/c layout, the SSM shall be connected to the s/c to the rectangular side of 20cm x 10cm. Therefore, the available height is 10cm. This fact requires the innovation of the structure layout with respect to other nanosatellites configuration. Note that in the case of NanoSail-D and –D2, LightSail-1 and CubeSail (Europe), the sail container (or deployment system) is located over the boom deployment mechanism and it occupies around 1.5U (10cm x 10cm x 15cm). In addition, the boom deployment mechanism is located just at the bottom occupying 0.5U (10cm x 10cm x 5cm). As this kind of design is incompatible with the structural layout of a 6U s/c, three different structural configurations for the SSM are analyzed in Table 16.

Structure configuration downselect	
Sail and booms coiled around two different axes 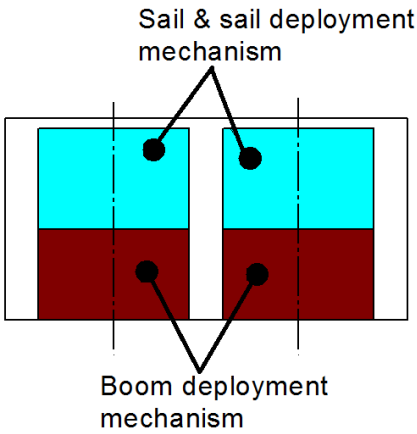 	This structural layout is an evolution of the one already used in Nanosail-D, -D2, LightaSail-1 and CubeSail. Two separated axes are used. Each axis guides a spool for two membrane quadrants (above) and the mechanism for two booms (under the sail mechanism). With this system longer booms can be coiled. Nonetheless, while the deployment of the booms is simple, the attachment of the sail to the booms and the sail deployment is really complex. Once deployed, due to the lack of complete symmetry, additional loads may be generated making more difficult the attitude control.

Deployable SSM 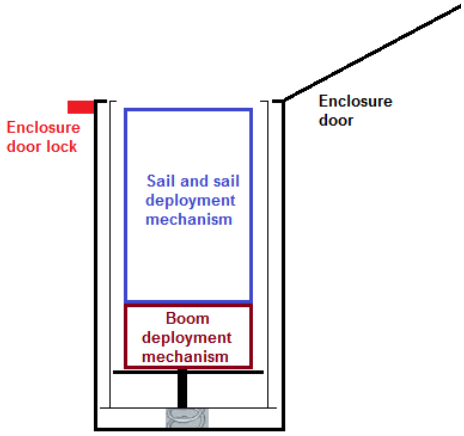	It is also similar to the structure used in NanoSail-D, -D2 and CubeSail. Indeed, in this case the sail deployment system is located over the boom deployment mechanism. Both deployment systems are attached through an axis to a platform that can be telescopically deployed once the 6U satellite is in space. The main advantage of this configuration is that it utilizes a space-tested configuration. Nonetheless, the reliability of the system is poor, since it requires a SSM pre-deployment before deploying the sail. Furthermore, the 2U volume is not entirely used for the sail.
Integrated SSM 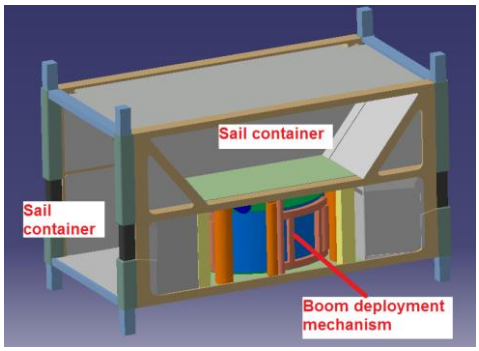	In this configuration the boom deployment mechanism is located in the middle of the 2U volume occupying around 0.5U. The rest of the volume is divided into four different compartments to keep the sail membrane quadrants. It is compact and efficient and after deployment, the sail keeps symmetric. Although the deployment of the booms may not be straightforward, the membrane may be easily deployed. Its main drawback is that the design is quite innovative and complex.

Table 16. Structure configuration downselect.

The analysis of Table 16 allows to conclude that the SSM is a challenging puzzle, due to the requirement of fitting many elements into a limited volume. In this way, in order to reduce the risk of failure, from the three configurations the most reliable one should be selected. Consequently, the second structure configuration, called deployable SSM is discarded. In addition, taking into account that it is aimed to maximize the sail area while minimizing the mass, the SSM compactness is a fundamental factor. Moreover, the SSM structure should the deployment process, particularly in the case of the sail membrane. Note that from the two structure configuration potential candidates, the integrated SSM better fulfills both requirements. Therefore, it is selected as the SSM structure configuration.

To end up with the downselection process, it is required to define the material to be used in the structure of the SSM. In this case, the selected material is

constrained by the CubeSat general dimensional, structural, electrical, operational and testing requirements stated in [19] and adapted for the requirements of a 6U CubeSat. By considering characteristics such as manufacturability, availability and cost, three potential candidates are described:

- **Metallic: Steel alloys.** They have excellent mechanical properties at relatively low cost. Nevertheless, due to their high density. they are not very suitable for limited weight applications such as a nanosatellite. However, for some critical elements (e.g. screws, washes, shafts, joints, etc.) they are good candidates.
- **Metallic: Aluminum alloys.** They are very light materials and have good mechanical properties, yet not as good as steel alloys. Mainly, for these reasons, they have been widely used in aerospace for structural applications. Additionally, they have a great resistance to corrosion due to the phenomenon of passivation. Their cost is moderate.
- **Composites: Carbon-fiber Reinforced Plastic.** It is a very lightweight material with outstanding mechanical properties. It is a very stiff material, which is desirable for structure applications. However it is considerably more expensive than aluminum and steel. In addition, manufacturing with CFRP is a complex process when compared to steel or aluminum. Moreover, it is very vulnerable to UV because it is a polymer, so that its chemical chains tend to be degraded. Hence, for planetary missions where the space environment can be have large UV radiation dose it is recommended to protect the CFRP.

As already mentioned, [35] recommended constructing the s/c entirely of conductive materials in order to minimize the potential differentials and threats of discharges. Thereby, the composite materials are discarded. In addition, between the metallic materials, Aluminum alloys seem to be the best choice. This is in compliance with the CubeSat structural requirement stated in [19][19], which proposed the use of materials with thermal expansion similar to that of Aluminum 7075-T73. Specifically, they suggested the utilization of Aluminum 7075 or 6061-T6 for the main structure of the s/c, which in this case corresponds with the structure of the SSM. From the two Aluminum alloys proposed by [23], the Al 7075-T6 has been chosen. Although the Al 7075-T6 is denser than Al 6061-T6, the mechanical properties of the former are better, as shown in Table 17.

Name	**Al 7075-T6**	**Al 6061-T6**
Ultimate Tensile Strength	572MPa	310MPa
Tensile Yield Strength	503MPa	276MPa
Density	2810kg/m^3	2700kg/m^3

Table 17. Comparison table of Al 7075-T6 vs. Al 6061-T6 alloys (source [67] and [68]).

6.1.4. FINAL RESULT OF THE CONFIGURATION DOWNSELECT

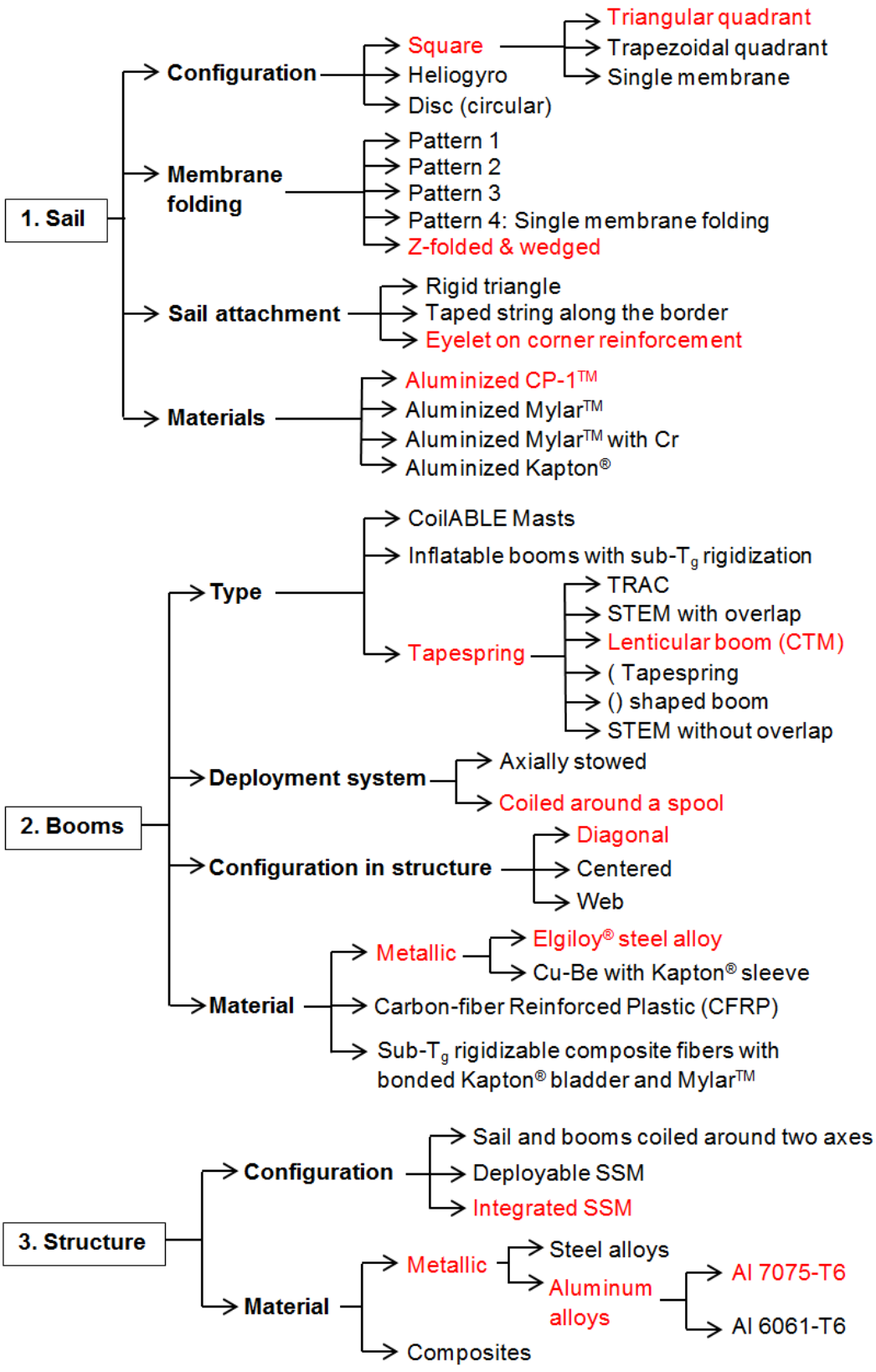

Figure 30. Scheme to summarize the downselection process.

The final result of the downselection process is summarized in Figure 30. The elements highlighted in red are the technologies to be applied in the detailed design of the SSM. Furthermore, here below the main characteristic of the downselected materials are listed. Note that the basically three materials have been selected for the SSM: Aluminized CP-1™ for the solar sail membrane, Elgiloy® steel for the booms and Al 7075-T6 for the SSM structure.

The commercial name of Aluminized CP-1™ is LaRC™-CP1 Polyimide. Most of the characteristics of the LaRC™-CP1 Polyimide are found in the datasheet published by ManTech International Corporation® [69]. Although the entire LaRC™-CP1 Polyimide datasheet is enclosed in the ANNEX D of this project, its most important properties are summarized in Table 18. Note that not all of the properties are included. As well, due to the fact that the Poisson ratio is not specified in the official datasheet, the value given by [44] is used as reference for further calculations.

Aluminized CP-1™ Properties			
Type of property	**Name**	**ASTM Method**	**Value**
Physical and Mechanical Properties	Tensile Strength (1 mil, 23ºC)	D882-02	87MPa
	Young Modulus (23ºC)	D882-02	2GPa
	Tensile Elongation at break	D882-02	16%
	Density	D792-08	1540kg/m^3
	Poisson ratio	--	0.35
Optical Properties	Solar Absorptance (1mil)	E903-96	0.08
	Solar Transmittance (1mil)	E903-96	0.83
	Solar Reflectance (1mil)	E903-96	0.09
	Infrared Emissivity (hemispherical & 1mil)	E408-71	0.45
Nominal thicknesses	$2.5\mu\text{m}, 5\mu\text{m}, 12\mu\text{m}$ & $25\mu\text{m}$.		

Table 18. Summary of the main properties of the Aluminized CP-1™. The ASTM refers to the American Section of the International Association for Testing Materials.

Note that 1mil shown in the Table 18 refers to $\frac{1}{1000}\text{inch}$, which is equivalent to $25\mu\text{m}$.

The physical and mechanical properties of the Elgiloy® steel, used in the booms, are summarized in the Table 19. The source for most of these characteristics is [36], except for the Poisson ratio, which is found in [45].

Elgiloy® Steel Properties			
Name	**Value**	**Name**	**Value**
Tensile Strength	1600MPa	Density	8300kg/m^3
Young Modulus (23ºC)	190GPa	Poisson ratio	0.226
Tensile Elongation at break	$\geq 1\%$		

Table 19. Summary of the main physical and mechanical properties of Elgiloy® steel.

Finally, for the structure of the SSM Al 7075-T6 is going to be used. The typical composition of this Aluminum alloy is shown in Table 20 (source [67]).

7075 Aluminum alloy composition			
Component	**Amount (wt. %)**	**Component**	**Amount (wt. %)**
Aluminum	$87.1 - 91.4$	Manganese	$\text{Max. } 0.3$
Chromium	$0.18 - 0.28$	Silicon	$\text{Max. } 0.4$
Copper	$1.2 - 2$	Titanium	$\text{Max. } 0.2$
Iron	$\text{Max. } 0.5$	Zinc	$5.1 - 6.1$
Magnesium	$2.1 - 2.9$	Other, total	$\text{Max. } 0.15$

Table 20. Summary of the typical composition of 7075-T6 Aluminum alloy (source [67]).

As well, the main physical and mechanical properties of the 7075 alloy with T6 temper are listed in Table 21. The source is also [67].

Properties of the 7075-T6 Aluminum alloy			
Name	**Value**	**Name**	**Value**
Ultimate Tensile Strength	572MPa	Density	2810kg/m^3
Tensile Yield Strength	503MPa	Poisson ratio	0.33
Elongation at Break (1.6mm thickness)	11%	Fatigue Strength	159MPa
Brinell Hardness (500kg load, 10mm ball)	150	Shear Modulus	26.9GPa
Young Modulus (23ºC)	71.7GPa	Shear Strength	331MPa

Table 21. Summary of the main properties of Al 7075-T6 (source [67]).

6.2. DESIGN SIZING

In this subsection the sizing of the solar sail is presented. The sizing process encompasses determining the longitude of the booms as well as the area of each sail's triangular quadrant. Thus, once both are calculated, from the matching process the total area of the sail is obtained. The decisions made in this last stage are driven basically by the first two design criteria mentioned in the introduction of the section 6.1: fulfillment of mission propulsive requirements and maximizing the solar sail area while minimizing the SSM mass. It should be pointed out that the available volume is really limited (only 2U) and so that, the maximum sail area and the length of booms is sized by considering the volume that they occupied in the stowed conditions. Note that the booms first are flattened and then coiled around a spool through the second deployment mechanism shown in Table 12. In the case of the sail, as it is not feasible to include a spindle, the Z-folded & wedged folding method, also used in LightSail-1 is implemented. Both stowing methods shall be fitted in the integrated SSM shown in Table 16.

From some preliminary calculations has been proved that the maximum sail area is limited by the maximum booms length. That is to say, the volume occupied by the folded sail triangular quadrants is not the problem, because it exceeds the volume required to fold the maximum sail area given by the booms longitude. So, as the booms are the critical part, first its sizing process is described in section 6.2.1. Then, the sizing of the membrane is presented in section 6.2.2. Finally, the matching of the sizing process of the booms and membrane is enclosed in section 6.2.3.

6.2.1. SIZING OF THE BOOMS

During the launch phase of the nanosatellite, the booms are flattened and coiled around the spool though the second mechanism shown in Table 12. In order to estimate the total longitude of the booms coiled around the spindle, the following hypothesis is going to be assumed: one boom is coiled around the spindle. Once the total longitude is estimated, it will be divided by four approximating the longitude of each boom. From this value, the available square-shaped area as well as the volume occupied by the coiled booms is calculated. Although it is not the exact method to find longitude of each boom, it is an excellent approximation. Indeed, the final longitude of booms calculated by this method is gives an overestimated value and so that, it is a conservative assumption.

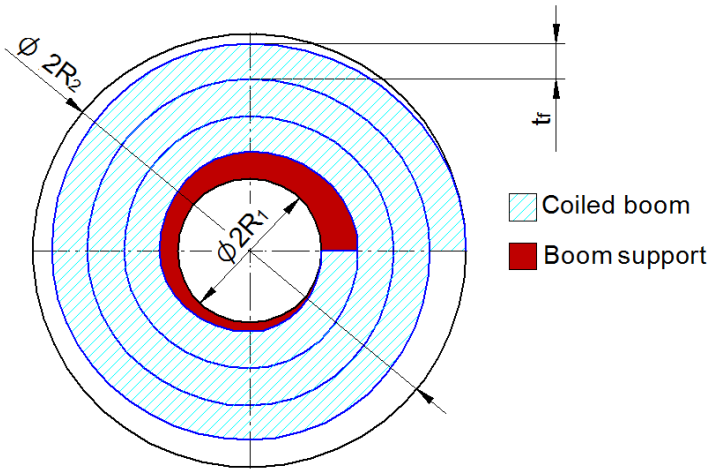

Figure 31. Scheme of a unique boom coiled into the deployment mechanism.

In Figure 31 how a boom is stowed inside the deployment mechanism is schematized. In this figure, R_1 is the radius of the spool and R_2 corresponds to the maximum available radius of the deployment mechanism. As shown, the boom cannot be coiled directly to the spool because it has a constant thickness. Therefore, it is necessary to add a boom support, which shown in brown in Figure 31. This support helps making the transition soft during the first turn of the boom turn so that the strain level is acceptable. As already mentioned, this scheme does not correspond to what happens in the reality. Indeed, in the physical deployment system, there are four booms whose starting point is located at the North, South, East and West of the spindle, respectively. In this way, during the real coiling, the booms are overlapped.

If m_{turn} is the integer number of turns that one boom performs around the spindle, Figure 31 allows to conclude that

$$(m_{turn} + 1)t_f = R_2 - R_1 \rightarrow m_{turn} = \text{integer}\left(\frac{R_2 - R_1}{t_f}\right) \quad (6.1)$$

where R_1 is the radius of the spool, R_2 corresponds to the maximum available radius of the booms deployment mechanism (BDM) and t_f is the flattened thickness of the boom. Note that if t_w is the thickness of the wall of the boom, t_f is equal to $t_f = 2t_w$. As well, the units of R_1, R_2 and t_f in equation (6.1) must be the same. Assuming a conservative sizing, the longitude of the boom when $m_{turn} = 1$, called L_1, can be estimated through the mean radius $r_{mean} = R_1 + \frac{t_f}{2}\ [m]$ as follows:

$$L_1 = 2\pi\left(R_1 + \frac{t_f}{2}\right)\ [m] \quad (6.2)$$

Analogously, with the second turn the longitude gained by the coiled boom due to the second turn L_2 is:

$$L_2 = 2\pi \left(R_1 + \frac{t_f}{2} + t_f\right) = 2\pi \left(R_1 + t_f\left(2 - \frac{1}{2}\right)\right) \text{ [m]} \quad (6.3)$$

So, the total longitude of the boom L_T if $m_{turn} = 2$ is obtained from the addition of (6.2) and (6.3) as follows:

$$L_T = L_1 + L_2 = 2\pi \left(R_1 + \frac{t_f}{2}\right) + 2\pi \left(R_1 + t_f\left(2 - \frac{1}{2}\right)\right) \text{ [m]} \quad (6.4)$$

Generalizing the expression (6.4) for any integer value of m_{turn}, it is provides:

$$L_T = \sum_{i=1}^{m_{turn}} L_i = 2\pi\left(R_1 - \frac{t_f}{2}\right) m_{turn} + 2\pi \cdot t_f \sum_{i=1}^{m_{turn}} i \quad \text{[m]} \quad (6.5)$$

where R_1 is the radius of the spool, t_f is the flattened thickness of the boom and the value of m_{turn} is found through (6.1). Then, if four booms are coiled around the spool, the longitude of each boom, L_{boom} is calculated from expression (6.5) as:

$$L_{boom} = \frac{L_T}{4} = \frac{1}{4} \sum_{i=1}^{m_{turn}} L_i = \frac{1}{2}\pi\left(R_1 - \frac{t_f}{2}\right) m_{turn} + \frac{1}{2}\pi \cdot t_f \sum_{i=1}^{m_{turn}} i \quad \text{[m]}. \quad (6.6)$$

Furthermore, once calculated the longitude of each boom, the corresponding sail area is obtained from:

$$A = 2\, {L_{boom}}^2 \quad [m^2] \quad (6.7)$$

where L_{boom} is defined in expression (6.6).

With expression (6.5), constraining the value of R_2 the total conservative longitude of a coiled boom for different values of R_1 and t_f can be calculated. Then, with the equations (6.6) and (6.7), the longitude of each boom (real) and sail area as a function of R_1 and t_f can be approximated. With these, some graphs to be used in the matching can be performed. Precisely, to obtain these graphs a Matlab® code has been developed implementing expressions (6.1), (6.5), (6.6) and (6.7). The Matlab® code is included in the ANNEX C of this project. The graphs achieved from the compilation of this code are shown and utilized in the matching process of section 6.2.3.

6.2.2. SIZING OF THE SOLAR SAIL QUADRANTS

During the launch phase of the nanosatellite, the four triangular quadrants of the membrane are Z-folded and wedged into the sail containers. Note that due to space limitations, the use of spindles to wrap the four quadrants has been discarded during the downselection process (see 6.1.1). Consequently, in order to avoid possible tearing as well as to facilitate the deployment process of the sail

four individual and separate sail containers (one container per sail quadrant) have been considered in the detailed design.

In this section, a way to assure the maximum sail volume and area that can be fitted in these containers is presented. It should be pointed out that the final aim of the methodology hereunder attached is not to optimize the folding of the sail assuring compactness with minimum Creasing Indicator (CI) (for further information of CI, please see [32]). Indeed, the objective of this section is to describe a conservative procedure to validate that the final sail area is able to be fitted in the 2U SSM with the Z-folded and wedged folding method. For that, it is assumed that its container is a rectangular cuboid of $W_{cont} \times P_{cont} \times H_{cont}$, such as the one shown in Figure 32.

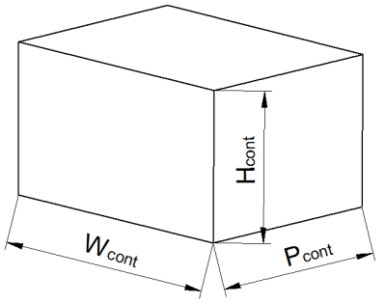

Figure 32. Scheme of the container's volume used to fit the sail.

Furthermore, although the sail quadrant to be fitted is triangular, with the formulation here presented it is approximated to a rectangle of $L \times L/2$, similar to that shown in Figure 33 (Left), where L is the hypotenuse of the triangular shape quadrant. Note that the rectangle area is the double of the real triangular quadrant. The thickness is supposed to be the same as the triangular membrane. Once the rectangular sail is folded, the volume occupied is a rectangular cuboid of $W_{sail} \times P_{sail} \times H_{sail}$ such as the one shown in Figure 33 (Right). Consequently, in this rectangular cuboid two triangular quadrants can be theoretically filled.

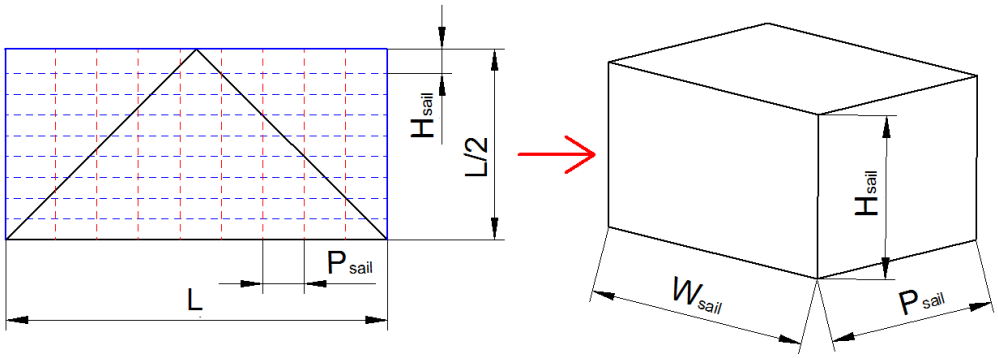

Figure 33. Triangular sail and it approximated rectangular sail (Left) and the volume occupied by the rectangular sail once folded (Right).

Following the concept of the Z-folding, the height of the triangle $L/2$ should be divided in n_h folds so that each fold sizes H_{sail} (see Figure 34 (Left)). So, the required number of n_h fold sizing each one H_{sail} is:

$$\begin{aligned} n_h &= \text{integer}\left(\frac{L}{2H_{sail}}\right) \qquad \text{if } L - 2n_h H_{sail} = 0 \\ n_h &= \text{integer}\left(\frac{L}{2H_{sail}}\right) + 1 \qquad \text{if } L - 2n_h H_{sail} > 0 \end{aligned} \tag{6.8}$$

where L and H_{sail} must be expressed in the same units.

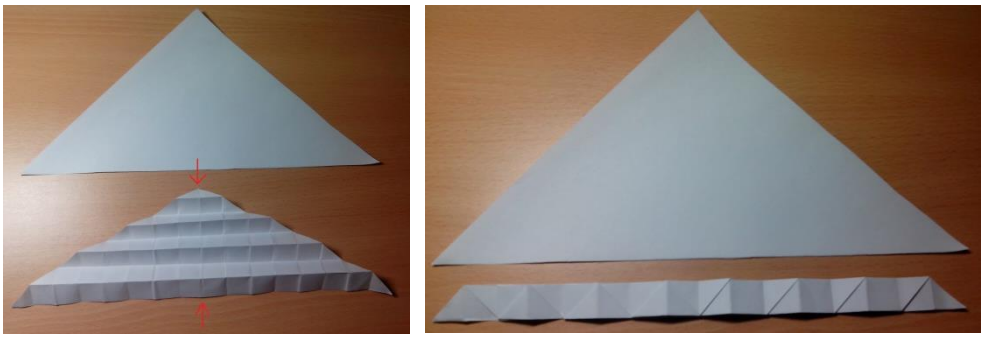

Figure 34. Z-folding process of a triangular shape quadrant (Left) and comparison between not folded and Z-folded triangular shape quadrants (Right).

Once the sail quadrant is Z-folded, it is obtained a rectangular cuboid of longitude L and height H_{sail}, such as the one shown at the bottom of Figure 34 (Right). Considering the aforementioned approximation of rectangular quadrant instead of triangular one, the thickness of the Z-folded rectangular cuboid is constant and equal to:

$$t_1 = n_h t_s \quad [m] \tag{6.9}$$

where n_h is found in expression (6.8) and t_s is the thickness of the sail membrane in $[m]$. Now, the longitude L of this Z-folded rectangular cuboid should be divided into n_p folds so that each fold sizes P_{sail}, as shown in Figure 35 (Left). Thus, the required number of n_p folds sizing each one P_{sail} is:

$$\begin{aligned} n_p &= \text{integer}\left(\frac{L}{P_{sail}}\right) \qquad \text{if } L - n_p P_{sail} = 0 \\ n_p &= \text{integer}\left(\frac{L}{P_{sail}}\right) + 1 \qquad \text{if } L - n_p P_{sail} > 0 \end{aligned} \tag{6.10}$$

where L and P_{sail} must be expressed in same units. The final result after completely folding will be a rectangular cuboid similar to the one shown in Figure 35 (Middle & Right). Nonetheless, as a rectangular shaped quadrant is considered for the formulation instead of a triangular one, the thickness of the rectangular quadrant can be considered constant and equal to:

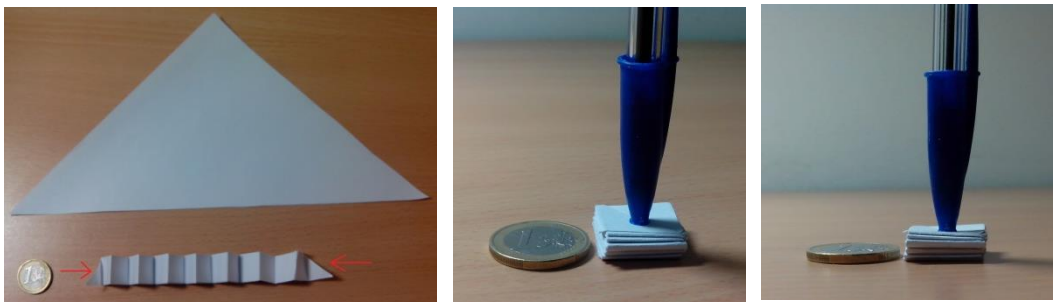

Figure 35. Folding of the longitude L in n_p folds (Left) and completely folded triangular shape quadrant (Middle & Right).

$$W_{sail} = n_p t_1 \quad [m] \tag{6.11}$$

where n_p is found in expression (6.10) and t_1 is found in (6.9). So, substituting the equation (6.9) into (6.11) is finally achieved:

$$W_{sail} = n_p n_h t_s \quad [m] \tag{6.12}$$

where n_h is found in expression (6.8), n_p is found in expression (6.10) and t_s is the thickness of the sail membrane in $[m]$. Finally, in order to verify that the sail can be fitted into the sail container shown in Figure 32, if it is assumed that $H_{cont} = H_{sail}$ and $P_{cont} = P_{sail}$, the requirement to be fulfilled is:

$$W_{sail} \leq W_{cont} \qquad \text{if } H_{cont} = H_{sail} \,\&\, P_{cont} = P_{sail} \tag{6.13}$$

So, substituting expressions (6.12), (6.10) and (6.8) into (6.13) and applying $H_{cont} = H_{sail}$ and $P_{cont} = P_{sail}$, it can be rewritten as:

$$\frac{L^2}{2P_{cont}H_{cont}} t_s \leq W_{cont} \qquad \text{if } H_{cont} = H_{sail} \,\&\, P_{cont} = P_{sail} \tag{6.14}$$

where P_{cont}, H_{cont}, L and t_s must be in same units. To sum up, in Figure 36 the formation of creases due to the folding of the triangular shape sail is shown.

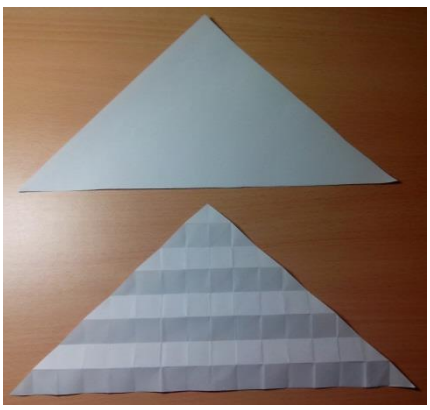

Figure 36. Comparison of a triangular shape quadrant before folding (Top) and after folding and deploying (Bottom). In the latter, the creases due to the folding process are observed.

6.2.3. MATCHING OF THE BOOMS AND SAIL QUADRANTS

In this section the matching of the boom sizing and sail sizing is made. Basically, results applying the formulation presented in sections 6.2.1 and 6.2.2 are obtained and then, from those values a final decision is made.

Firstly, a Matlab® code attached in the ANNEX C of this project has been developed to calculate boom sizing graphs. Precisely, constraining the value of the maximum available radius of the BDM R_2 for different values of radius of the spool R_1 and flattened thicknesses of the boom t_f, the total longitude of a boom (6.5), the longitude of each boom (6.6) and the sail area obtained with this longitude of booms (6.7) is calculated. The range of R_1 and values of t_f studied are:

$$\begin{matrix} R_1 \in [0.015, 0.0425]\ [\mathrm{m}] \\ t_f = \{0.1, 0.15, 0.20, 0.25, 0.30, 0.35, 0.40\}[\mathrm{mm}] \end{matrix} . \quad (6.15)$$

Note that the study if smaller values of R_1 has not got sense due to the fact that they provoke not acceptable strain levels. As well, the maximum value of R_1 corresponds with the maximum available radius of the deployment mechanism. That is to say, the constrained value of R_2 is $R_2 = 0.0425\mathrm{m} = 42.5\mathrm{mm}$. Furthermore, in case of flattened thicknesses of the booms, the analyzed range has been determined from the state of the art [36]. In this way, a total longitude vs. spool radius for different flattened boom thicknesses (Top, left), each boom longitude vs. spool radius for different flattened boom thicknesses (Top, right) and sail area vs. spool radius (Bottom, left) for different flattened thickness are shown in Figure 37.

In addition, in order to have an idea of the order of the magnitude of the mass, the mass of the booms, m_{booms} has been calculated. For that, only the volume of the stowed booms is considered (not the boom deployment mechanism) as a function of R_1 as follows:

$$m_{booms} = \rho_{Elgiloy} h_f \pi (R_2^2 - R_1^2)\ [\mathrm{kg}] \quad (6.16)$$

where $\rho_{Elgiloy}$ is the density of the Elgiloy® steel found in table Table 19 and equal to $\rho_{Elgiloy} = 8300\mathrm{kg/m^3}$, R_2 is $R_2 = 0.0425\mathrm{m}$ and h_f is the height of the flattened boom, which has been constrained to $h_f = 0.035$. The graph of this boom mass is shown in Figure 37 (Bottom, right).

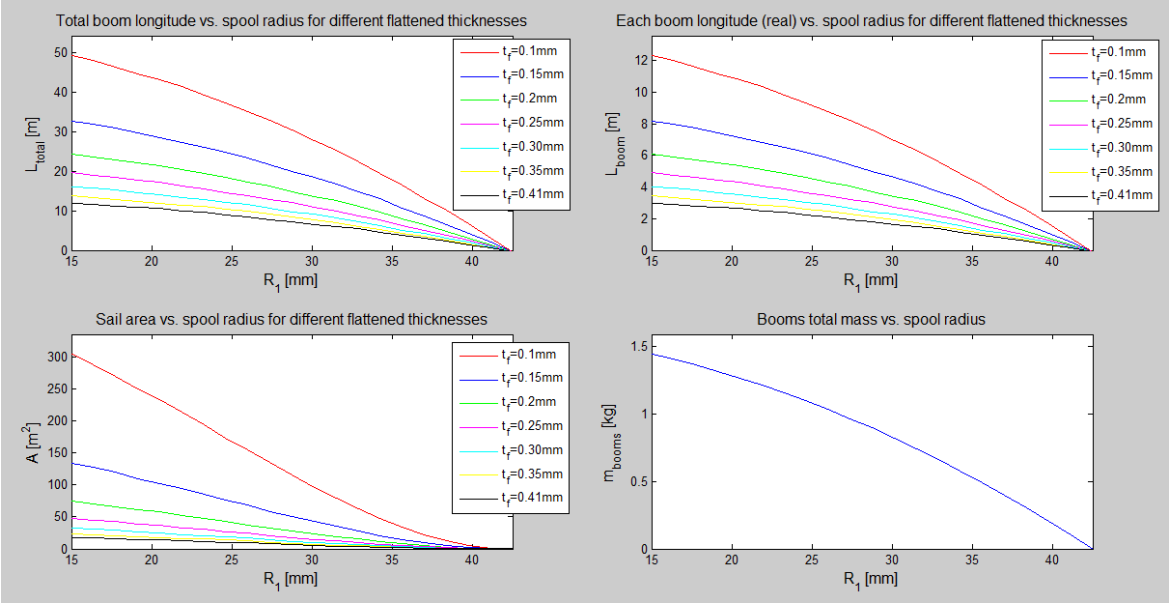

Figure 37. A total longitude vs. spool radius (Top, left), each boom longitude vs. spool radius (Top, right), sail area vs. spool radius (Bottom, left) for different flattened thickness and booms total mass vs. spool radius (Bottom, right).

As observed from the three first graphs of Figure 37, the thinner the boom flattened thickness, the greater the longitude of booms coiled around the spool and consequently, the area of the feasible solar sail is also bigger. Besides, if the radius of the spool is increased, the total longitude of the coiled boom decreases. Analogously, with bigger R_1 the longitude of each boom is also reduced and consequently, the sail area diminishes too. Nonetheless, it should be pointed out that with thinner booms (and so with thinner flattened thicknesses), the radius of spool can be reduced thanks to the fact that strain level compared to a thicker boom is less severe. Therefore, if thinner booms are possible to withstand external solicitations, smaller spool can be implemented in the deployment mechanism being able to coil longer booms.

In case of the booms total mass, its value decreases as the value of R_1 increases. The main reason of this tendency is that in this graph the volume occupied is only considered and not boom's longitude or different thicknesses. Nonetheless, it is evident that if the maximum boom longitude is stored with the minimum spool radius, the booms itself will be very heavy ($> 1\text{kg}$). Bearing in mind that the mass of the 2U SSM shall be up to 2kg (nominal value), this maximization of booms longitude is not convenient. Furthermore, with longer and thinner booms although greater sail area can be achieved, due to having small moment of inertia, the problem of buckling appears. Thereby, even though the theoretical formulation indicates that thinner and longer booms can be coiled in the mechanism, due to the mass limitations and the buckling phenomenon, shorter booms are adapted to be used in SSM.

Secondly, in the case of the sail sizing, the SSM structure configuration gives rise to two different types of containers: North/South (N/S) sail containers illustrated in Figure 38 and East/West (E/W) sail containers shown in Figure 39.

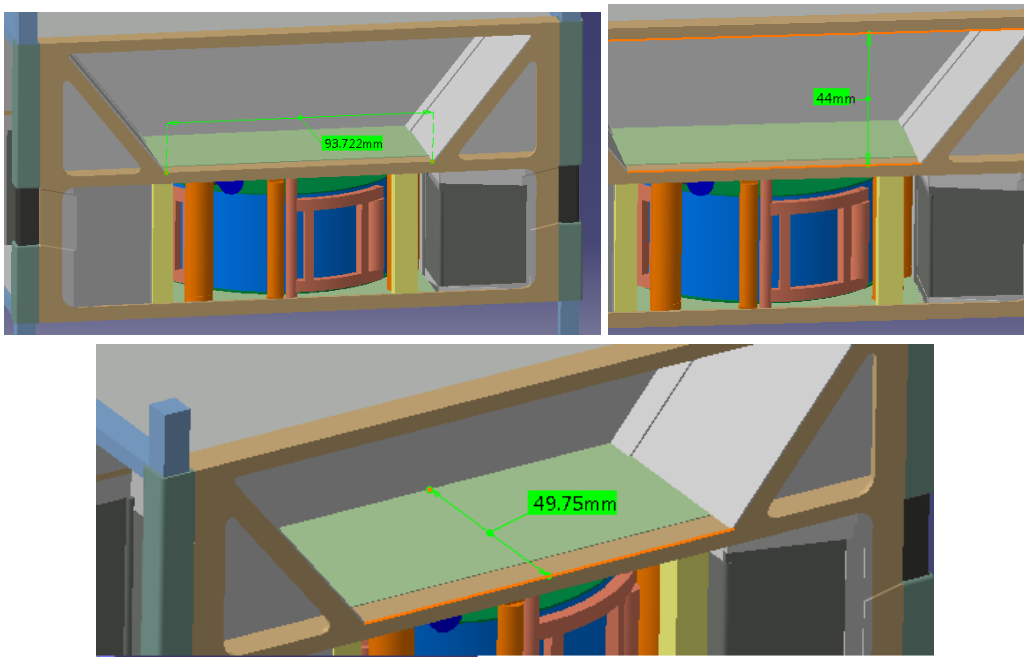

Figure 38. South sail container: $W_{cont} = 93.7mm$ (Top, left), $H_{cont} = 44mm$ (Top, right) and $P_{cont} = 49.7mm$ (Bottom). The sizes and shape are analogous for the North sail container.

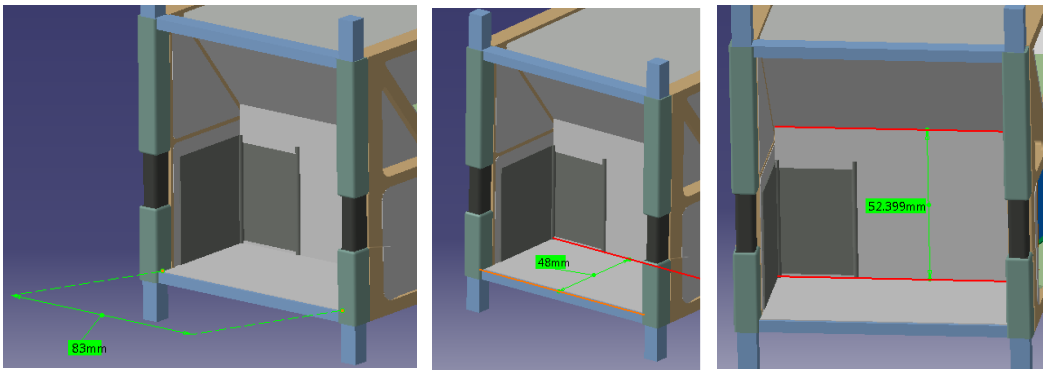

Figure 39. West sail container: $W_{cont} = 83mm$ (Left), $P_{cont} = 48mm$ (Middle) and $H_{cont} = 52mm$ (Right). The sizes and the shape are analogous for the East sail container.

Approximating the containers shown in Figure 38 and Figure 39 to a rectangular cuboid such as the one shown in Figure 32, conservative values of P_{cont}, H_{cont} and W_{cont} can be established. With these conservative values and assuming that $H_{cont} = H_{sail}$, $P_{cont} = P_{sail}$ and $W_{cont} = W_{sail}$, the maximum hypotenuse of the triangular shape quadrant (L_{max}) that can be fitted in these containers is estimated. For that, L_{max} is isolated from equation (6.16) as follows:

$$\frac{L_{max}^2}{2P_{cont}H_{cont}}t_s = W_{cont} \rightarrow L_{max} = \sqrt{\frac{2W_{cont}P_{cont}H_{cont}}{t_s}} \quad [m] \tag{6.17}$$

where $t_s$is the thickness of the membrane in $[m]$. In Table 22 for each type of container the value of L_{max} is calculated substituting the dimensions shown in Figure 38 and Figure 39 in expression (6.17). With the aim of being conservative, a $5\mu m$ thick sail has been adopted. Moreover, in order to analyze the order of magnitude of the creases generated during folding, the folds n_h and n_p given by equations (6.8) and (6.10) are also included. In addition, the mass of the sail membrane fitted into each type of sail container m_{s_c} is also estimated. Note that m_{s_c} has been calculated considering that two triangular-shaped quadrants can be theoretically fitted as:

$$m_{s\_c} = \rho_{CP-1^{TM}} \frac{W_{sail} \text{ x } P_{sail} \text{ x } H_{sail}}{2} \quad [kg] \tag{6.18}$$

where $\rho_{CP-1^{TM}}$ is the density of Aluminized CP-1^{TM} ($\rho_{CP-1^{TM}} = 1540 kg/m^3$, see Table 18).

Parameter	N/S containers	E/W containers
W_{cont} $[m]$	0.0937	0.083
P_{cont} $[m]$	0.0497	0.048
H_{cont} $[m]$	0.044	0.052
t_s $[m]$	$5 \cdot 10^{-6}$	$5 \cdot 10^{-6}$
L_{max} $[m]$	9	9.1
A_{max} $[m^2]$	81	82.8
n_h	103	88
n_p	181	188
m_{s_c} $[kg]$	0.16	0.16
$m_{s\_cT} = 4m_{s\_c}$ $[kg]$	0.64	0.64

Table 22. Comparison of the sail sizing values for N/S vs. E/W containers.

As shown in Table 22, the containers may be capable of fitting up to $9m$ side sail, which may total membrane mass of $1.28kg$. Nonetheless, in order to generate $9m \text{ x } 9m$ square-shaped sail, each boom shall be $9/\sqrt{2}m$ long. This boom longitude is unfeasible due to strict volume, excessive weight and buckling. So, it is concluded that the restrictive elements during the sizing process of the solar sail are the booms: the maximum solar sail area is limited by the booms' length,

mass and buckling stiffness and not by the membrane folding volume. Thereby, in order to begin with the detailed CAD design, it is necessary to constraint the mass of the booms, their length and their thickness as well as the inner R_1 and outer radii R_2 of the BDM. Once these five parameters are constrained, the rest of the sizing values (A, n_h and n_p inter-alia) are estimated. Note that the length L_{boom} and thickness of the booms determine their bucking resistance as well as booms' total mass. In addition, the mass of the booms, which is usually around the 50% of the total mass of the module, determines the mass of the final of the SSM. Finally, inner and outer radii of the BDM determine the boom deployment (e.g. torque of the motor used) and the manufacturability of the mechanism itself.

In Table 23 are summarized the solar sail sizing results. The values of $L_{boom} = 5m$ and $t_f = 0.1524mm$ have been adopted after several interactions between the booms' total mass and buckling stiffness. For that, the maximum boom mass has been constrained to $< 1kg$ and the buckling stiffness of the different booms has been simulated in Abaqus® 6.10 Computer-aided Engineering (CAE) software. In case of R_1 and R_2, they have been determined considering the state of the art ([30]) . Additionally, in case of R_1, the maximum acceptable strain level has been also taken into account. The rest of the parameters haven been calculated following the formulation presented in sections 6.2.1 and 6.2.2. Note that, the folding of the sail has been decided by means of keeping the symmetry between N/S and E/W containers.

Booms sizing results						
A $[m^2]$	**L_{boom}** $[m]$	**L_T** $[m]$	**t_f** $[mm]$	**R_1** $[mm]$	**R_2** $[mm]$	**m_{booms}** $[kg]$
50	5	20	0.1524	20	42.5	0.9

Triangular quadrants sizing results									
A $[m^2]$	**L** $[m]$	**Cont.**	**n_h**	**n_p**	**H_{sail}** $[m]$	**P_{sail}** $[m]$	**W_{sail}** $[m]$	**t_s** $[\mu m]$	**m_{s_c}** $[g]$
50	$5\sqrt{2}$	**N/S**	89	156	0.040	0.045	0.070	5	97
		E/W	89	156	0.040	0.045	0.070	5	97
Total estimated mass: $m_{booms} + 2m_{s\_c\_N/S} + 2m_{s\_c\_E/W} = 1.288kg$									

Table 23. Summary of the results of the sizing of the booms and triangular-shape quadrants.

6.3. DETAILED DESIGN

In this section, the 3D CAD design of the SSM is described. In order to do the CAD design, CATIAv5R17 software has been used. Furthermore, from this CAD design, drafts of the SSM are done. These drafts are presented in another document. Moreover, further information about the detailed design of the SSM is also included in the technical datasheet. The original CAD design of the SSM is included in the CD of the project.

The section begins with the presentation of the main parts of the SSM. In this case, images obtained from the CAD design are briefly described. Then, the mass busget of the SSM is presented. Finally, the position of the CM and the matrices of inertia for the launch and operartional configuration are given.

6.3.1. SOLAR SAIL MODULE

The Solar Sail Module is basically descomposed into four main elements: the four quadrants of the sail, the four booms, the Booms Deployment Mechanism (BDM) and the structure. In Figure 40 the general view of the deployed SSM is shown.

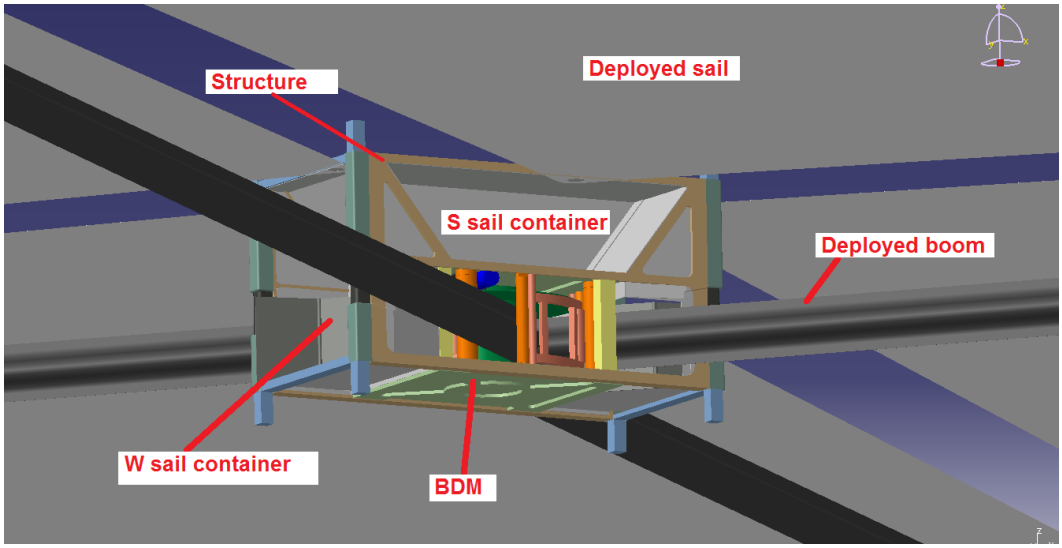

Figure 40. General view of the SSM.

As illustrated in Figure 41 (Top, left), once they are deployed, the four sail quadrants are symmetric. It should be pointed out that, due to the volume distribution of the SSM, the sail quadrants lie above the booms. The greater height difference between booms and the sail quadrants exist just in the vicinity of the s/c, as shown in Figure 41 (Bottom). As moving away from the position of the satellite, this height difference is reduced. In addition, note that the attachment of the quadrants to the s/c is does not lie just in the middle of each

side of the s/c. Indeed, these attachments are displaced counterclockwise as illustrated in Figure 41 (Top, right). The main reason of this displacement is found in the distribution of the booms with respect to the s/c structure. As shown in Figure 42 (Left), the deployment of the booms is constrained by the columns used in the SSM structure not forming a perfect diagonal. Consequently, the middle point for each pair of booms does not lie on the middle point of each side and thus, the sail membranes shall be attached to the s/c as shown in Figure 41 (Top, right) in order to be symmetrically distributed with respect to the two booms used to tauten each quadrant. Note that this symmetric distribution of quadrants avoids the generation of undesired internal stresses.

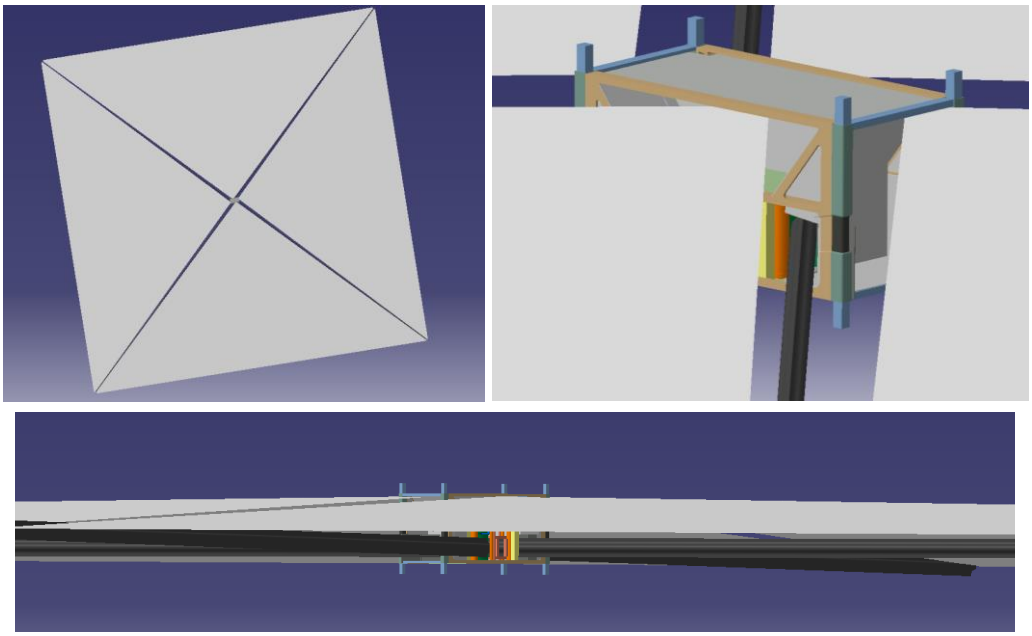

Figure 41. Upper view of the deployed sail (Top, left), detail view of the quadrant attachments to the s/c bus (Top, right) and side-view of the deployed sail (Bottom).

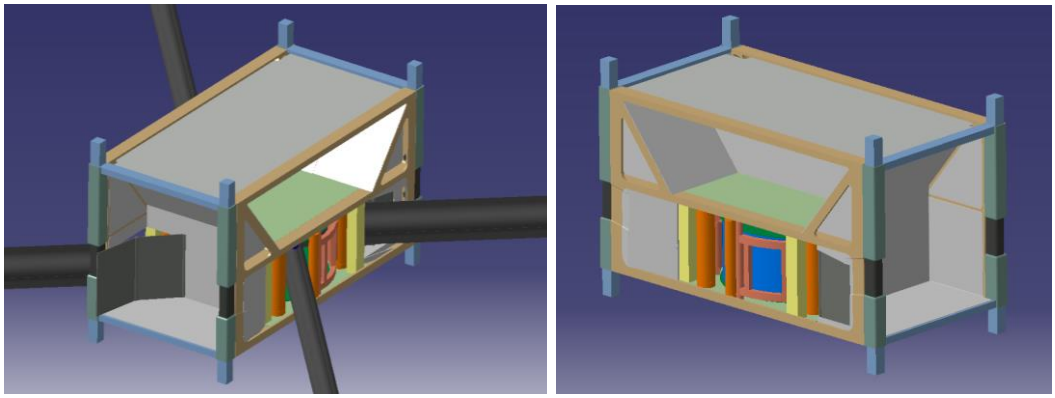

Figure 42. SSM with the booms deployed (Left) and its structure and BDM overview (Right).

In Figure 42 (Right) a general overview of the SSM not showing the deployed sail and booms is presented. In this way, it is easier to appreciate the distribution of

volume between the four sail containers and the BDM. Note that as shown in Figure 43 (Left), the BDM is located just at the bottom of the SSM providing stiffness to the structure. Indeed, although the BDM is considered as a part of the SSM structure, it also helps the structural withstanding the stresses. In case of the structure, four main elements are considered: horizontal supports, vertical columns, sail cavities and screws. The horizontal supports and the vertical columns form the primary structure, whereas the sail cavities and the screws are part of the secondary structure. All of the elements are made of Al 7075-T6, except for the screws which are made of steel. In addition, following the concept of PnP connectors have been added at the end of the vertical supports. These connectors, which are also part of the secondary structure, are used to connect the SSM to the rest of the 6U s/c structure. Thereby, their shape can be adapted to join the shape of the vertical columns of the s/c structure.

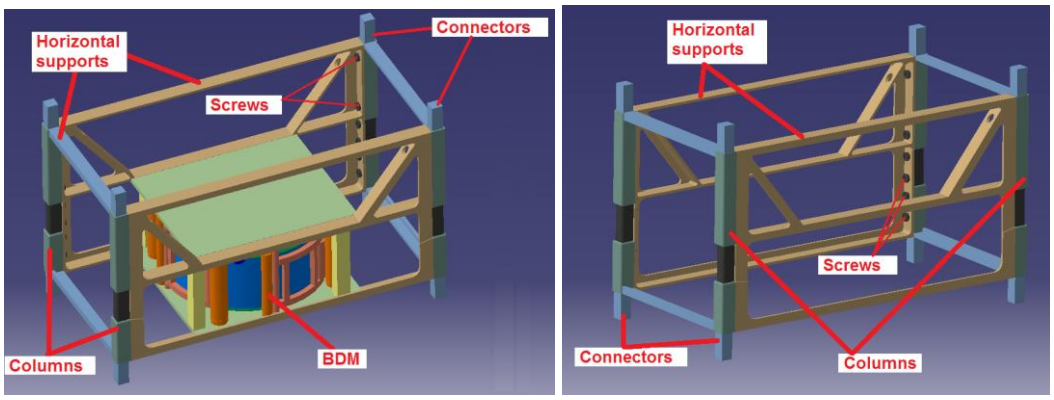

Figure 43. Image of the SSM structure and the BDM (Left) and different elements of the structure (Right).

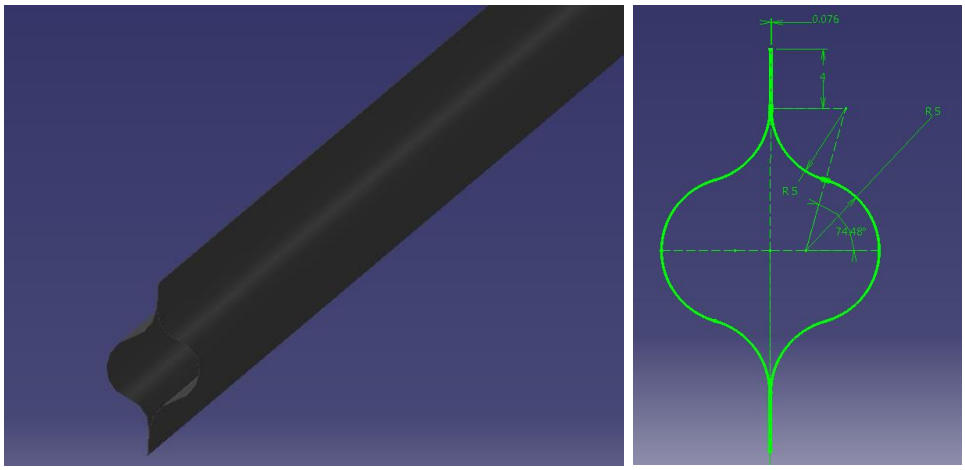

Figure 44. Boom cross-section image (Left) and sizes of the cross-section (Right).

In case of the booms, several iterations with Abaqus® 6.10 have been done to determine their cross-sectional sizes and maximum feasible length. In this way, Figure 44 (Left) illustrates their final deployed design. Note that the in Figure 44

(Right) the cross-sectional sizes of the adopted lenticular boom are shown. These sizes have been determined following the indications given in [43] and [46] about lenticular booms.

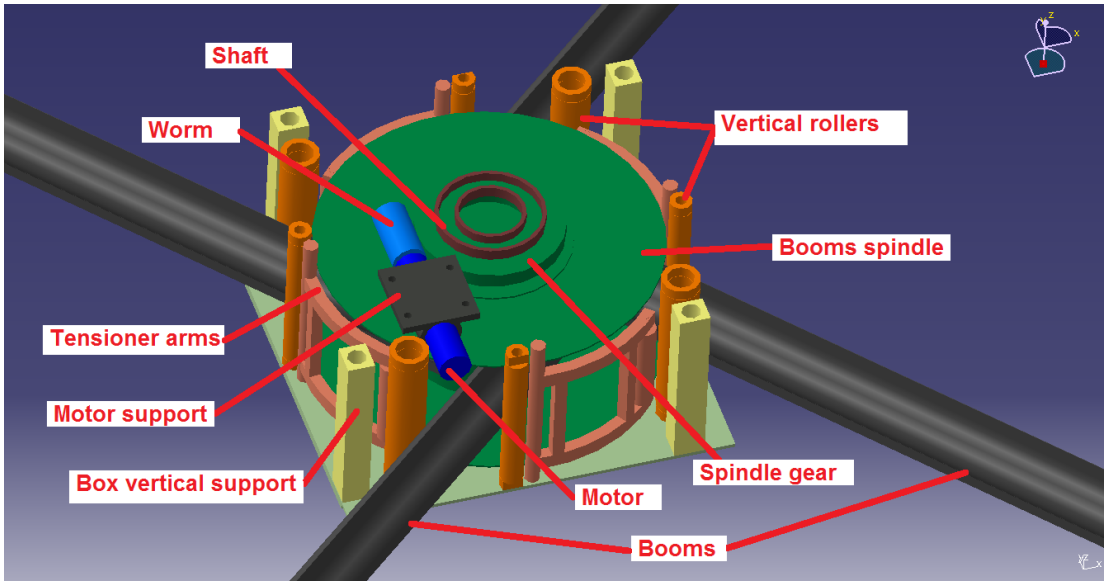

Figure 45. Different components of the Booms Deployment Mechanism (BDM).

In Figure 45 the different components of the BDM are indicated. By far, the BDM is the most complex part of the SSM. The core of the mechanism is the booms spindle, used to coil the booms. This spindle has a worm-gear at the top that is part of a worm-drive. Note that a worm-drive is very suitable for his application because it multiplies the engine torque and has the characteristic auto-blocking. Firstly, with very little motor torque it is possible to generate a high torque at the output gear, hence allowing a small engine to deploy the booms overcoming the friction forces. Secondly, a worm-drive does not rotate unless the motor provides a torque. It is not possible to move the worm-drive from the output gear, i.e. if the booms generate an undesired torque to the boom spindle because the worm-drive blocks the shaft the spindle will not move. So, once deployed no matter what external torques is applied to the spindle (e.g. satellite vibrations, boom dynamics, etc.) the spindle shaft will be block by the worm-drive.

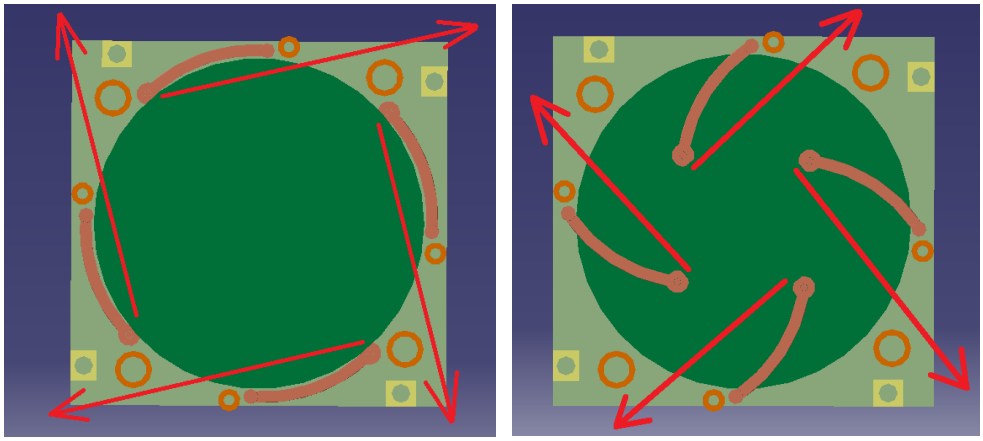

Figure 46. BDM: fully stowed state (Left) and fully deployed state (Right). The red arrows indicate the booms exit.

In addition, the BDM has a system composed by vertical rollers and tensioner to aid and guide the deployment process of the booms. This system provides normal reaction force against the booms all times. As shown in Figure 46 (Left), in the fully stowed state, the tensioner is at the corner and it moves towards the center of the spindle while the booms are deploying, as illustrated in Figure 46 (Right). Then, once the deployment process ends, the tensioners achieved a blocked stage similar to that presented in Figure 47 (Left and Right). Finally, it should be pointed once deployed, due to the SSM structure limitations the booms occupied part of the E/W sail containers. In order to not to interfere the boom deployment with the sail quadrant stowage and initial deployment, four flexible cavity doors (one per each boom) have been added between the E/W sail containers and BDM. During the launch configuration, when the booms are fully stowed, these doors are closed enabling the protection of the E/W sail quadrants from the booms. However, when the deployment process beings, these doors are opened interfere aiding the sail to be unfurled. Then, once the deployment ends, the doors are fully opened as shown in Figure 48.

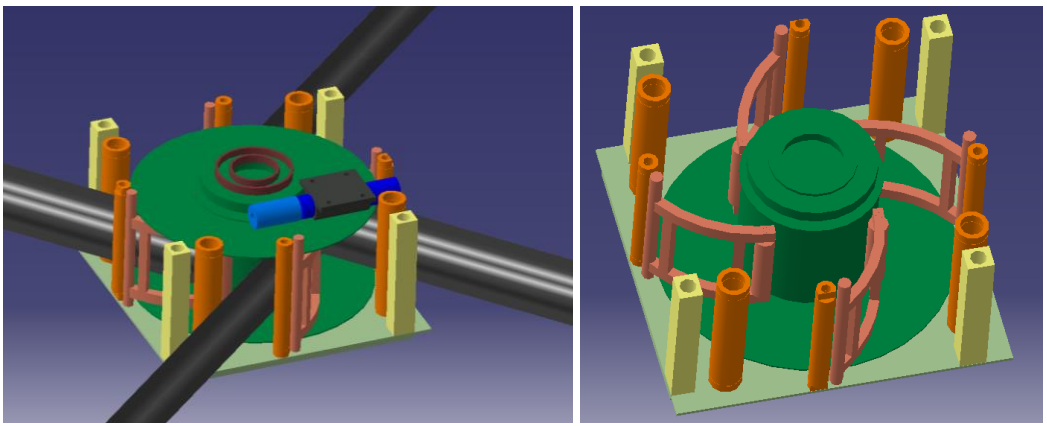

Figure 47. General view (Left) and sectioned-view (Left) of the BDM once the booms are fully deployed.

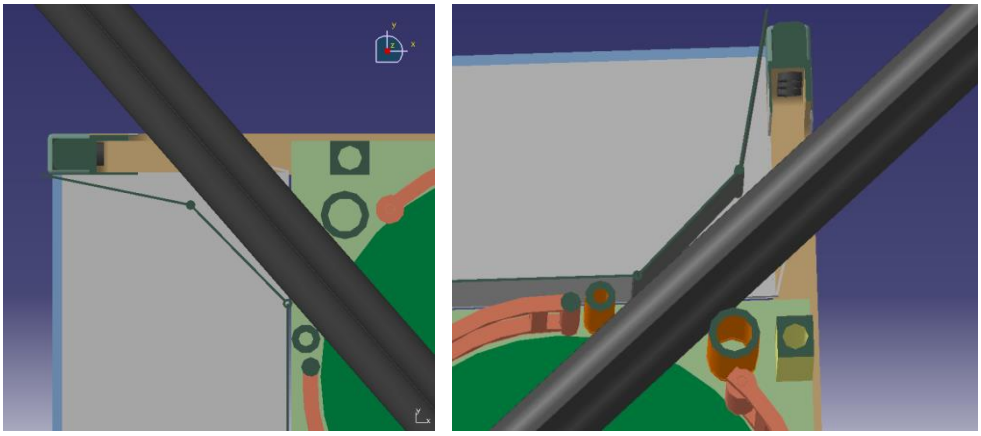

Figure 48. Detail view of the boom exiting from the N-W side with the cavity door opened (Left) and from the N-E side (Right).

Finally in Figure 49(Right), the detailed view of the joint between the eyelet corner of the membrane and that of the boom is presented. In this case, strings and springs have been implemented. The strings are used to allow for the booms to be stored in the BDM and the four quadrants to be stored in a nearby location with only the string having to pass through the interface. In order to pass these strings four recesses have been made to the structure as shown in Figure 49(Left). During the launch phase, these recesses shall be protected with the lateral solar sail panels of the 6U s/c. The design of these lateral solar panels is not included into the design of SSM because they belong to the s/c and not to the SSM. Finally, the springs are included in the boom-to-sail attachment to withstand thermal distortions enabling the adjustment of the stress caused by the different dilation coefficients between the booms and the membrane.

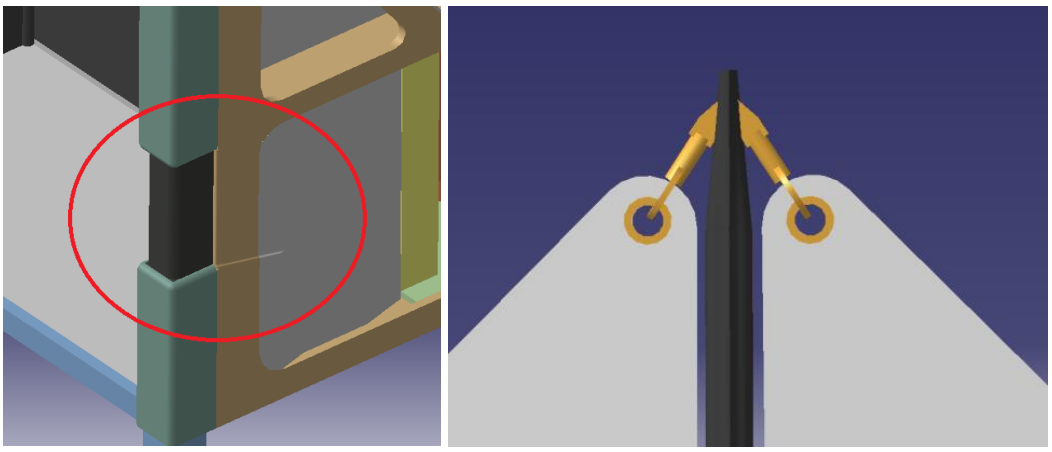

Figure 49. Detailed view of the recess made to structure (Left) and image of the eyelet attachment with corner reinforcement (Right).

6.3.2. MASS BUDGET

In Table 24 the mass budget of the SSM is presented. The mass of the four elements mentioned before is given in grams as well as with respect to the total.

Mass budget of the SSM		
SSM element	**Mass [g]**	**% of Total**
Sail (4 quadrants)	385	21.23
Booms (4 booms)	888	48.98
Booms Deployment Mechanism (BDM)	238	13.13
Structure (total)	302	16.66
Total mass of SSM	**1,813**	**100**

Table 24. Mass budget of the SSM.

Comparing the mass distribution of the detailed design (Table 24) with that of the sizing process of the (Table 23), it should be pointed that sizing process provides accurate mass values of booms as well as sail quadrants. In this way, in the sizing thee booms is estimated as $m_{booms} = 900g$, almost the same as the given in Table 24. Furthermore, in case of the sail quadrants, the mass of each one is estimated as $m_{s\_c} = 97g$, which gives a total mass of $388g$, slightly bigger than the given by the CAD model. In addition, it is important to point out that the E/W and N/S sail quadrants of the CAD model are not exactly of the same sizes. Precisely, due to the distribution of the sail with respect to the s/c, the N/S sail quadrants are quite bigger: $m_{s\_c\_N/S} = 96.5g$ compared to $m_{s\_c\_N/S} = 96g$ for the E/W sail quadrants. To sum up with Table 24, note that the CAD design does not consider the rivets used to join the different Aluminum sheets of the containers. Thereby, in the constructed SSM, the total mass may be rounded to $2kg$.

Mass budget of the SSM structure		
SSM structure element	**Mass [kg]**	**% of Total**
Columns (4 columns + joints)	45	14.90
Sail cavities	108	35.76
Horizontal supports	135	44.70
Screws	14	4.64
Total mass structure	**302**	**100**

Table 25. Mass budget of the SSM structure.

Finally, in Table 25 the mass budget of the SSM is presented, which is realistic. In this case, the horizontal supports represent around the 45% of the total structural mass. However, note that the connectors identified in Figure 43 are included into the budget of these horizontal supports.

6.3.3. CENTER OF MASS AND INNERTIA MATRIX

Next, the Center of Mass (CM) and the inertia matrix of the SSM are presented. Basically, with the CAD design two SSM configurations are represented: the launch configuration and operational configuration. Note that in the launch configuration, the solar sail quadrants and the booms are completely stowed into the structure of the SSM. Analogously, in the operational configuration, both the sail qiadrants and the booms are totally deployed. It should be pointed out that the transitory state from stowed to completely deployed is not taken into account, due to its complexity to be simulated.

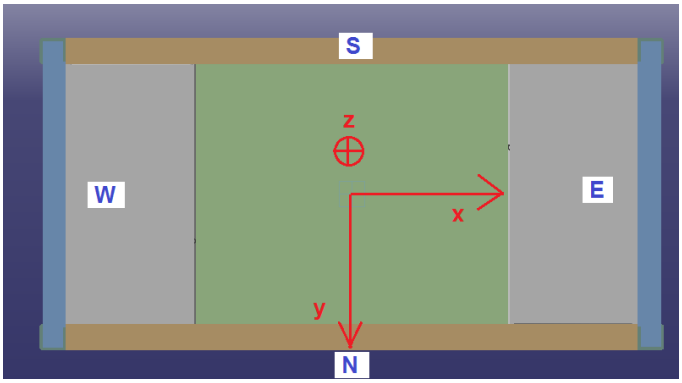

Figure 50. Origin of the reference system used in the CAD design (bottom surface of SSM).

For both configurations, using the CAD design the postion of the CM is calculated. Note that, as illustrated in Figure 50, the reference system used in the CAD design has been located at the center of the bottom surface of the SSM (just under the boom deployment mechanism). In this way, the values of CM given in Table 26 for both configurations are refered to the reference frame indicated in Figure 50.

Position of CM for different configurations of SSM		
Parameter	**Launch**	**Operational**
$G_x\ [mm]$	-0.448	-0.448
$G_y\ [mm]$	-0.364	-0.364
$G_z\ [mm]$	33.83	33.74

Table 26. Position of the CM for different configurations of SSM.

As shown in Table 26, the CM does not change a lot from one configuration to other. This is due to the fact that the mass is distributed similarly and symmetrically in both configurations.

The inertia matrix for both configurations is given with respecto to the CMs defined in Table 26. In this way, the matrices of launch $[\mathrm{I}_{\mathrm{launch}}]$ and operational $[\mathrm{I}_{\mathrm{operational}}]$ configurations are:

$$[\mathrm{I}_{\mathrm{launch}}] = \begin{bmatrix} \mathrm{I}_{\mathrm{xx}} & \mathrm{I}_{\mathrm{xy}} & \mathrm{I}_{\mathrm{xz}} \\ \mathrm{I}_{\mathrm{yx}} & \mathrm{I}_{\mathrm{yy}} & \mathrm{I}_{\mathrm{yz}} \\ \mathrm{I}_{\mathrm{zx}} & \mathrm{I}_{\mathrm{zy}} & \mathrm{I}_{\mathrm{zz}} \end{bmatrix} = \\ = \begin{bmatrix} 0.002 & -2.127 \cdot 10^{-5} & 1.04 \cdot 10^{-5} \\ -2.127 \cdot 10^{-5} & 0.005 & 8.672 \cdot 10^{-6} \\ 1.04 \cdot 10^{-5} & 8.672 \cdot 10^{-6} & 0.005 \end{bmatrix} [\mathrm{kg/m^2}] \tag{6.19}$$

$$[\mathrm{I}_{\mathrm{operational}}] = \begin{bmatrix} 5.582 & -1.104 \cdot 10^{-5} & 1.047 \cdot 10^{-5} \\ -1.104 \cdot 10^{-5} & 5.583 & 8.731 \cdot 10^{-6} \\ 1.047 \cdot 10^{-5} & 8.731 \cdot 10^{-6} & 11.163 \end{bmatrix} \left[\frac{\mathrm{kg}}{\mathrm{m^2}}\right] \tag{6.20}$$

Both inertial matrices are almost diagonal. So, the axes used in the CAD design and illustrated in Figure 50 are almost the principal axes of inertia. This results is expected given that it is aimed to make a symmetrical design. Furthermore, it should be pointed out that from launch to operational configuration the values of the diagonal increase considerably because the same quantity of mass is distributed further away. Finally, it should be pointed out that in order to design an altitude control for the sail, it is important to make use of $\mathrm{I}_{\mathrm{xx}} \cong \mathrm{I}_{\mathrm{yy}} = 5.583$. Indeed, due to this equality, altitude could be controlled in $\vec{\mathrm{x}}$ and $\vec{\mathrm{y}}$ axes (referred to Figure 50) through sliding masses as discussed in [47]. In case of the **z** axis, a reaction wheel could be used. However, in [18] recommended cated tips with individually controlled stationary electrochromic vanes to enable three-axis photon pressure actitude control. This last attitide system may eliminate the need of any consumables or moving parts after the sail deployment.

7. CONCLUSIONS

In this chapter the main conclusions of the project *Design of a Solar Sail as the Propulsion System for a Nanosatellite* are presented. Furthermore, some suggestions for future work are also given.

7.1. CONCLUSIONS

The main conclusions concerning each studied area are described below:

- **Mission analysis.** It is the first phase where decision making process begins. After researching the state of the art, the RAQL mission is selected due to being a natural step for solar sail technology applied to thrust nanosatellites. In this way, since only having solar sailing knowledge on 3U CubeSats, the RAQL mission gives a golden opportunity to develop an innovative design never done before. Furthermore, it should be pointed out that although the SSM here presented is designed to fulfill the requirements of this particular mission, it can be easily adapted to perform other type of selenocentric missions where solar sails are used to thrust 6U nanosatellites.
- **Mission trajectory analysis.** This chapter has been used to assess the feasibility of the solar sail design. In this way, the results of the trajectory study are only focused on simulating the spiral Earth escape departing from GEO. For this purpose, a basic solar sail steering law as well as a non-optimized trajectory have been used. The results obtained verified that a satellite of 6kg propelled by a solar sail of 50m^2 needs 2.784 years to Earth escape whereas that of 8kg lasts 3.607 years. It should be pointed out that in order to simulate the capture of the satellite by the Moon, an optimal control that assures the arrival of the s/c to the Sphere of Influence (SOI) of the Moon should be implemented. This is a complex and open problem that requires techniques such as low energy transfers ([48]), which are currently under development and out of the scope of this project. Additionally, after several simulations it is concluded that departing from a Geosynchronous Earth Orbit (GSO) coplanar to the Moons' orbit eases the Earth escape: the escape is quicker and the used steering law is simpler. Nonetheless, this departure orbit is unfeasible for nanosatellite due to the associated cost of GSO launching. Thereby, for them it is better to depart from GEO and optimize the trajectory utilizing an adequate steering law.
- **Solar Sail Module design.** This chapter is the core of the project. The chapter begins with a complete solar sailing technology downselection process, which was complicated due to the complexity of compacting broad information briefly in few pages. Furthermore, in order to select the best

configuration for the SSM, an overall solar sailing engineering criterion has had to develop. Note that the SSM design is like a puzzle of volumes where each element shall be located strategically in order to fulfill all the requirements of the mission. Moreover, with the purpose of not groping in the dark, formulation to size the booms and the solar sail quadrants has had to develop. The results obtained from this sizing process are truthful, as being proved afterwards with the CAD design. In addition, it should be pointed out that the booms limited the maximum achievable solar sail area due to their mass and buckling. To sum up, it is remarkable that the final result of this work is a SSM design that can be put into practice by the CubeSat community with a moderate engineering effort.

7.2. FUTURE WORK

In order to broad the design of the SSM, some of the steps that can be followed are:

- **Structural analysis of the SSM in Abaqus®.** Although some simulations of different configurations of booms have been done during the sizing process of the SSM, a further study is required. Particularly challenging are the structural analysis of the sail membrane and the simulation of wrinkles. For this purpose, the software Abaqus® is recommended: a) it has been already used by the NASA to validate structural testing ([5] and [6]) and b) it is also owned by Dassault Systèmes, fact that eases the exportation of the 3D CAD design.
- **Thermal analysis of the SSM in Abaqus®**. Analogously to the case of the structural analysis, a thermal simulation of the SSM must be done. If Abaqus® is used, this analysis can be combined with the structural analysis.
- **Improvement of the trajectory analysis.** Implementation in Matlab® code of the capture of the s/c by the Moon.
- **Implementation of attitude control.** The attitude control of solar sails is an open problem. A deep study of the attitude control is required in order to determine whether the sliding masses or cated tips with individually controlled stationary electrochromic vanes are the best system to control the SSM.
- **Solar sail charging analysis.** Due to being propelled by the sunlight, it is important to consider the charging of the SSM once deployed. A useful software for that is the NASCAP-2K, that has been already used to simulate the charging process of solar sails ([35]).

8. BUDGET

This chapter presents the budget for the realization of the project *Design of a Solar Sail as the Propulsion System for a Nanosatellite* called engineering work cost. This cost includes the author's hours, hardware and software licenses. Besides, the chapter also includes the development cost of the SSM product.

8.1. ENGINEERING WORK

Concept		**Quantity [h]**	**€/h**	**Cost**
Mission analysis	Research of mission state of the art	20	15	300
	Justified selection of the mission	3	15	45
	Systems engineering	7	15	105
	Subtotal of mission analysis	**30**	**15**	**450**
Mission trajectory analysis	Research of trajectories state of the art	10	15	150
	Formulation development	25	15	375
	Implementation of the formulation into Matlab®	25	15	375
	Basic steering law development	20	15	300
	Simulations and code validation	50	15	750
	Validation of the SSM design feasibility	5	15	75
	Subtotal of mission trajectory analysis	**135**	**15**	**2025**
Detailed design	Research of solar sailing technology	50	15	750
	Downselection of the configuration	20	15	300
	Sizing of the solar sail booms	10	15	150
	Sizing of the solar sail quadrants	12	15	180
	Matching of the sizing process	15	15	225
	3D CAD design development	80	15	1200
	Estimation of mass budget and matrices	4	15	60
	Subtotal of detailed design	**191**	**15**	**2865**
Writing of the project report, drafts and technical datasheet		85	15	1275
Subtotal of worked hours		**441**	**15**	**6615**
Hardware				150
Software	CATIAv5R17 & Abaqus® Student Edition			0
	Matlab® R2013a			500
	VCL media player			0
	Microsoft Office Home & Student 2013			107.70
Total		**441**		**7380**

Table 27. Engineering work cost.

The engineering work lasted for more than 6 months with an average of 20 days worked during each month. So, approximately 120 working days are computed, considering an average cost of 15€ per engineering hour. In Table 27, five main groups are taken into account: mission analysis, mission trajectory analysis, hardware and software. The generation of document is not part of these five groups. The first three main groups and the generation of documents are considered as working hours, having a total of 441 hours. In case of the hardware, the reparation of the computer graphic card is computed. Indeed, the graphic card was burnt due to the hours lasted in the mission trajectory simulation. Finally, in case of the software licenses, the use of student licenses was preferred. In this way, only two software licenses have additional cost: the Matlab® R2013a and the Microsoft Office Home and Student 2013 edition. In case of the former, it is necessary to register in the official web-page ([70]) to consult the price of the software; latter's license value is found in [71]. Note that in order to shown the values in Euros, an exchange rate of 1.3 is applied. The total cost of the engineering work has been rounded to 7380€. In this budget taxes are not taken into account.

8.2. SOLAR SAIL MODULE DEVELOPMENT COST

To date, most methods for predicting the development costs of a new satellite such as NAFCOM are based on parametric approaches using historical data from flown satellites. Thus, the development cost of a new satellite can be approximately estimated using historical data. However, since the establishment of the "Faster, Better and Cheaper" philosophy in late 1980's the trend has turned to reduce more and more the size and the cost of the satellites. Thereby, nowadays, in general, the development costs tend to be lower than compared to past projects thanks to the technology maturity and the availability of miniaturized flight-proven components. This fact makes it more difficult to estimate precisely the development costs using historical databases.

Nevertheless, the creation of the CubeSat concept in 1999 has split apart from this trend and has become a revolution in the space field. In this way, CubeSats have allowed to develop nanosatellites with very low budgets (less than 1M$) with very short development time (6 months in some cases). Therefore, the development cost of a CubeSat cannot be estimated with the previous parametric methods from past missions. Hence, the best way to estimate the development cost is by using similar nanosatellite missions as a reference.

As shown Table 1, the NanoSail-D and NanoSail-D2 program cost was $250,000, LightSail-1 is estimated in 2.2 M$ and the budget of CubeSail (US) is $600,000. Furthermore, in [49] the authors estimated that cost of a mission for performing

multiple rendezvous with Near Earth Objects using a solar sail may be $175.2 million (FY2011), from which around $35 million would be invested on the generation of a $85\text{m} \times 85\text{m}$ square-shaped solar sail. So, for the case of [49] the development of the solar sail is about 20% of the total budget. Bearing in mind these percentages and sizes, in case of the SSM it is desired to constraint the maximum budget used in the Research, Development, Test and Evaluation (RDT&E) to 1M$. Note that the RDT&E includes the design, analysis and test, prototypes and qualification unit. Hence, this budget does not consider the launching of the SSM or its integration within the 6U s/c structure. Note that the SSM would be around five times bigger than the NanoSail-D and –D2. Nonetheless, the conceptual design of the SSM is not as complex as CubeSail (US) and the aim is to use as many solar sailing technology from the current state of the art as possible.

9. ENVIRONMENTAL IMPACT

The Solar Sail Module would impact the environment negatively during three phases of its lifecycle as a real product: in the manufacturing process, in the launch phase and after completing its mission. Since in the production system of satellites the quality and the non-contamination of the manufactured good is the most important, few green manufacturing recommendations are implemented. Thereby, one of the alternatives to reduce the generated contamination is based on the careful control of the supply chain. However, in case of nanosatellites, the required production systems for COTS elements are more lax compared to those of the commercial big satellites (e.g. communication satellites or military satellites). Thereby, the application of more eco-friendlier manufacturing process is feasible.

The launching phase of the SSM would also contaminate the environment. Nonetheless, the launches of satellites are not as hazardous as though by ordinary citizens. Indeed, as stated in the report of the trade group Intellect [72], a satellite launch vehicle emits less CO_2 than a single transatlantic flight. Furthermore, the mission is a one-off event for each satellite. Consequently, as nanosatellites are launched as secondary payload attached to larger satellites, their contribution to the atmospheric pollution is even smaller. Additionally, Intellect also pointed out that at least one launch site, Arianespace's Kourou facility, relies on hydroelectric and ethanol power in order to protect the environment. Thereby, if nanosatellites are launched from Kourou their contribution to the environmental impact would be the least possible.

Finally, once the s/c completes the service, the SSM will become part of space debris. As stated in [13], space debris is becoming a problem mainly in LEO, where around 5000tones of debris are computed. This is becoming a threat to space environment as well as space assets, astronauts and space station. Nonetheless, due to being designed to operate in the vicinity of the Moon, the SSM would be disposed in deep space. Hence, its environmental impact may be lower than those GEO or LEO satellites.

To sum up, it is remarkable that the solar sails are the cleanest propulsion systems among the currently available ones (e.g. monopropellant thrusters). Consequently, although the solar sail has the aforementioned drawbacks, it is the most suitable propulsion system to produce green satellites.

10. REFERENCES

10.1. BOOKS, LECTURES AND ARTICLES

[1] B. Dachwald and B. Wie. *Solar Sail Trajectory Optimization for Intercepting, Impacting, and Deflecting Near-Earth Asteroids.* AIAA Guidance, Navigation, and Control Exhibit. AIAA 2005-6176, (August 2005).

[2] B. Dachwald et al. *Potential Solar Sail Degradation Effects on Trajectory and Attitude Control.* AIAA Guidance, Navigation, and Control Conference and Exhibit. AIAA 2005-6172, (August 2005).

[3] E. Fantino. *T08-Thermal Analysis.* Lecture notes of the subject *Design of Space Vehicles II*. ETSEIAT (Terrassa, Barcelona, SPAIN), Spring 2012.

[4] B. Diedrich and M. Leipold. *A Summary of Solar Sail Technology Development and Proposed Demonstration Missions.* JPC-99-2697.

[5] D.W. Sleight, Y. Michii, D. Lichodziejewski, B. Derbès, K.N. Slade and J.T. Wang. *Finite Element Analysis and Test Correlation of a 10-meter Inflation-Deployed Solar Sail.* AIAA-2005-2121, (Austin, TX, US), 2005.

[6] D.W. Sleight, T. Mann, D. Lichodziejewski and B. Derbès. *Structural Analysis and Test Comparison of a 20-Meter Inflation-Deployed Solar Sail.* AIAA 2006-1706, (Newport, RI, US), 2006.

[7] L. Johnson, R. Young, E. Montgomery and D. Alhorn. *Status of the solar sail technology within NASA.* Advanced in Space Research 48 (2011).

[8] U. Geppert, B. Biering, F. Lura, J. Block and R. Reinhard. *The 3-Step DLR-ESA Gossamer Roadmap to Solar Sailing.* Proceedings of the 2nd International Symposium on Solar Sailing, (New York, NY, US), 2010.

[9] G. Laue and C. Adams. *NanoSail-D: The First Flight Demonstration of Solar Sails for Nanosatellites.* SSC08-X-1. 22nd AIAA/USU Annual Conference of Small Satellites, (Logan, Utah, US), 2008.

[10] E.E. Montgomery IV and C.L. Adams. *NanoSail-D*. 2008 CubeSat Developers Workshop, (San Luis Obispo, CA, US), 2008.

[11] D.C. Alhorn, J.P. Casas. *NanoSail-D: The Small Satellite That Could!* 25th Annual AIAA/USU Conference on Small Satellites, (Logan, Utah, US), 2011.

[12] M. Nehrenz, A. Diaz, T. Svitek and C. Biddy. *Initial design and simulation of the attitude determination and control system for LightSail-1.* 2nd International symposium on Solar Sailing (ISSS 2010), (New York, NY, US), 2010.

[13] V. Lappas. *Gossamer Systems for Satellite Deorbiting: The Cubesail and DEORBITSAIL Missions.* Notes from the *Space Vehicle Control Group.* University of Surrey. (Guildford, Surrey GU2 7XH, UK).

[14] A. Pukniel, V. Coverstone, R. Burton and D. Carroll. *Attitude Control of the CubeSail Solar Sailing Spacecraft in Low Earth Orbit.* Proceedings of the 2nd International Symposium on Solar Sailing, (New York, NY, US), 2010.

[15] J.K. Laystrom. *Design and Testing of the CubeSail Payload.* 7th Annual CubeSat Developer's Workshop, (San Luis Obispo, CA, US), 2010.

[16] L. Friedman. *History of Solar Sail Flight Test.* 2nd International Symposium on Solar Sailing (ISSS 2010), (New York, NY, US), 2010.

[17] R.L. Staehle et al. *Interplanetary CubeSats: Some Missions Feasible Sooner than Expected.* First Interplanetary CubeSat Workshop, Massachusetts Institute of Technology (Cambridge, MA, US), May 2010.

[18] R. Staehle et al. *Interplanetary Cubesats: Opening the Solar System to a broad Community at Lower Cost.* Final Report on Phase 1 to NASA Office of the Chief Technologist, December 2008.

[19] S. Lee, A. Hutputanasin, A. Toorian and W. Lan. *CubeSat Design Specification (CDS).* The CubeSat Program. California Polytechnic State University (San Luis Obispo, CA, US).

[20] SpaceFlight Services. *Secondary Payload Planners Guide.* (Tukwila, WA, US).

[21] J. Calaf. *Astrodinàmica. 2.2 Els elements orbitals.* Lecture notes of the subject *Astrodynamics*. ETSEIAT (Terrassa, Baecelona, SPAIN), Spring 2011.

[22] E. Fantino. *T05-Space and Time Reference Systems*. Lecture notes of the subject *Space Vehicles.* ETSEIAT (Terrassa, Barcelona, SPAIN), Spring 2011.

[23] J. Calaf. *Astrodinàmica. 1.2 Sistemes de referencia (Astronomia de posición 2).* Lecture notes of the subject *Astrodynamics*. ETSEIAT (Terrassa, Barcelona, SPAIN), Spring 2011.

[24] E. Cardoso Vilana. *Study of Spacecraft Orbits in the Gravity Field of the Moon.* Final Year Project Report submitted to the ETSEIAT (Terrassa, Barcelona, SPAIN), January 2012.

[25] J. Calaf. *Astrodinàmica. 3.3 Pertorbacions. Equacions de Gauss.* Lecture notes of the subject *Astrodynamics*. ETSEIAT (Terrassa, Baecelona, SPAIN), Spring 2011.

[26] B. Dachwald. *Interplanetary Mission Analysis for Non-Perfectly Reflecting Solar Sailcraft Using Evolutionary Neurocontrol.* AAS 03-579. AAS/AIAA Astrodynamics Specialist Conference, (Big Sky, MT, US), 2004.

[27] E. Fantino. *T-15. Power subsystem*. Lecture notes of the subject *Space Vehicles*. ETSEIAT (Terrassa, Barcelona, SPAIN), Spring 2011.

[28] H.D. Curtis. *Orbital Mechanics for Engineering Students*. *2nd Edition*. Butterworth-Heinemann (Elsevier), (Burlington, MA, US), 2010. ISBN: 978-0-12-374778-5.

[29]R.L. Burton, J.K. Laystrom-Woodard, V.L. Coverstone, et al. *Initial Development of the CubeSail/UltraSail spacecraft.* JANNAF Conference, (Colorado Springs, CO, US), 2010.

[30] C. Biddy. *Challenges and Design of LightSail-1 Boom Deployment Module.* Stellar Exploration Inc.

[31] O. Mori et al. *World's First Demonstration of Solar Power Sailing by IKAROS.* 2nd International Symposium on Solar Sailing (ISSS 2010), (New York, NY, US), 2010.

[32] S.N. Adeli. *Deployment System for the CubeSail nano-Solar Sail Mission.* SSC10-VIII-3. Surrey Space Center (Guildford, Surrey GU2 7XH, UK).

[33] W. E. Landford. *Folding apparatus*. US Patent 3,010,372. (NASA, US), 1961.

[34] F. Dalla Vedova, H. Henrion, M. Leipold, Th. Girot, R. Vaudemont, Th. Belmonte, K. Fleury and O. Le Couls. *The Solar Sail Materials Project-Status of Activities.* 2nd International Symposium on Solar Sailing (ISSS 2010), (New York, NY, US), 2010.

[35] L. Neergaard Parker, J.I. Minow, et al. *Analysis of Surface Charging for a Candidate Solar Sail Mission Using Nascap-2k.* 9th Spacecraft Charging Technology Conference (Tsukuba, JAPAN), 2005.

[36] G. M. Thomas. *Prototype Development and Dynamic Characterization of Deployable Cubesats Booms.* Master's Thesis presented to Air Force Institute of Technology. AFIT/GA/ENY/10-M10, (Wright-Patterson Air Force Base, Ohio, US).

[37] C. Garner, B. Diedrich and M. Leipold. *A Summary of Solar Sail Technology Developments and Proposed Demonstration Missions.* JPC-99-2697, 1999.

[38] Dr. C. M. Stevens. *New Millennium Program. Back-up Quad Charts.* Jet Propulsion Laboratory, California Institute of Technology (Long Beach, CA, US), 2000.

[39] W. A. Hollerman. *The Physics of Solar Sail.* 2002 NASA Faculty Fellowship Program. Marshall Space Flight Center, University of Alabama (Tuscaloosa, AL, US), 2002.

[40] L. Johnson. *Status of Solar Sail Technology Within NASA*. Paper and PPT.

[41] NASA. *DEPLOYTECH*. *Deployment Technology Survey.* Deployable systems Review. PDF.

[42] J.A. Banik and T. W. Murphey. *Performance Validation of the Triangular Rollable and Collapsible Mast.* SSC10-II-1. Air Force Research Laboratory (Edwards, CA, US).

[43] M. Aguirre-Martinez, D.H. Bowen, R. Davidson, R.J. Lee and T. Thorpe. *The Development of a Continuous Manufacturing Method for a Deployable Satellite Mast in CFRP.* British Plastic Congress, 107-110, 1986.

[44] B. J. de Blonk. *Optical-Level Structural Modeling of Membrane Mirrors for Spaceborne Telescopes*. Final thesis submitted to the Department of

Aeronautics and Astronautics in partial fulfillment of the requirements for the degree of Doctor of Philosophy at the Massachusetts Institute of Technology (Cambridge, MA, US), June 2003.

[45] ASME. *ASM Specialty Handbook: Nickel, Cobalt, and Their Alloys.* Ed. Upd Sub, 2001.

[46] S.K. Michael. *On-orbit Space Shuttle Inspection System Utilizing an Extendable Boom*. Master thesis submitted to the Faculty of the Graduate School of the University of Maryland, (College Park, MD, US), 2004.

[47] C. Scholz, D. Romagnoli and B. Dachwald. *Performance Analysis of an Attitude Control System for Solar Sails Using Sliding Masses.* 2nd International Symposium on Solar Sailing (ISSS 2010), (New York, NY, US), 2010.

[48] W.S. Koon, M.W. Lo, J.E. Marsden and S.D. Moon. *Low Energy Transfers to the Moon.* Celestial Mechanics and Dynamical Astronomy 81: 63-73, (NETHERLANDS), 2001

[49] L. Johnson. *Multiple NEO Rendezvous Using Solar Sails.* MSFC Advanced Concepts Office. PDF.

10.2. WEBSITES

[50] A Discovery Company. *How Solar Sails Work.* http://science.howstuffworks.com/solar-sail.htm (last access April 2013).

[51] Quark Web. *Space sailing activity section*. http://sail.quarkweb.com/activity.htm (last access April 2013).

[52] NASA. *A Brief History of Solar Sailing.* http://science.nasa.gov/science-news/science-at-nasa/2008/31jul_solarsails/ (last access April 2013).

[53] NASA. *Office of the Chief Technologist.* http://www.nasa.gov/images/content/581469main_solar_sails2_1210x794.jpg (last access April 2013).

[54] The Planetary Society. *Planetary Society to Sail Again with LightSail.* http://www.planetary.org/press-room/releases/2009/1109_Planetary_Society_to_Sail_Again_with.html (last access April 2013).

[55] *1st International Symposium on Solar Sailing (ISSS 2007).* 27-29 June 2007. Herrsching (Germany). http://www.isss.spacesailing.net/ (last access April 2013).

[56] *2nd International Symposium on Solar Sailing (ISSS 2010).* 20-22 July 2010. New York City College of Technology (NY, US). http://www.citytech.cuny.edu/isss2010/ (last access April 2013).

[57] *3rd International Symposium on Solar Sailing (ISSS 2013)*. 11-13th June 2013. (Glasgow, UK). http://www.solarsailing2013.com/ (last access May 2013).

[58] Spaceflight Now. *NASA's first solar sail makes unlikely comeback in orbit.* http://www.spaceflightnow.com/news/n1101/22nanosail/ (last access May 2013).

[59] NASA. *NanoSail-D*. http://www.nasa.gov/mission_pages/smallsats/nsd_team .html (last access May 2013).

[60] The Planetary Society. *LightSail-1*. http://www.planetary.org/explore/projects/ lightsail- solar-sailing/ (last access May 2013).

[61] Spacenews. *Spotlight: Stellar Exploration, Inc*. http://www.spacenews.com/ article/spotlight-stellar- exploration-inc#.UYk3ScrZ5f0 (last access May 2013).

[62] Surrey Space Centre & Astrium: An EADS Company. CubeSail. http://www. cubesail.net/science.php?ScienceType=history (last access May 2013).

[63] National Debate Coaches Association. *Space Debris Neg-Wave 1*. www.de batecoaches.org/files/download/1421 (last access May 2013).

[64] CubeSatShop.com. *6-U Unit CubeSat Structure.* http://www.cubesatshop. co m/index.php?page=shop.product_details&flypage=flypage.tpl&product_id=45 &category_id=1&option=com_virtuemart&Itemid=66 (last access May 2013).

[65] PoleCATS. *Coordinate Systems.* http://rexuscats.wikispaces.com/Coordin ate+Systems (last access April 2013).

[66] ESR Technology. *MaterialsSolutions: Polymer Composites. Design Example: SPACE collapsible tube mast*. http://www.admc.esrtechnology.com/CDKB/ CaseStudies/SPACE%20Collapsible%20Tube%20Mast/ (last access May 2013).

[67] ASM Aerospace Specification Metals Inc. *Aluminum 7075-T6; 7075-T651*. http://asm.matweb.com/search/SpecificMaterial.asp?bassnum=MA7075T6 (last access May 2013).

[68] ASM Aerospace Specification Metals Inc. *Aluminum 6061-T6; 6061-T651.* http://asm.matweb.com/search/SpecificMaterial.asp?bassnum=MA6061t6 (last access May 2013).

[69] ManTech International Corporation®. *Products*. http://www.mantechmaterials. com/products.asp (last access May 2013).

[70] MathWorks®. *Product and Services*. http://www.mathworks.com/products/ ?s_cid=global_nav. (last access May 2013).

[71] Microsoft. *Office. Software for the things you do most.* http://www.microsoftstore.com/store/msusa/en_US/cat/categoryID.62684700 ?icid=USGobalNav_TopCat_3_Office2013_041713 (last access May 2013).

[72] Satellite today. *Green satellites*. http://www.satellitetoday.com/via/globalreg/ Green-Satellites_22875.html (last access May 2013).

11. LIST OF DRAFTS

No.	Title
1	Solar Sail
2	Solar Sail Module
S	Primary Structure
4	BDM

Table 28. List of drafts.

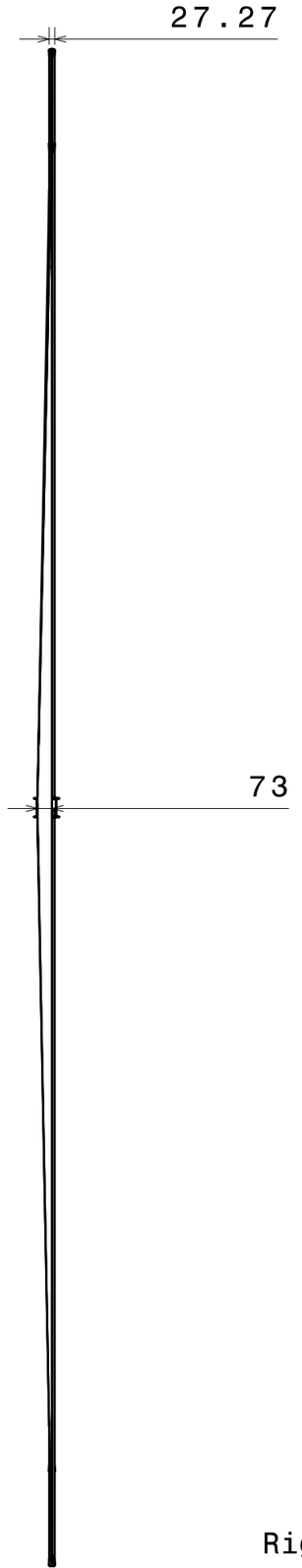

Right view
Scale: 1:30

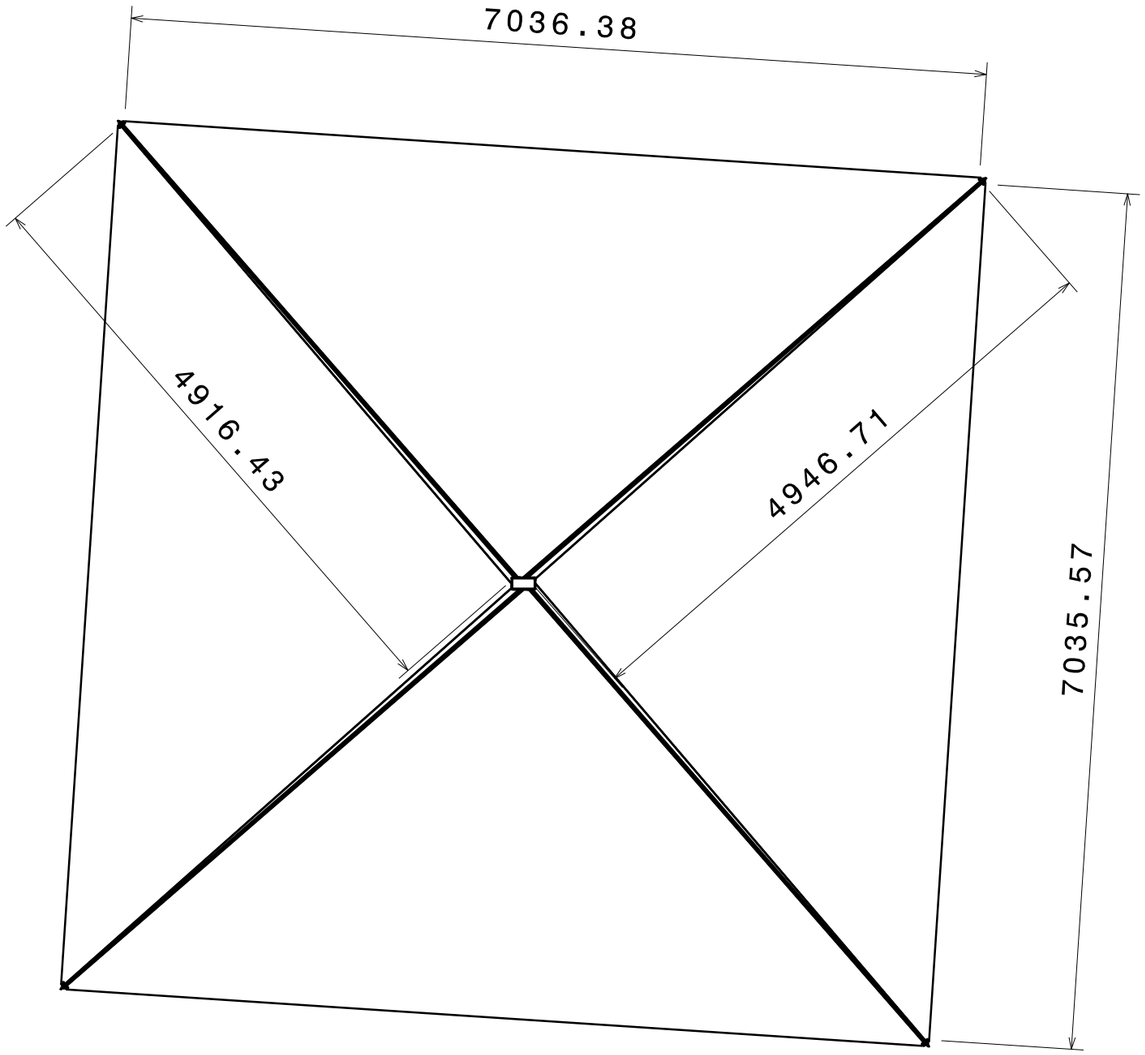

Front view
Scale: 1:50

Number	Quantity	Name	NORM	Sizes	MATERIAL
	1	Solar sail		7036 x 7036	CP-1

Solar Sail

PFC	ETSEIAT-UPC
Rique Garaizar, Orzuri	
Date: June 6, 2013	Nº 1

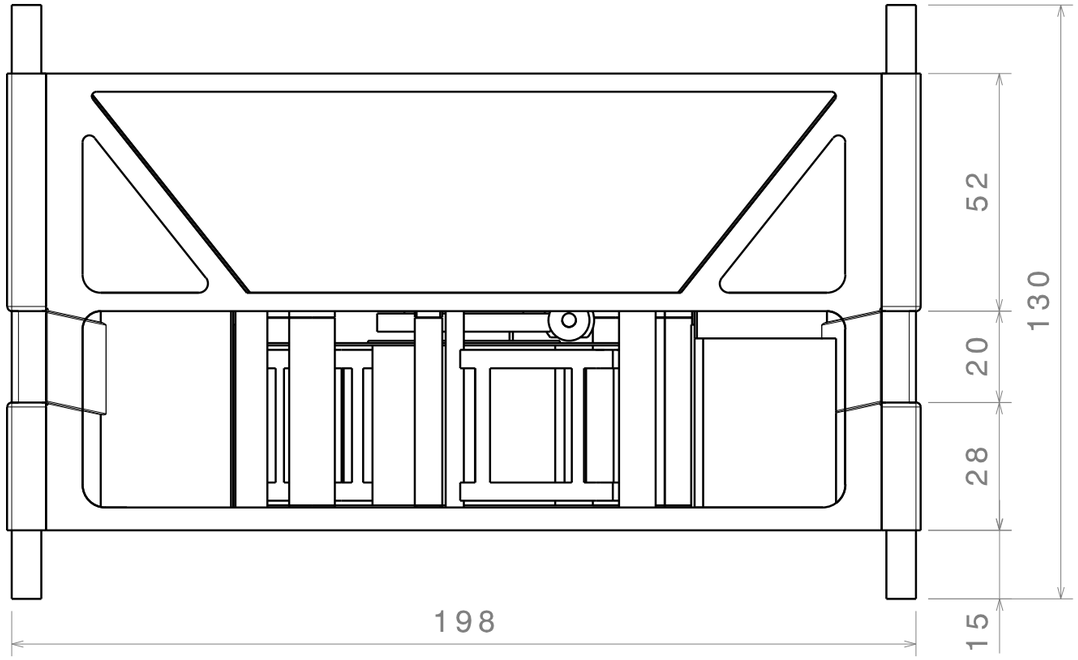

Front view
Scale: 3:4

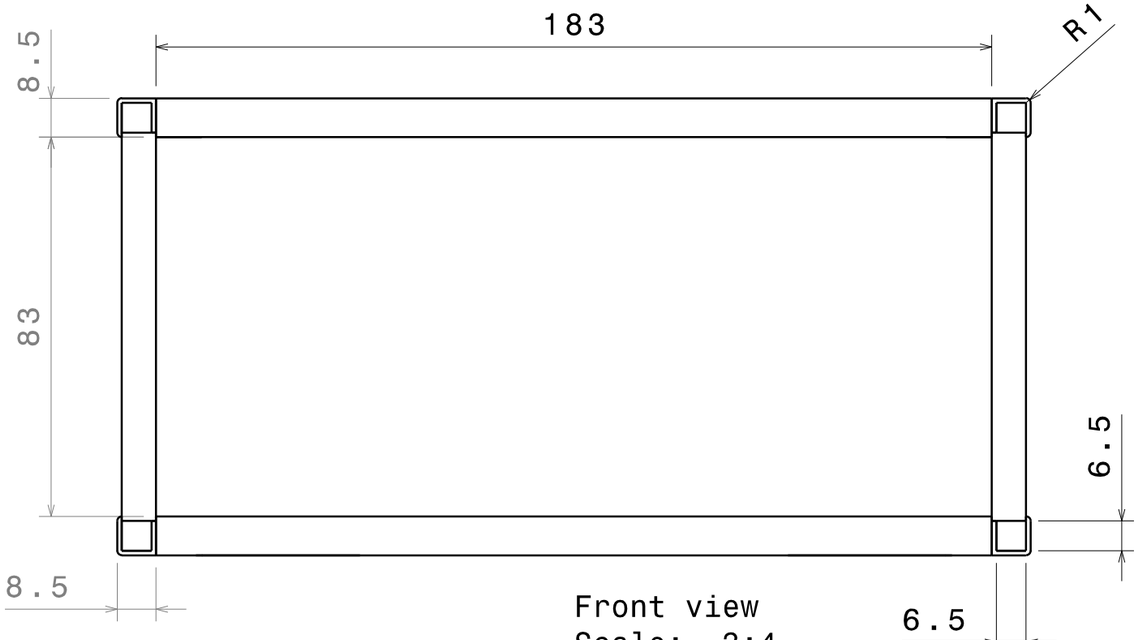

Front view
Scale: 3:4

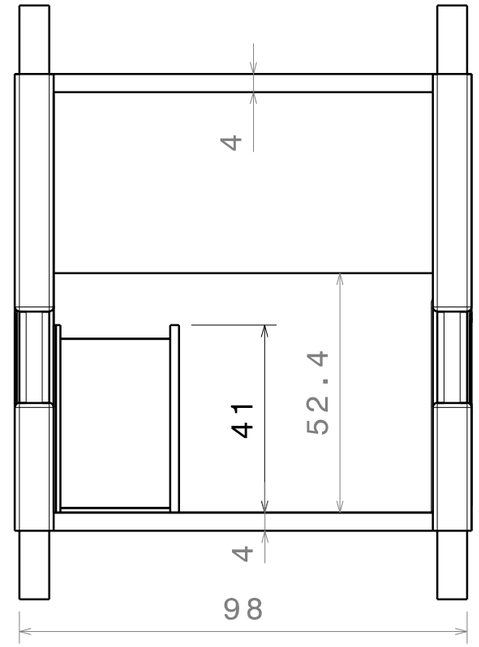

Front view
Scale: 3:4

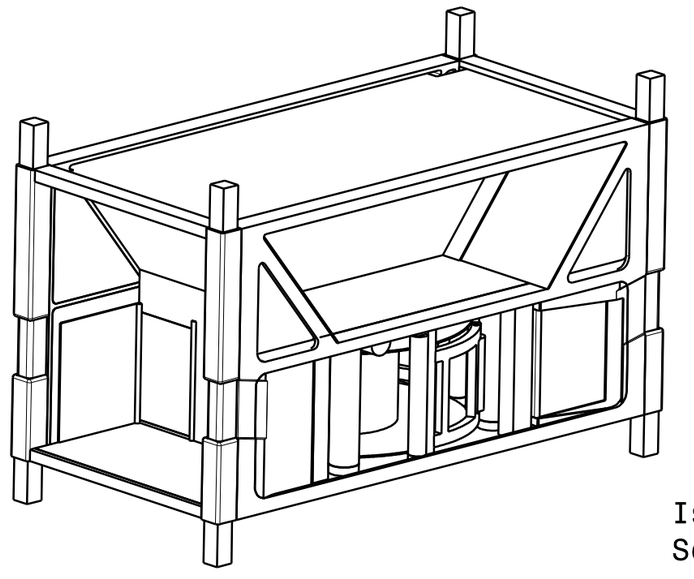

Isometric view
Scale: 1:2

Number	Quantity	Name	NORM	Sizes	MATERIAL
	1	SSM		200x100x130	Al 7075T6

Solar Sail Module

PFC	ETSEIAT-UPC
Rique Garaizar, Orzuri	
Date: June 6, 2013	Nº 2

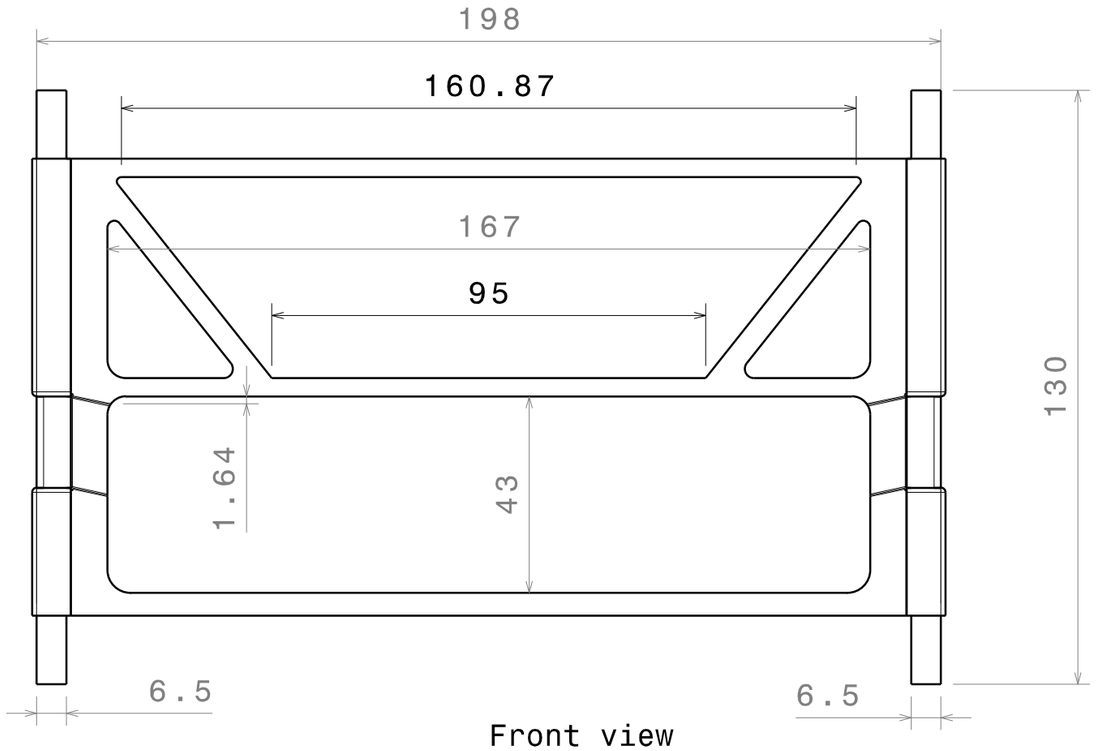

Front view
Scale: 3:4

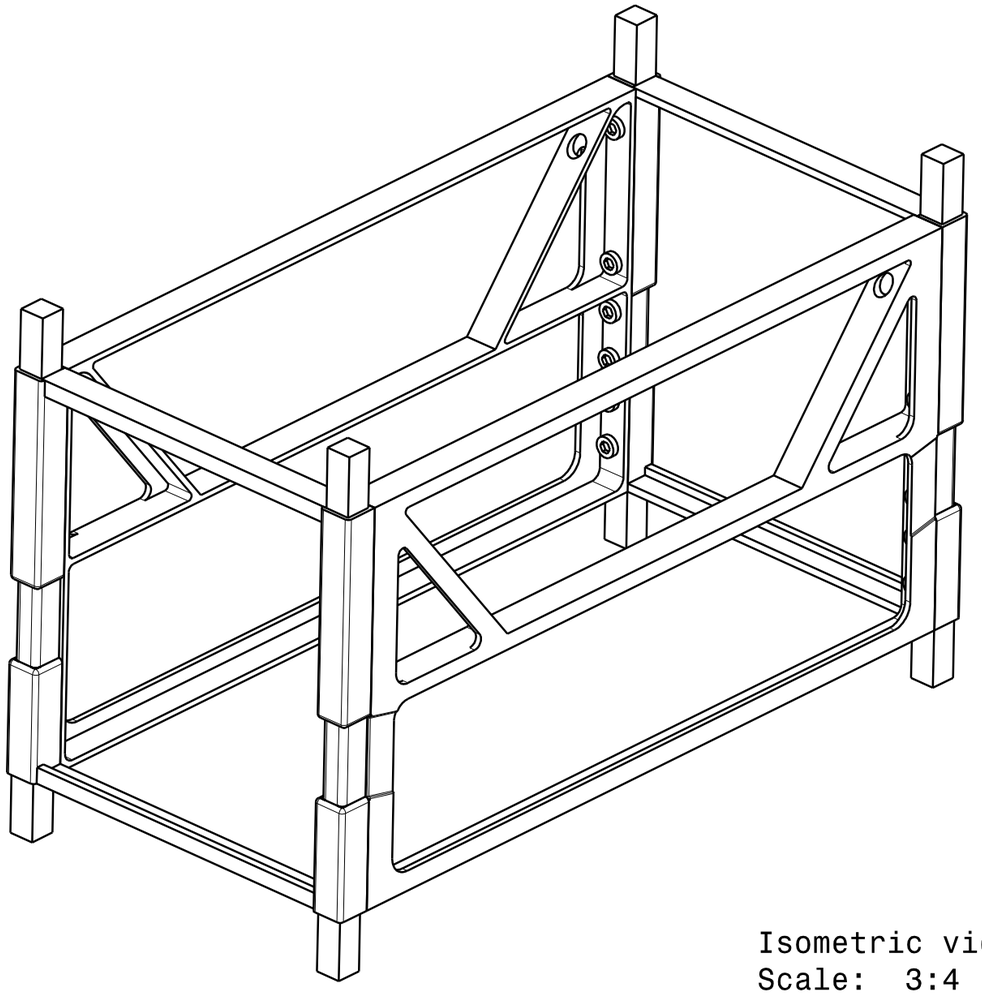

Isometric view
Scale: 3:4

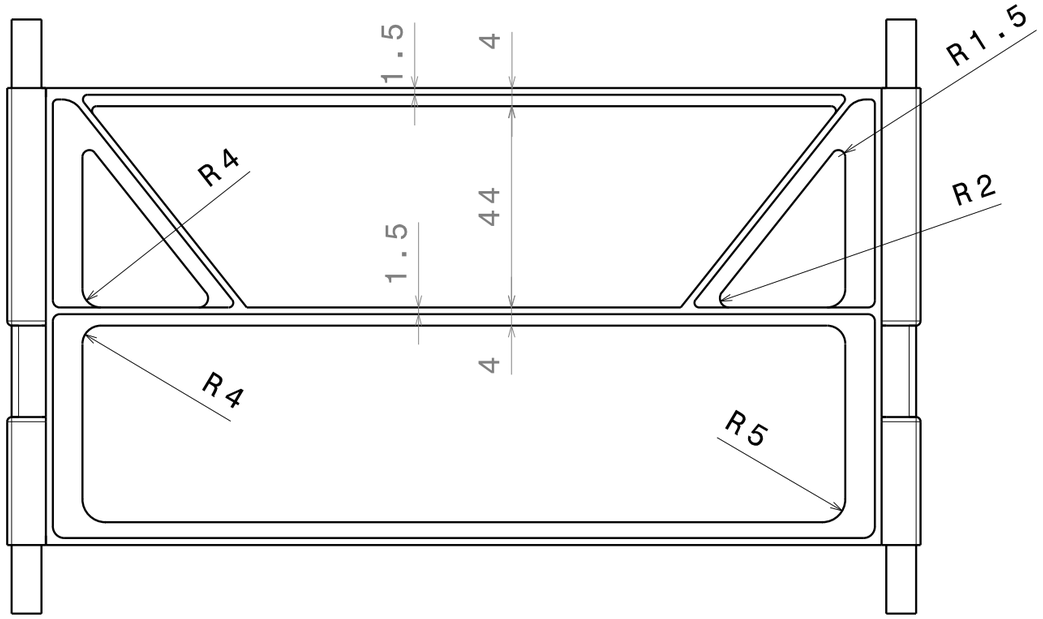

Front view
Scale: 3:4

Number	Quantity	Name	NORM	Sizes	MATERIAL
	1	Primary structure		200x100x130	Al 7075T6

Primary structure

PFC

ETSEIAT-UPC

Rique Garaizar, Orzuri

Date: June 6, 2013

Nº 3

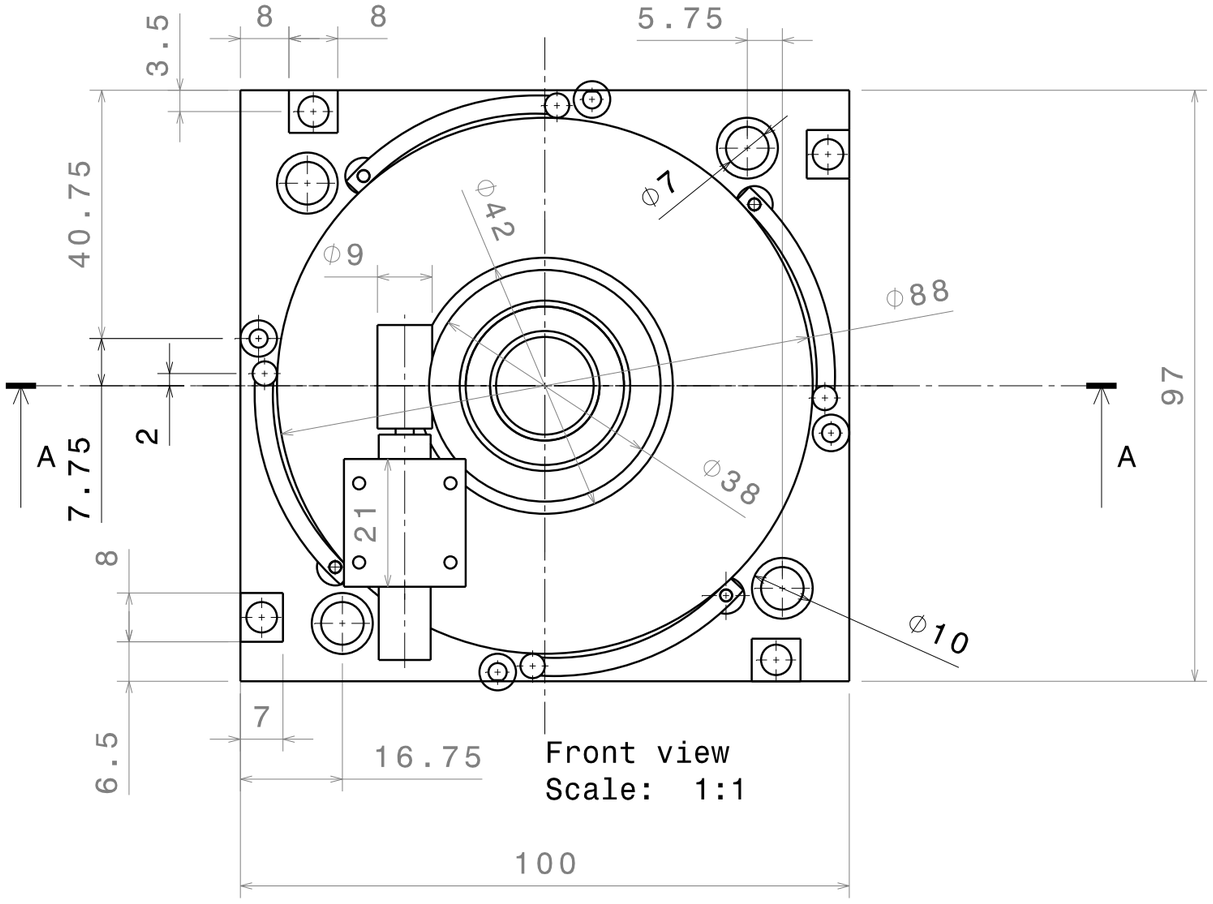

Front view
Scale: 1:1

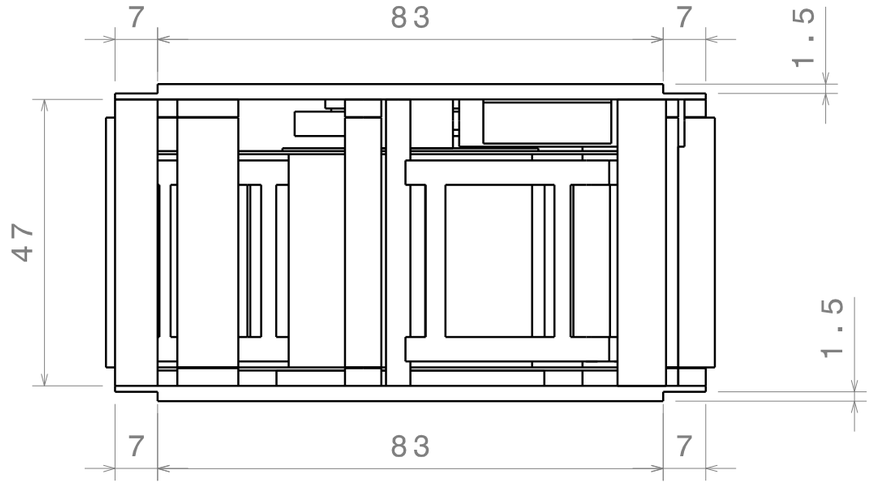

Front view
Scale: 1:1

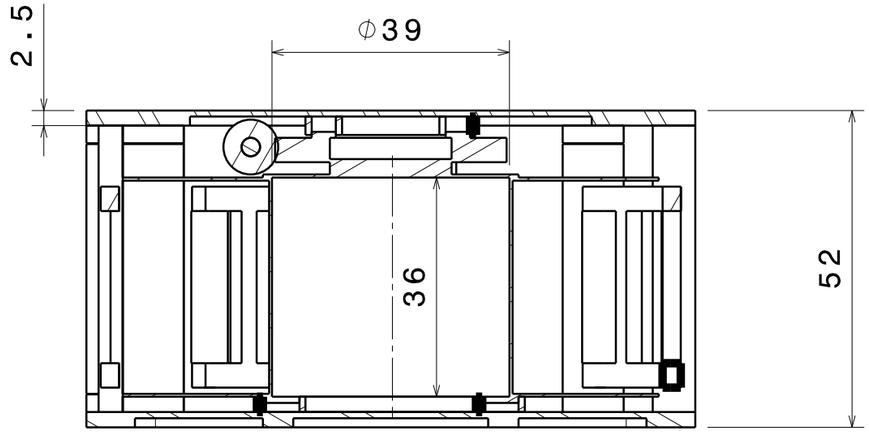

Section view A-A
Scale: 1:1

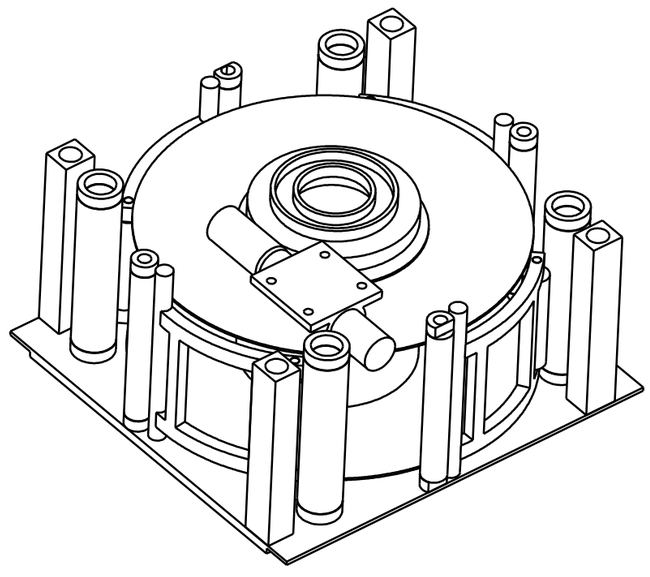

Isometric view
Scale: 3:4

Number	Quantity	Name	NORM	Sizes	MATERIAL
	1	BDM		100x100x52	Al 7075T6

BDM	PFC	ETSEIAT-UPC
	Rique Garaizar, Orzuri	
	Date: June 6, 2013	Nº 4